Linear stability analysis of a supercritical water loop driven by natural convection

by

T. N. C. de Vries

to obtain the degree of Bachelor of Science in Applied Physics
at the Delft University of Technology,
to be defended publicly on Wednesday March 2, 2016 at 4.00 PM.

Student number:	4153502	
Project duration:	November 9, 2015 – March 2, 2016	
Thesis committee:	Dr. ir. M. Rohde,	TU Delft (TNW), supervisor
	Dr. ir. D. Lathouwers,	TU Delft (TNW)

An electronic version of this thesis is available at
http://www.nera.rst.tudelft.nl/en/publications/
and http://repository.tudelft.nl/.

TU Delft

Nomenclature

Roman characters		
A	[m^2]	Channel flow area
A_w	[m^2]	Wall cross-sectional area
C_i	[m^{-3}]	Precursor concentration
D_H	[m]	Hydraulic diameter
E_f	[J]	Energy per fission event
H	[J kg^{-1}]	Specific enthalpy
K		Pressure loss coefficient
L	[m]	Length
M	[g mol^{-1}]	Molar mass
N	[m^{-3}]	Number density
N_A	[mol^{-1}]	Avogadro constant
P_{in}	[m]	Perimeter
Q	[J s^{-1}]	Core heating power
Q_w	[J s^{-1}]	Fuel-to-wall heat flow
$\mathscr{R}$		Reactivity
T	[K]	Temperature
V	[m^3]	Volume
V_f	[m^3]	Fuel volume
W	[kg s^{-1}]	Mass flow rate
c_p	[J kg^{-1} K^{-1}]	Fluid specific heat
$c_{p,w}$	[J kg^{-1} K^{-1}]	Wall material specific heat
f		Darcy friction factor
g	[ms^{-2}]	Gravitational acceleration
h	[J kg^{-1}]	Specific enthalpy
n	[m^{-3}]	Neutron concentration
p	[N m^{-2}]	Pressure
t	[s]	Time
v_n	[ms^{-1}]	Neutron velocity
Greek characters		
Λ	[s]	Mean generation time
Σ_f	[m^{-1}]	Macroscopic neutronic cross-section for thermal fission
α_r	[m^3 kg^{-1}]	Density reactivity feedback coefficient
β		Delayed neutron fraction
ε		Enrichment
θ	[K]	Temperature perturbation
λ		Eigenvalue
λ_f	[J s^{-1} m^{-1} K^{-1}]	Fluid thermal conductivity
λ_i	[s^{-1}]	Precursor decay constant
λ_w	[J s^{-1} m^{-1} K^{-1}]	Wall thermal conductivity
μ	[N s m^{-2}]	Dynamic viscosity
ρ	[kg m^{-3}]	Density
ρ_w	[kg m^{-3}]	Wall material density
σ_f	[m^{-3}]	Microscopic neutronic cross-section for thermal fission
τ	[s]	Fuel heat transfer time constant

v	$[\mathrm{m^3\ kg^{-1}}]$	Fluid specific volume

Dimensionless numbers

N_{Fr}	Froude number
N_{sub}	Subcooling number
$N_{\Delta h}$	Pseudo phase change number
Nu	Nusselt number

Subscripts	Value taken at:
0	Bottom core node
1	Top core node
B	Buffer vessel node
D	Downcomer node
F	Fuel node
R	Riser node
pc	Pseudo-critical point
w	Wall node (low heating model)
$w,0$	Bottom wall node (high heating model)
$w,1$	Top wall node (high heating model)

Other

$\overline{X}$		Steady state value of variable
$\underline{X}$		Dimensionless variable
$\check{x}$		Perturbation
$\widehat{Nu}$	$[\mathrm{J^{0.66}\ s^{-0.66}\ m^{-0.66}\ K^{-0.66}}]$	Adjusted Nusselt number

Common abbreviations

BWR	Boiling Water Reactor
ESBWR	Economic Simplified Boiling Water Reactor
DWO	Denisty Wave Oscillations
GIF	Generation IV International Forum
HPLWR	High Performance Light Water Reactor
NIST	National Institute of Standards and Technology
NSB	Neutral Stability Boundary
PDO	Pressure Drop Oscillations
PWR	Pressurised Water Reactor
SCWR	Supercritical Water Reactor

Abstract

The Supercritical Water-cooled Reactor (SCWR) is one of the six Generation IV reactor concepts, designed to be more efficient, highly economical, inherently safer and more environmentally friendly than earlier-generation reactors. The European SCWR design concept is named High Performance Light Water Reactor (HPLWR). Its safety is partly enhanced as its core heat is removed by water that circulates through natural convection instead of being driven by active pumps. In order for the HPLWR concept to be viable, the flow stability of supercritical water has to be understood for all possible operating conditions. This thesis extends research done by an existing computational model that calculates the stability of a HPLWR reactor at different operating conditions.

In the model, the reactor is simplified to several nodes. For each node, conservation balances are set up regarding mass, heat and momentum. The system is reduced to an eigenvalue problem by linearising the balanced equations. Once the steady state solutions are found by an iterative process, the stability of operational conditions is found by investigating the response of the system to introduced perturbations. Stable and unstable regions are displayed in map of non-dimensional operating conditions. The goal of this research was to investigate why numerical results of the model deviate from experimental data of similar systems and investigate what physical mechanisms are causing the different unstable operating conditions that occur in our model.

Throughout the model, the hydraulic diameter of the system had been kept constant. To investigate the implications of this simplification with respect to a real HPLWR, a parametric study was carried out for the stability of the model with a varying hydraulic diameter of the riser. It was found that increasing the hydraulic diameter of the riser resulted in stabilisation of the system in both a high power and a lower power unstable area. It was also found that increasing the riser length causes significant destabilisation of the low power unstable region and decreasing the volume of the buffer resulted in similar effects.

To get a better insight in the origin of unstable regions found by the model, the eigenvalue problem was solved as a function of time. Fluctuations in system variables were plotted against time and convincingly showed converging and diverging behaviour according to stable and unstable operating conditions respectively.

Terms associated with gravity and friction throughout the system were determined out of the linearised balance equations. Their time-dependent behaviour was concluded to be according to stable and unstable operating conditions. In general, it was shown that the fluctuation amplitude of the friction term was larger than the amplitude of the gravitation term. It was concluded that fluctuations in friction play a more important role in destabilising the model for the operating conditions that were investigated. However, due to the oscillatory and exponential behaviour of both terms, a time-dependent ratio between the two terms turned out to be quantitatively meaningless.

Contents

1 Introduction

1.1. Background of research

As the world's population is expected to grow to 10 billion by 2050 and the energy consumption per capita is increasing, so has the the demand for reliable energy sources [7]. Since the increase of CO2 levels in the atmosphere is considered one of the main causes for global warming, there is a great need for generating electricity without CO2 production. With the combustion of fossil fuels emitting 8 million tons of CO2 per year, nuclear energy is already saving approximately 2.5 billion tons of CO2 emission per year, while providing more than one billion people with electrical power [7]. Nowadays more than 90% of thermo-hydraulic research in nuclear reactors belongs to the field of nuclear safety [22]. The Nuclear Energy and Radiation Applications (NERA) section of Delft University of Technology performs research on the analysis and development of nuclear reactors that excel on safety and sustainability.

Over 400 nuclear power reactors are currently operating worldwide, of which most are Boiling Water Reactors (BWR) or Pressurized Water Reactors (PWR), being second or third generation reactor types. The Generation IV International Forum (GIF) is an international organisation which was set up to carry out the research and development needed to establish the next generation nuclear energy systems. By 2030 the world is set out to start using generation IV reactors, being highly economical, with enhanced safety, producing minimal waste and used only by the parties that originally designated the reactor. GIF selected six nuclear reactor types for further development [6]. One of these Generation IV reactors that NERA focusses on is the Supercritical Water-cooled Reactor. Like a conventional BWR or PWR, a SCWR uses light water as both a coolant and a moderator. It operates under pressures and temperatures above the supercritical point of water.

1.2. Supercritical fluids

As shown in figure 1.1, water can exist in various states. Liquids or gasses become supercritical fluids under extremely high pressures and temperature. The critical point of water lies at T_C=373.946 $^\circ C$ and 22.0640 MPa. Most supercritical water reactors operate in the range of liquid and supercritical fluids, keeping the pressure throughout a system constant like is indicated in the figure. They are considered to be a one phase system, other than a BWR, in which one liquid undergoes boiling in the transition to a gaseous state.

Table 1.1: Properties of water at the pseudo-critical point. [19]

PROPERTY	VALUE
T_{pc}	384.9 °C
h_{pc}	$2.1529 \cdot 10^6$ J/kg
ρ_{pc}	316.82 kg/m^3
v_{pc}	$3.1564 \cdot 10^{-3}$m^{-3}/kg
μ_{pc}	$4.2797 \cdot 10^{-5}$ Pa·s

Several properties of water, such as the density, viscosity, and specific heat capacity, exhibit highly non-linear behaviour around this point, as shown in figure 1.2. Although supercritical fluids do not undergo a phase transition (like boiling), some characteristics change significantly. For water, density decreases drastically. As the temperature increases from 280 °C to 500 °C, the density drops from 780 kg/m^3 to 90 kg/m^3 [7]. This drop in density makes supercritical water suitable for natural circulation, if the core is placed vertically.

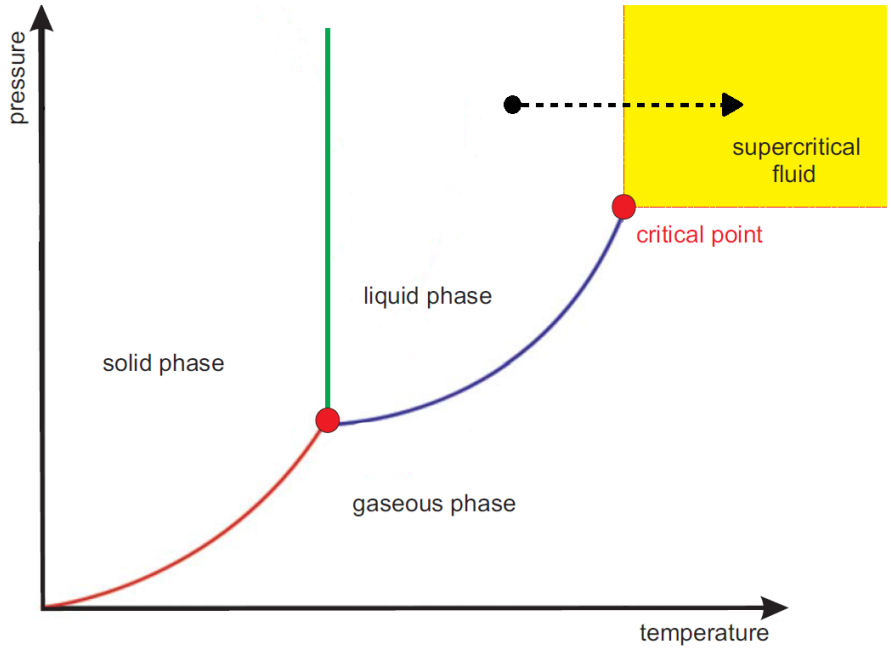

Figure 1.1: Phase diagram of water. The dashed black line shows the operating range of the HPLWR, showing the phase change from liquid to supercritical water as temperature rises. [13]

The specific heat capacity of water peaks in the supercritical region, and its value is highest at the so-called pseudo-critical point. The corresponding temperature is called the pseudo-critical temperature. The peak in heat capacity enables water to store a lot of heat with only a small change in temperature, making it a good cooling fluid. In table 1.1, different pseudo-critical properties are listed for water, like the pseudo-critical enthalpy h_{pc}.

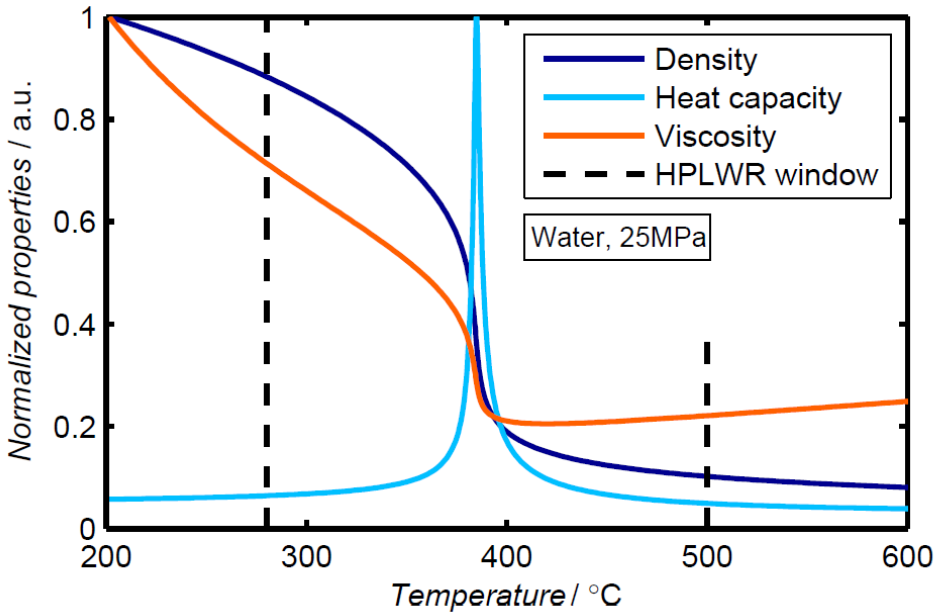

Figure 1.2: Properties of water around the pseudo-critical point. The dashed black lines show the operating range of the HPLWR. [27]

1.3. Supercritical water-cooled reactors

Figure 1.3 shows the schematic overview of a supercritical water-cooled reactor. Liquid water flows into the core at the bottom of the Reactor Pressure Vessel (RPV). The pressure inside the reactor is continuously kept at 25MPa (above the critical pressure of 22.1 MPa), so that the water passes the maximum specific heat capacity while being heated in the reactor core. The nuclear process within the core is heating the water and causing it to become supercritical. The supercritical water is brought into a turbine, where the heat is converted to electricity through a generator. In a condenser, the water cools down to the inlet temperature.

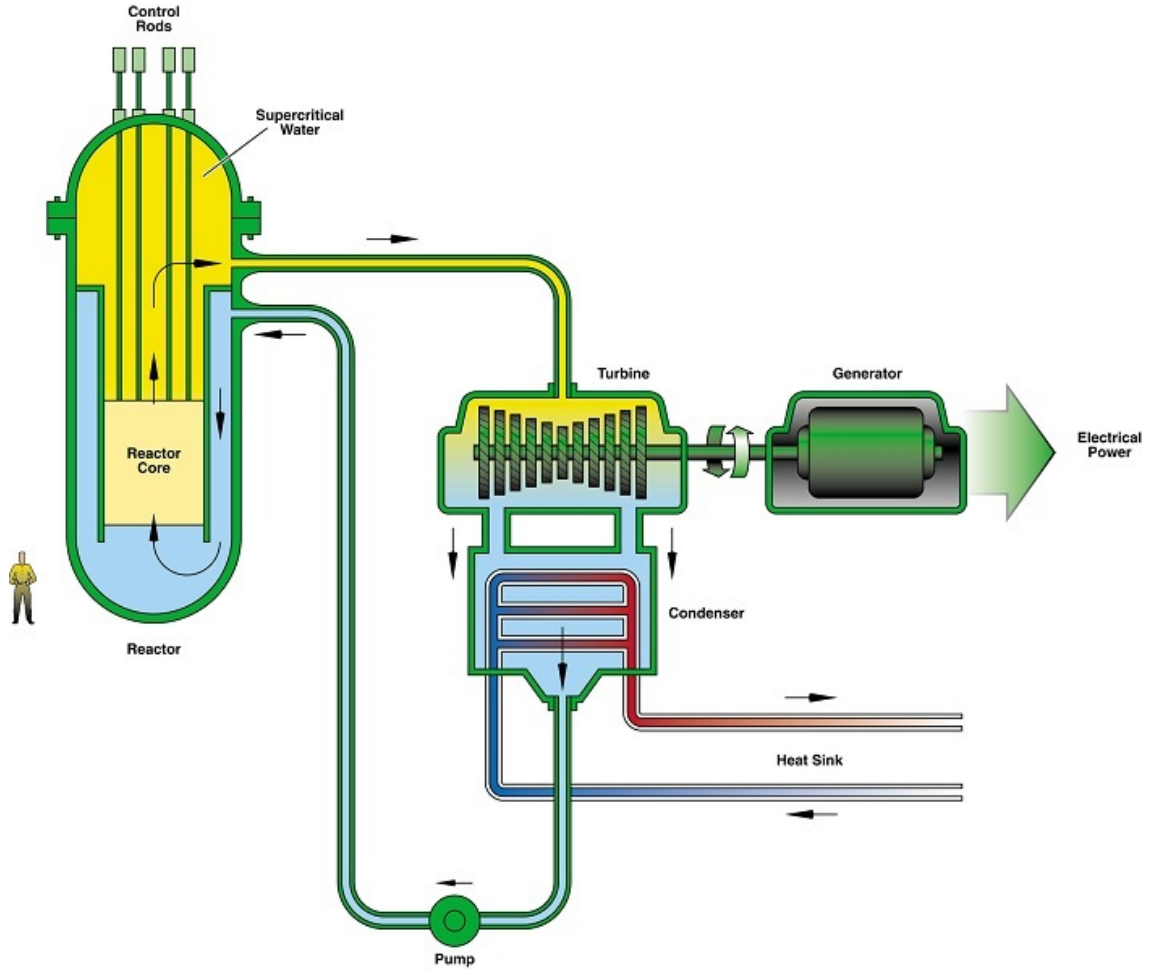

Figure 1.3: Schematic overview of the SCWR concept. In the natural convection driven HPLWR, a riser is present on top of the core (not shown in figure) and the active pump is absent. [6]

The SCWR has a thermal efficiency of 44% against 33% of a boiling water reactor [6]. Apart from this major improvement in efficiency, there are several other properties that are very promising. As the coolant has a higher enthalpy content, it needs a lower coolant mass flow rate per unit of thermal core power. This enables a supercritical fluid to cool the core at lower flow rates. As the coolant goes through the reactor vessel only once, less coolant mass inventory is needed. This opens the possibility of smaller containment buildings.

As there is no second phase in the reactor, there will be no boiling crisis, thereby avoiding discontinuous heat transfer regimes within the core during normal operation. A last advantage is that steam dryers, steam separators, recirculation pumps, and steam generators are eliminated. Therefore, the SCWR could be a simpler plant with fewer major components [6].

1.3.1. High Performance Light Water Reactor

The European version of a SCWR is named a High Performance Light Water Reactor. A consortium of 10 partners out of 8 European countries is developing this reactor which is funded by the European Commission. The target for completion of the essential Reserch and Development in order to start a definite design has been set at 2020 [11]. The HPLWR mainly differs from other supercritical water reactors in its core design. The core of a HPLWR consist of three heating sections and mixing chambers in between. The three-pass core design was first proposed by Schulenberg et al [25], to avoid hotspots in the core. Each heating stage consists of 52 fuel assembly clusters, containing nine fuel assemblies in which water flows along the fuel rods. The mixing chambers are designated so that the temperature of water is more uniform before entering the next heating section. While the coolant flows upward in the evaporator, it is heated to 390 °C. After this the coolant will flow downwards through the first superheater and upwards again through the second superheater, reaching a temperature of 435 °C and 500 °C respectively.

Apart from transporting the fuel heat, water is also used as a moderator for neutrons. Fast neutrons lose part of their kinetic energy when they collide with the hydrogen atoms in water. Therefore, the moderation of neutrons is dependent on the density of water in the core. The moderation in the core decreases as the density of decreases while being heated. This is why neutron thermal-hydraulic coupling takes place between the power delivered by the core and the properties of the coolant.

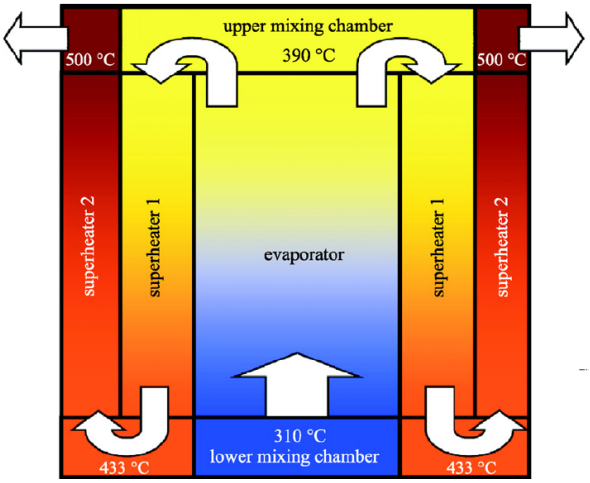

Figure 1.4: Diagram of the coolant flow in the three pass HPLWR core. Mixing chambers are located between every heating stage. [7]

For this thesis, a natural circulation variant of the HPLWR design was investigated, so the water flows without the use of active pumps. In Boiling Water Reactors natural circulation is possible thanks to the phase transition, as steam is much lighter than liquid water. The density difference between water in liquid and gaseous phase is creating a gravitational pressure drop in the system, which drives the circulation. The HPLWR also has the potential to operate by natural circulation, as the density drop of the supercritical water is large enough to drive the flow. A riser is placed on top of the core to increase the gravitational pressure drop, enhancing the process of natural convection. After extraction of heat by the turbines, a downcomer is placed to let relatively cold and heavy water flow downwards.

The mechanism behind natural circulation also induces a negative feedback loop. A decrease in mass flow would give the cooling water a longer time in the reactor core, causing to reach supercritical properties earlier in the core. As the density will decrease significantly after the pseudo-critical point, the gravitational pressure difference between the core and the downcomer increases. A larger net force on the water will lead to an increase in mass flow rate, eventually causing it to return to its steady state.

Natural circulation may enhance the inherent safety of the HPLWR design. Technical failure or natural disasters may cause power outage, that could cause circulation pumps to stop working. In combination with other unwanted circumstances this could lead to a core meltdown. This is why the natural circulation of a cooling fluid might be considered as an extra safety feature during emergency situations.

1.4. Stability of reactors

The stability of a system is determined by its reaction to perturbations, being small fluctuations in steady state operating variables. If we investigate the amplitude of oscillations caused by perturbations throughout time, we can determine the decay ratio. The decay ratio is defined as the ratio between two consecutive peaks. If the decay ratio is smaller than one, the system will go back to its original state, meaning it is stable. The system is unstable if the decay ratio is larger than one. Then the amplitude of an oscillation keeps increasing and the system does not go back to its steady state. A decay ratio less than 1 (e.g. 0.25) is set for core stability

during normal operation for a margin to the design criterion [20]. In experiments, an amplitude of a certain percentage of the mean value (10%-30%) is often considered as an indication for instability [18].

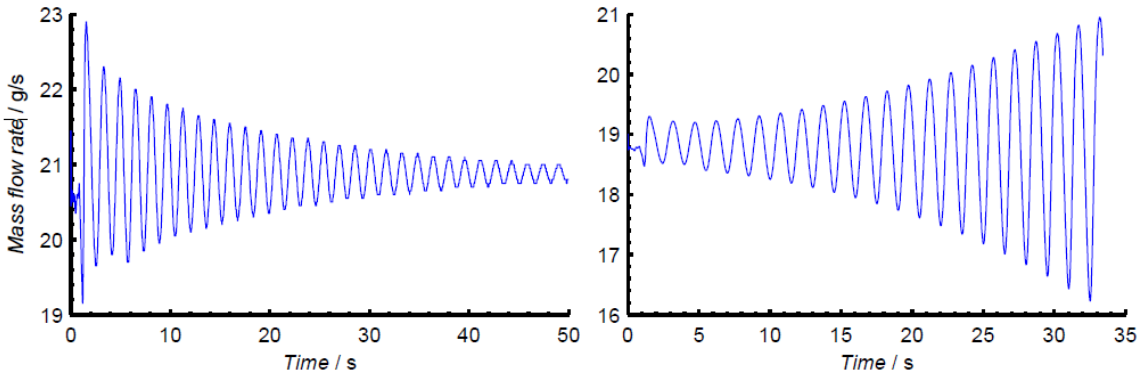

Figure 1.5: Example an oscillation that is showing exponential decay (left) and exponential growth (right). [27]

Instability results in an unstable mass flow, which may cause additional issues. As water is used as a moderator, flow instability of the water may induce power instability. This decreases the reliability of continuous power delivery. Another disadvantage of unstable flow is, that high fluctuations in local pressure can lead to component fatigue or even damage of reactor components [9]. The most significant risk however, is that at low flow rates water would be unable to cool the core, causing it to overheat.

The stability of a reactor depends on both design parameters and operating conditions. The core layout and system geometry therefore play a big role in reactor design. Operating conditions like the core power affect stability together with the coolant and moderator flow rate and inlet temperature of the coolant of the reactor.

1.4.1. Types of flow instability

First off all, a distinction has to be made between microscopic and macroscopic instabilities. Microscopic stabilities, occurring at the interface of a two-phase flow, are out of the scope of this research. Further research in the field of microscopic instabilities like Rayleigh-Taylor instability, Miles instability or shear mode instability has been done by Boomkamp [2] amongst others. The focus of this research is kept on macroscopic phenomena, as they involve the integral system.

Different types of two-phase flow instability were classified by Bouré et al [3] in 1973. As many two-state flow instabilities are also expected to occur within a SCWR, it is relevant to know the main principles that cause them to take place. The most used classification divides macroscopic instabilities in static and dynamic instabilities. Static instabilities can be explained from the steady-state equations governing the system, while dynamic instabilities follow from feedback mechanisms in the transient behaviour. Furthermore, when several instability mechanisms interact, the term compound instability is used. In the coming paragraphs a static instability called Ledinegg instability and a pure dynamic instability type called Density Wave Oscillations will be introduced.

Ledinegg instability

For determining static stability, the steady states of an internal and external system are compared. Comparing the internal pressure drop with the external pressure drop characteristic, i.e. related to a pumping system, one can find intersecting points as shown in figure 1.6. These intersections define the steady state operating points of the entire system. The pressure drop vs. flow rate characteristic curve of a boiling system (internal curve) often exhibits an N-shaped or S-Shaped curve. Depending on the external curve, operational points can be stable or unstable. If the slope of the internal curve is smaller than the external characteristic curve, the operational point is called stable. In natural circulation systems, the external characteristic is defined by the driving head due to buoyancy [18]. Equation 1.1 is showing the stability condition [22].

$$\frac{\partial \Delta P}{\partial G}_{int} > \frac{\partial \Delta P}{\partial G}_{ext} \tag{1.1}$$

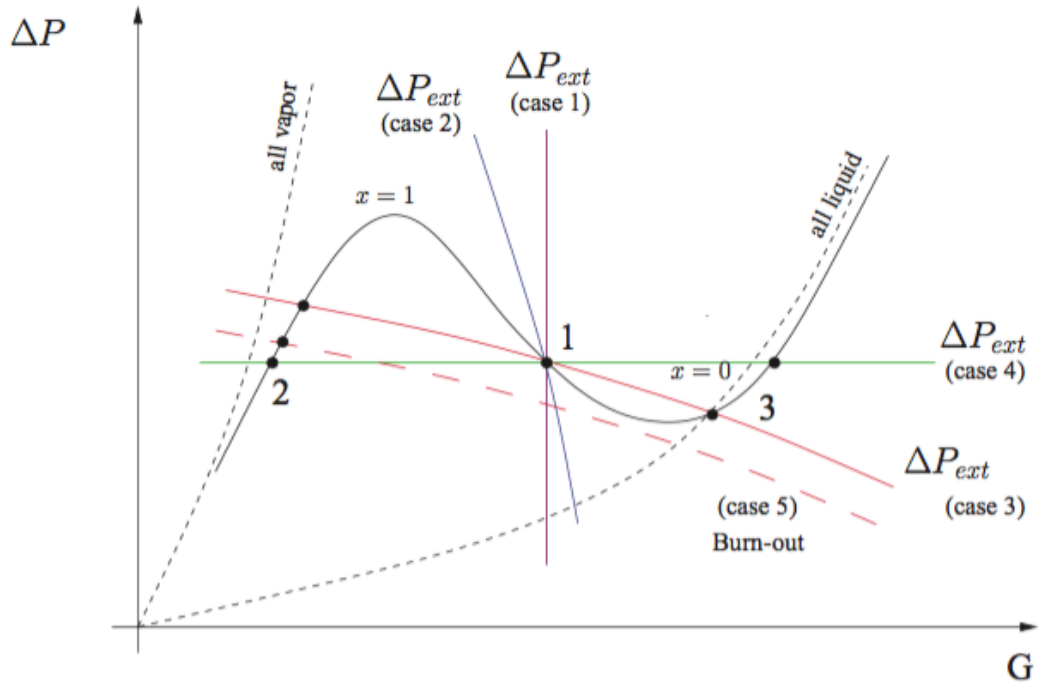

Figure 1.6: Internal pressure drop vs. flow rate characteristic curve for a boiling system. In addition, five different external characteristic curves are presented. [22]

In figure 1.6, one can see the theoretical BWR cases of all vapor and all liquid. The two curves represent the limit cases for the pressure drop within a two-phase system. It is clearly visible that for case 1 and 2 the external characteristic results in only one (stable) steady state intersection point, whereas the external curves for case 3 and 4 have multiple intersection points with the internal characteristic. In these cases, point 1 is unstable, as the stability condition is not fulfilled.

Ledinegg instability is also referred to as flow excursion and it is one of the most analysed instabilities in literature, first introduced by M. Ledinegg [14]. Ledinegg found out that the gradient of the steady state pressure drop curve could become negative, depending on operating conditions. Ledinegg instability is non-periodic and transient, and it is highly related to the pressure characteristic curve of a heated pipe throughout literature [5].

The origin of a Ledinegg instability is shown in figure 1.6. A small perturbation causes an abrubt flow excursion to a new stable operating condition. Ledinegg instability only occurs if the stability criterion shown in 1.1 is not fulfilled. If this is the case, unstable mass flow rates may suddenly change to another mass flow rate, which can be both stable or unstable again. In case 3 the system has 3 steady state operating points. If the external characteristic is modified to case 5, the system will experience a flow excursion from point 3 to point 2 [22]. As the HPLWR has no external pumping system and it is driven by natural convection, other means of determining Ledinegg unstable conditions were used. These are explained in section 4.3.3.

Density wave oscillations

This dynamic instability is caused by the delay and feedback effects relating flow rate, density and pressure drop. Density wave oscillations (DWO), also named enthalpy wave oscillations, are the most common type of encountered flow instability in two-phase flow systems like a BWR. BWR are highly susceptible for DWO at low mass flow rates of a coolant and high power operating conditions. [7] Three types of DWO can be caused by either gravity, friction or momentum. They are referred to as Type I, Type II and Type III density wave oscillation respectively.

DWO are associated with low frequencies of 0.1-1 Hz, related to the residence time of fluid in a channel. Classically, the period of DWO is considered to be between 1.5 and 2 times the time that a fluid requires to flow through a system [22]. Type II DWO is therefore associated with frequencies that are slightly higher than type I DWO, as friction often starts to play a role at higher mass flow rates.

Both type I and II DWO are proven to be present in boiling water reactors. Type I DWO is generally found in upward vertical systems with a long unheated riser placed downstream from a heating section [22]. In a BWR, this type of DWO is mainly caused by the difference in gravitational head between (relatively) cold water and hot steam, resulting from the density differences between water in liquid and gaseous phase. In a SCWR the coolant does not undergo a phase transition, but since a similar density drop takes place from subcritical to supercritical water, type I DWO is expected to occur in our system. Moreover, the change in coolant density is even bigger for a HPLWR than for a BWR [7]. As this phenomenon is particularly important in natural convection loops, it is a significant subject of this research.

Type II DWO is the most common density wave oscillation. It is caused by the difference in propagation speed of flow perturbations in the single phase and two phase region. As type II DWO is induced by frictional component of pressure losses at higher mass flow rates, this instability is predicted to occur in our model at approximately the same region as type II DWO in a BWR.

Momentum-based (type III) DWO has attracted very little attention throughout literature and will not be taken into account for this research.

Since the 80's, coupled neutronic thermo-hydraulic instabilities have been considered as compound DWO [22]. As water is used as a moderator in both a BWR and a SCWR, the feedback caused effect is comparable. The neutron flux and thus the power depends strongly on the density of the cooling and moderating fluid. This feedback effect is called reactivity feedback and can cause so-called neutronic-coupled DWO.

1.4.2. Flow instability in natural circulation systems

During the last decade, researchers like Nayak and Vijayan have mainly focussed on flow instabilities within natural circulation systems. Due to the non-linearity of the natural circulation process and their low driving force, NC systems tend to be more inherently unstable. A regenerative feedback system is inherent in the mechanism causing NC flow due to the strong coupling between the flow and the driving force [18]. In general, most instabilities observed in forced circulation systems are also observed in natural circulation systems.

In 2008, Nayak and Vijayan also investigated the effects of loop diameters in single and two phase natural circulation loops [33]. Single-phase loops turned out to be more stable for small loop diameters. Fort two-phase systems, both Type I and Type II instabilities turned out to be present in small diameter loops. In large diameter loops, only Type I instabilities were present. The latter can be avoided by implementing a pressurized start-up (increasing the K value at the entrance of a heating section).

1.4.3. Stability of reactors driven by natural circulation

The stability of Boiling Water Reactors has been widely researched during the last decades. In 1988, Van Bragt, among others, analysed the stability of BWRs, by simplifying the reactor type to a two-phase water loop driven by natural circulation [31].

Although the dimensionless numbers used by van Bragt are defined slightly different in magnitude from the ones that have been used in this model, the qualitative behaviour of a boiling water reactor is expected to be comparable with a supercritical water reactor [13]. The area denoted by roman number I is caused by the density difference of liquid water and steam, indicating gravitational (type I) DWO. This unstable region is only present if a riser is placed vertically on top of the core. Thinking about the change in density around the pseudo-critical point of a supercritical water reactor, we would expect a similar instability near the border of sub and supercritical operating conditions. The right area is related to friction, type II DWO, and is also expected in SCWR.

Although much experimental data is available about the stability of boiling water reactors, only few experiments have been done with supercritical fluids.

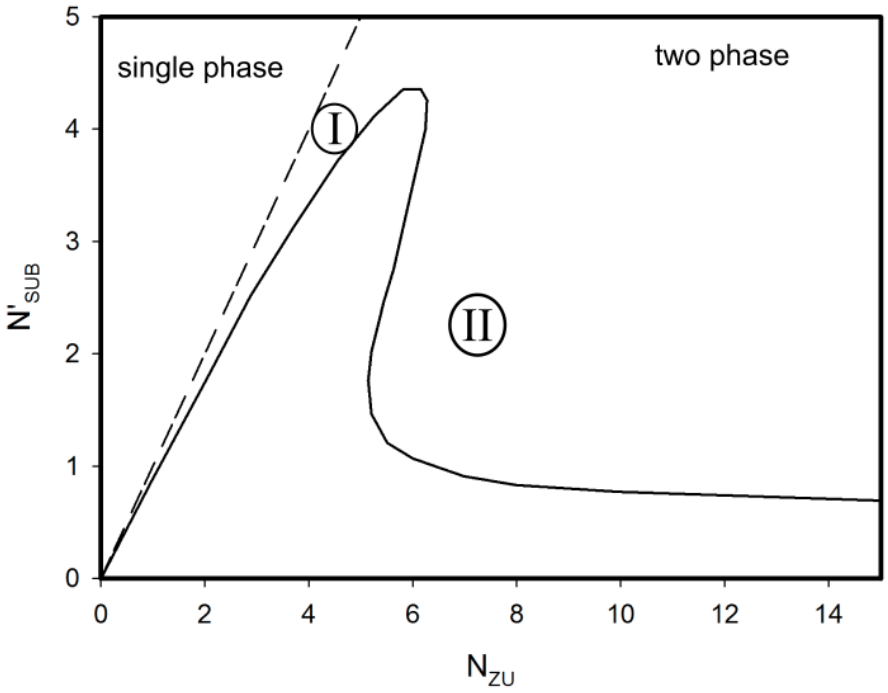

Figure 1.7: This is a stability map for a natural circulation driven water loop under the circumstances of a BWR. It is clear that there are two unstable areas in the two-phase region (right from the boiling line). They are denoted by roman number I and II. The neutral stability boundary (NSB) is the line between unstable and stable regions and the dotted line between single phase and two phi is the boiling line. [31]

1.4.4. Flow stability of supercritical fluids

Since 2001 Chatoorgoon has carried out various experimental studies on supercritical water [4]. He has used dimensionless numbers to evaluate the flow stability of super critical water loops driven by natural convection.

Lomperski did an experimental research supercritical on CO_2 in 2004 [23]. No flow instabilities were observed in their tests; a result that deviated from the predictions of a numerical model developed to study natural circulation flow behavior under these particular conditions. Jain and Rizwan-Uddin did a numerical analysis for a supercritical loop of CO_2 in 2008 [9]. Their parametric studies for different operating conditions revealed similarity of stability characteristics of flow under supercritical conditions with those in two-phase flows. In 2009 Gomez investigated the stability of a HPLWR core, driven by forced circulation [7]. Steady-state analysis showed that Ledinegg instabilities, flow maldistribution, and pressure drop oscillations did not occur at normal operation conditions of the HPLWR. Density Wave Oscillations (DWO) were shown to be the most important instability phenomena in a HPLWR.

In 2011, Ambrosini investigated flow stability boundaries in a heated channel driven by forced circulation for different supercritical fluids [1]. Flow instabilities in supercritical pressure fluid systems were predicted in close similarity with those observed in two-phase flow. A wide variety of tools and theories developed for boiling channel instabilities turned out to be available to be used with supercritical fluids. In comparison with the two-phase flow case, the complexity of tools to analyse supercritical flow phenomena can be considerable, including the coupling with neutronics reported in works like that of Oka [20]. However, still more experimental data needed to confirm stability predictions done in his research.

An unstable area between the critical and subcritical region, like the one near the boiling line of a BWR, was experimentally found by Tjoen and Rohde in 2011 with their scaled version of a supercritical water reactor, named DeLight [29]. DeLight is using Freon (R-23) as a cooling fluid instead of water, as it becomes supercritical at lower temperature and pressure [21]. In figure 1.8, the black line denotes the neutral stability line, and the black dotted line stands for the pseudo-critical boundary, while the intensity of colours indicates the decay ratio of oscillations at different operating conditions. The pseudo-critical boundary refers to operat-

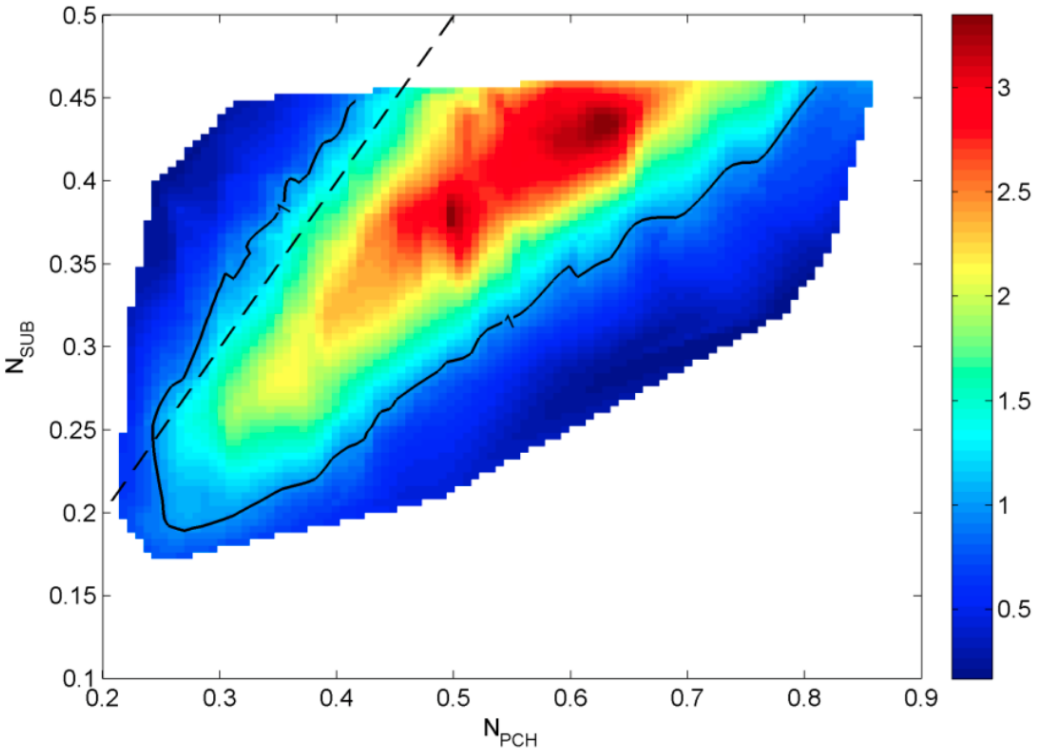

Figure 1.8: Contour plot of measured decay ratio values for the Delight facility. The black line indicates DR=1, the neutral stability line, and the black dotted line stands for the pseudo-critical boundary, while the intensity of colours indicates the decay ratio of oscillations at different operating conditions. [29]

ing conditions $N_{sub} = N_{\Delta h}$, at which the coolant reaches supercritical temperature at exactly the end of the core.

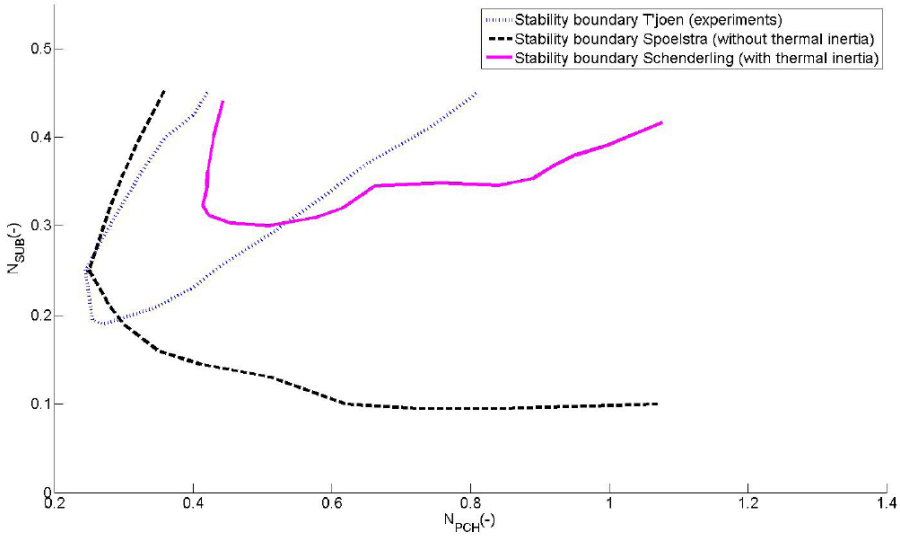

Figure 1.9: The Delight experimental data is shown in the blue striped line. The black dotted line shows the numerical model data of Spoelstra. Schenderlings data, plotted in the pink line originates from om model that includes thermal inertia effects. [24]

Up to now, numerical results [24][10][27] that included the effects of the thermal inertia of the core wall, did not match the experimental data of the DeLight facility sufficiently. This created urgency for a simplified model that is able to find the same qualitative stability behaviour.

1.4.5. Stability investigation by current model

According to this thought, Krijger [13] performed a numerical analysis on the natural circulation driven supercritical water loop, breaking the system down into a handful of nodes, based on a model for a parallel boiling channels used by Guido et al. [8]. Krijger derived heat, mass, and momentum balances for the water loop and investigated the stability by linearising these balances, reducing the single-loop system to an eigenvalue problem. Krijger's analysis did not take the thermal inertia of the internal core structure or neutronic thermal-hydraulic coupling into account. A reference case, shown in figure 1.10 was set by Krijger, after a parametric study was done for various design decisions of the supercritical water loop. It was found that increasing the length of the riser has a destabilising effect on the system, whereas increasing the volume of the buffer vessel he included in the model improved the system's stability.

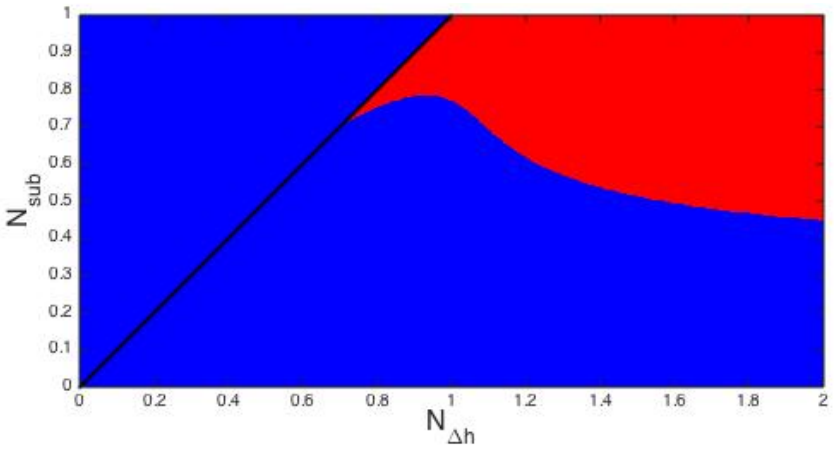

Figure 1.10: In this stability map stable and unstable regions are denoted in blue and red respectively. The black line indicates $N_{sub} = N_{\Delta h}$. The reference case of Krijger shows some resemblance with figure 1.7 of van Bragt, however, the unstable zone near the pseudo-critical boundary (indicated by the black line) is much smaller. [13]

By analysing the frequency map for this same reference case, displayed in figure 1.11, the system was expected to house three kinds of instability. The zero-frequency unstable region would be expected to house Ledinegg instability, whereas the other unstable regions could be the result of density wave oscillations. As Type I DWO is gravity-based, this is expected to happen at a moment of large differences in density, however at lower powers than Type II DWO. Type Is unstable regions occur near the boiling boundary of a BWR (van Bragt), so in a SCWR they are expected to take place near the boundary of subcritical and supercritical operating conditions. Type II DWO is friction-based and occurs at higher operating powers and somewhat higher frequencies. This is why it was expected that the low-frequency region in the frequency map indicated type I DWO and the higher frequency region denotes type II DWO.

In 2014, Lippens [15] elaborated on Krijger's work with the inclusion of the internal core structure thermal inertia, also extending the reference case, shown in figure 1.12. Lippens found that, while the inclusion of the thermal inertia effect improved stability, the stabilising effect is reduced when the wall cross-sectional area is increased. In addition, agreement with T'Joen's and Rohde's experiments in another numerical study with Freon (R-23) improved [29].

A notable side effect of including the thermal inertia of the core wall was that Krijger's low frequency unstable zone disappeared, as shown in figure 1.13. This could mean that only static instabilities, like Ledinegg, take place at lower power.

In 2015 Zonneveld [35] further developed the model by including the feedback mechanisms of neutronic thermal-hydraulic coupling. The neutronics and fuel heat transfer turned out to generally destabilize the system, as shown in figure 1.14. He also performed parametric studies for the heat transfer time constant, the density reactivity feedback coefficient and the fuel enrichment. The heat transfer time constant was set at 6 seconds, being within the reasonable range set by Van der Hagen [32]. A new unstable region was found adjacent to the previously found region that was thought to house Ledinegg instability only.

When investigated in the frequency plane, figure 1.15 shows that the low power unstable area is now showing very low frequency unstable behaviour, so possibly Ledinegg instability combined with another type of

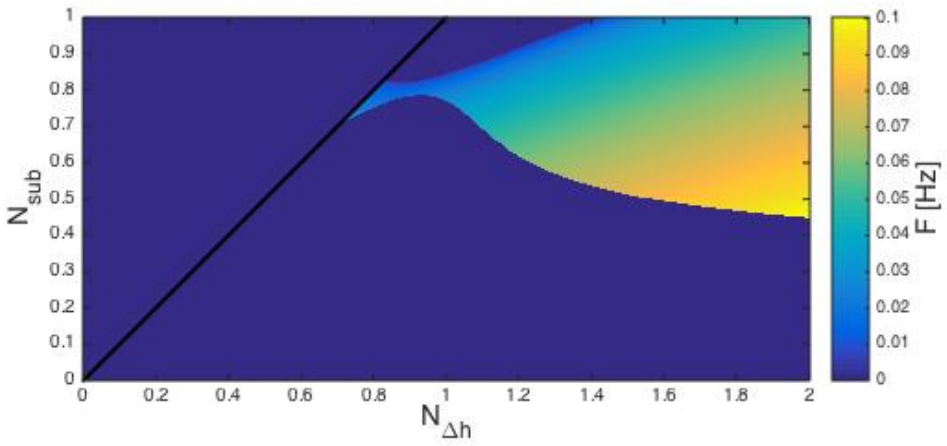

Figure 1.11: In this frequency map, the frequency of unstable operating points is indicated by color. The frequency map for reference case of Krijger shows three unstable zones. At higher powers, the frequency is higher than at the low power periodic unstable area. Around N_{sub} and N_{Δ} values of 1, also a non-periodic unstable area was found. [13]

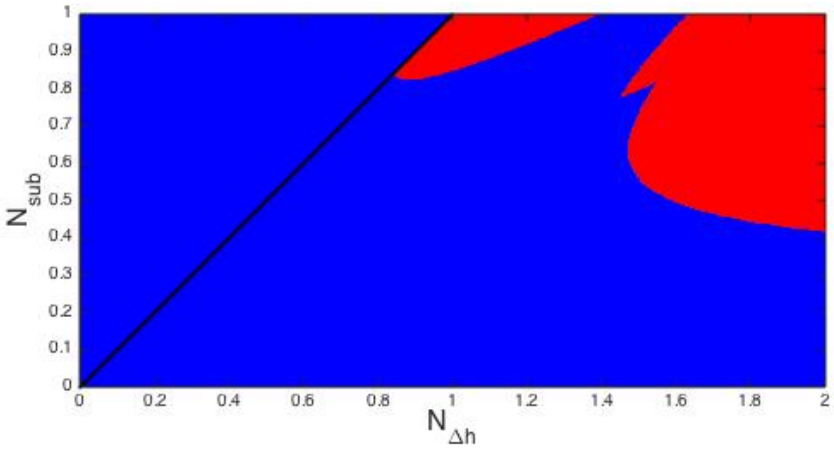

Figure 1.12: In this stability map stable and unstable regions are denoted in blue and red respectively. The black line indicates $N_{sub} = N_{\Delta h}$. In the reference case of Lippens, the system stabilised for lower powers. The unstable plane splitted in two parts. [15]

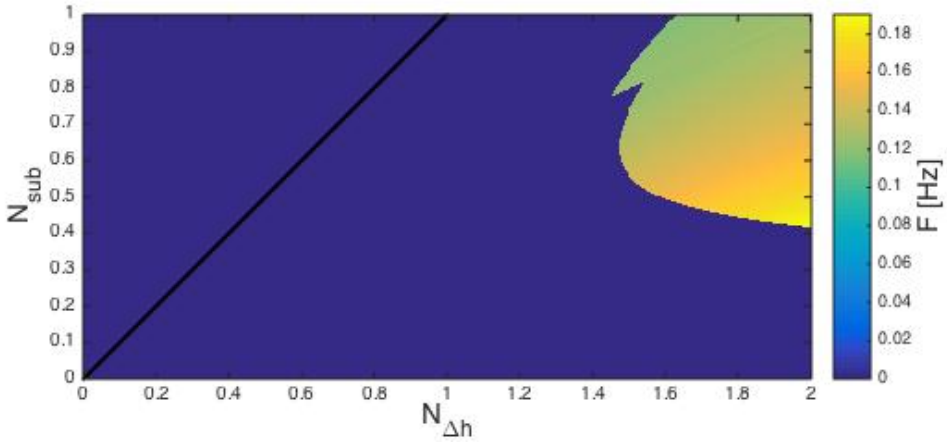

Figure 1.13: In this frequency map, the frequency of unstable operating points is indicated by color. In the frequency map for Lippens' reference case, it is visible that the unstable area at lower powers is non-periodic. [15]

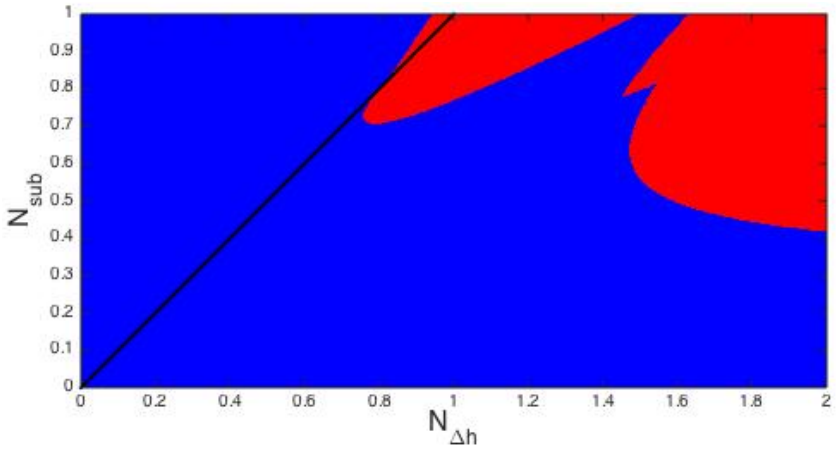

Figure 1.14: In this stability map stable and unstable regions are denoted in blue and red respectively. The black line indicates $N_{sub} = N_{\Delta h}$. The reference case of Zonneveld shows destabilisation at lower powers. The unstable zone is extended to within the subcritical region. [35]

instability, which had to be enforced by Zonneveld's implementations.

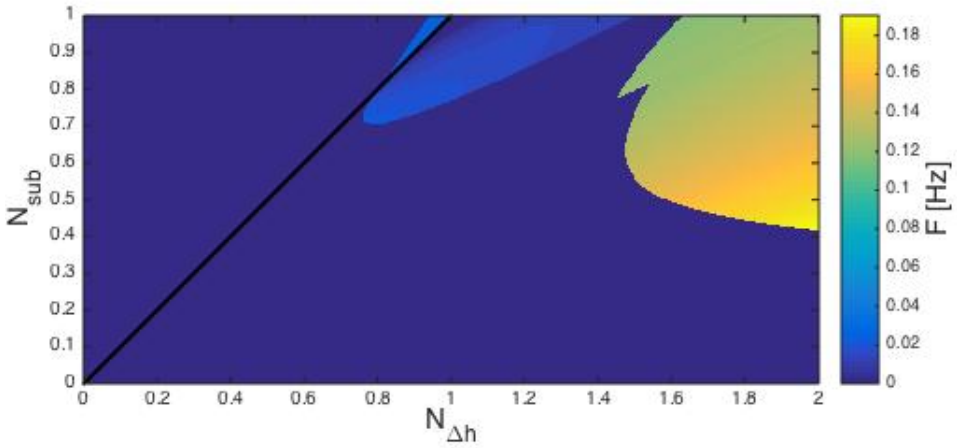

Figure 1.15: In this frequency map, the frequency of unstable operating points is indicated by color. The frequency map for reference case of Zonneveld shows a return of low-frequency periodic behaviour at the low power unstable zone. [35]

1.5. Aim of this research

In order to investigate why numerical results of the model deviate from experimental data of similar systems (e.g. Delight [29]) the dependency of stability on different geometrical parameters will be analysed. Since the hydraulic diameter of the single channel model has been set constant in every section of the loop, a simplification was made compared with the actual HPLWR geometry. The influence of this simplification will be investigated.

After investigating the effects of the hydraulic diameter of the riser, the dependency on other parameters that might lead to destabilisation of the system at lower powers will be investigated. In this way, it can be seen if the current choice for these parameters used in a reference case (see Appendix C) has been of great influence for the model's deviation in stability from experimental data.

To get a better insight in the origin of unstable regions found by the model, the influence of gravity and friction in destabilisation of the system will be clarified. To be able to identify the existence of Type I (gravity-based) and Type II (friction-based) density wave oscillations in the model, the eigenvalue problem will be solved as a function of time. By doing so, the time-dependent behaviour of system variables becomes known after a small disturbance has been introduced to one of the variables.

It is expected that knowing the development of variables related to gravity and friction throughout the system, can improve the understanding of the origin of instabilities that occur in our system. The ratio between gravity and friction could prove which of the two is more dominant in destabilising the system at certain operating conditions.

1.6. Thesis Outline

This thesis will shed new light on the model developed by Krijger, Lippens and Zonneveld, and will further investigate its theoretical background. The research will generally follow the same document structure as their reports.

In the next chapter, the physical model used for investigating the stability of the loop will be introduced. This includes the geometrical loop structure and the approximations made for several water properties. Also the balance equations that govern the loop will be shortly introduced, where the momentum balance will be used as a visual example. This balance will be made dimensionless and linearised.

Chapter 3 covers the stability investigation. It will describe the various steps to solve the matrix equations extracted from all linearised balance equations. After that, the dimensionless numbers chosen to reflect different operating conditions will be introduced.

Chapter 4 will present the computational implementations used to obtain results. After stating the considerations that affected our model, the general algorithm will be introduced step by step. The way of solving the generalised eigenvalue problem will be discussed and lastly additional analyses that have been implemented in the model will be introduced shortly.

In Chapter 5, the results will be presented. After a parametric study of several variables, perturbed variables will be plotted with respect to time. Additionally, the effects of both gravitation and friction were investigated in different areas of the stability map.

Finally, conclusions about the results have been drawn in Chapter 6. Furthermore, recommendations have been done for further research and improving the accuracy of the model.

2

Physical Model

2.1. Loop structure

In 2013, Krijger[13] investigated the stability of a natural convection supercritical water loop through an analytical model developed by Rohde, inspired by the analytical model for boiling water channels used by Guido et al in 1991 [8]. One of the simplifications that was implemented is that the core is reduced to one single channel, in which the cooling fluid is heated.

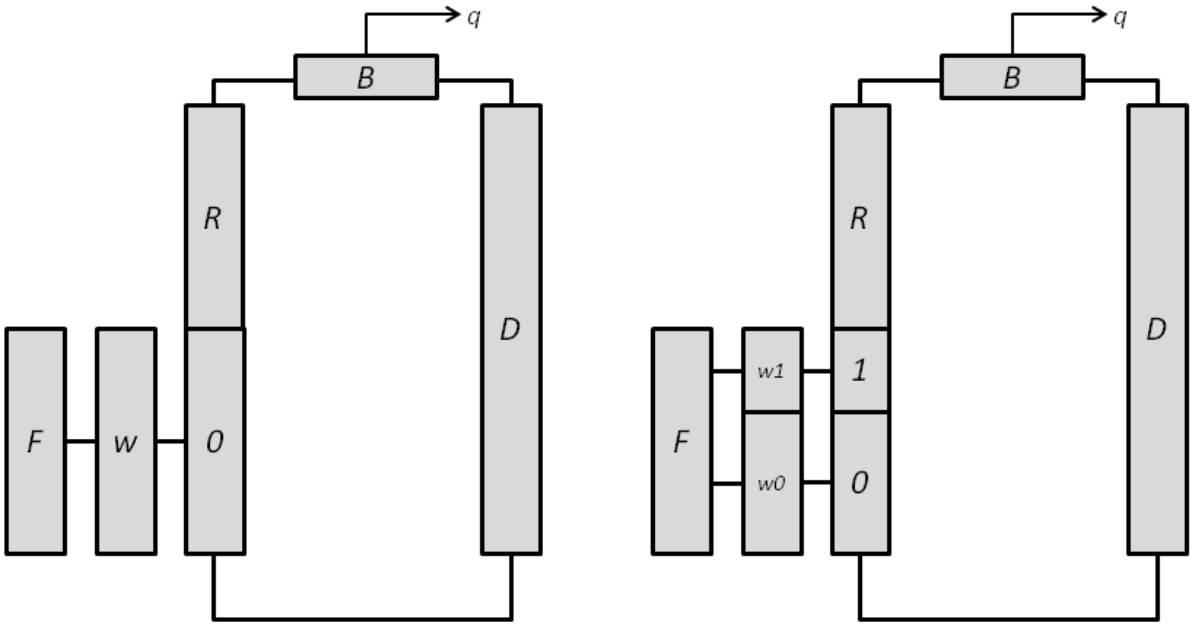

Figure 2.1: Overview of the supercritical water loop model. The left figure shows the low-heating model, with the high-heating model to the right. The coolant flows in the clockwise direction. Node labels: *0*: Core node 0; *1*: Core node 1; *w0*: Wall node 0; *w1*: Wall node 1; *F*: Fuel; *R*: Riser; *B*: Buffer; *D*: Downcomer [35]

Subcritical water enters the reactor core at node '0', and it has thermal interaction with the core wall and fuel. If the water does not become supercritical in the core, the left model applies. If water is heated past the pseudo-critical point, the core is split into two nodes '0' and '1', the subcritical and supercritical part, as can be seen on the right-hand side of figure 2.1. These models will be referred to as the Low Heating Model (LHM) and High Heating Model (HHM) respectively. Note that the border between 0 and 1, just as their relative lengths, shift with the moment that the water becomes supercritical.

The core channel has a constant flow area and a riser with the same area is placed on top of it. After the core, the water will enter the riser by natural convection, thanks to the difference in density between the cold and hot water. In the buffer, the water loses energy like it would in a turbine or heat exchanger. Since the riser and downcomer are assumed to be perfectly insulated, the buffer is the only part where heat is exchanged with surroundings of the system. The energy exchanged at the buffer is denoted by 'q' in the figure. After this, the coolant has cooled down to the specific inlet temperature. The subcritical water will enter the core again after passing a downcomer, with the same geometrical parameters as the core and the riser combined.

In 2014, Lippens[15] enhanced the original single loop model of Krijger with the thermal inertia effects of the core wall (denoted by w, w_0 and w_1 in the loop structure). One year later, the model was augmented further by including the neutronic thermal-hydraulic coupling (denoted by F in the figure).

Figure 2.2 is showing the geometry of the core channel. The cladding surrounding the fuel is referred to as the channel wall. The model represents each part of the loop as a node, assuming there are no additional position dependencies apart from the presence of the coolant in a particular section. The state variables per section can be time-dependent, but are never dependent on the axial or radial position within a section. This is a clear simplification, as in reality the fuel's heat generation and the coolant's enthalpy would be position-dependent. The nodes indicating the fuel and core wall only interact with heat exchange to the coolant, but do not affect the flow of the coolant directly.

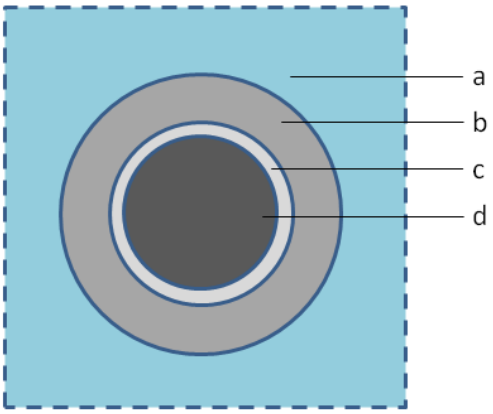

Figure 2.2: Top-down view of the channel geometry. The coolant (*a*) flows around the fuel rod (*b*, *c* and *d*). *b* is the channel wall – the cladding surrounding the fuel. The thin layer of gas (*c*) present in fuel rods is neglected in this research. The fuel itself is labeled *d*. Not to scale. [35]

2.2. Water properties

As water properties change significantly throughout the loop, density, temperature and thermal conductivity are approximated for both the subcritical and supercritical region. One of the main assumptions in the model is the equation of state. If the pressure is kept constant within the reactor, the density of water can be supposed to be only dependent on the section's specific enthalpy. Although in reality the pressure would undergo gravitational and frictional pressure drops, the pressure is assumed to be constant throughout the system. This principle was found to hold for multiple cooling fluids by Ambrosini and Sharabi [26]. In our model, a linear two-region approximation was used to give the dependency of the density on the waters enthalpy, intersecting at the pseudo-critical point of water [13]. In literature, approximating the density of supercritical water by a two-state equation was already done by Zuber in 1966 [36], and more recently linear approximations are regularly made at supercritical conditions, as the three-state approximation was done by Swapnalee and Vijayan in 2012 [28]. The gradients of the linear functions are $C_1 = -4.7877 \cdot 10^{-4} kg^2 m^{-3} J^{-1}$ and $C_2 = 0.80 \cdot 10^{-8} m^3 J^{-1}$ respectively.

$$v_i = \begin{cases} \frac{1}{\rho_{pc} + C_1(H_i - h_{pc})} & (H_i < h_{pc}) \\ v_{pc} + C_2(H_i - h_{pc}) & (H_i \geq h_{pc}) \end{cases} \tag{2.1}$$

Additionally, the temperature was approximated from the enthalpy using quadratic functions in both regions, as they can be linearized quite easily. Both the approximation and its slope are continuous around the pseudo-critical point. This led to the following equation with coefficients $\alpha_0 = -1.1 \cdot 10^{-10} KJ^{-1}$ and $\alpha_1 = 1.0 \cdot 10^{-10} KJ^{-1}$ [15].

$$T_i = \alpha_i (H_i - h_{pc})^2 + \frac{1}{c_{p,pc}} (H_i - h_{pc}) + T_{pc} \tag{2.2}$$

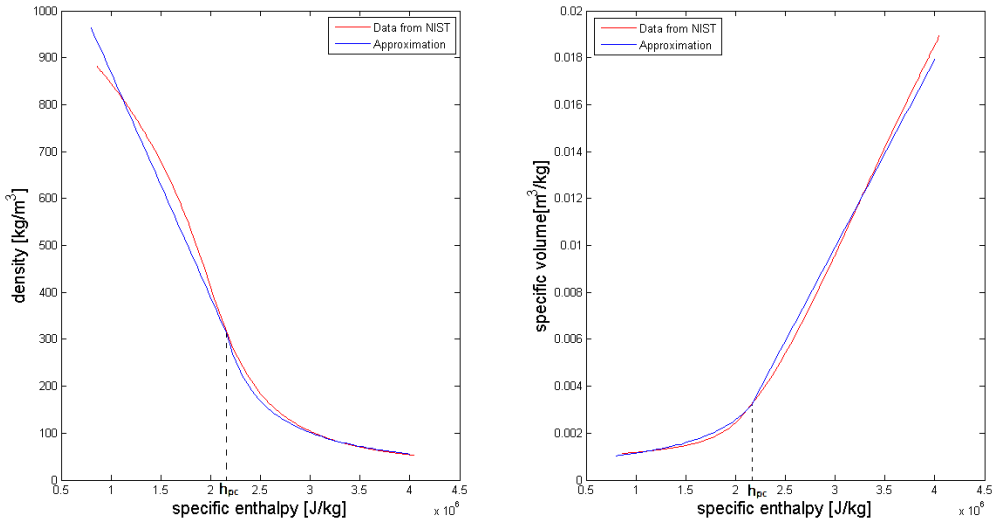

Figure 2.3: Approximation of density (left) and specific volume (right). [13] The red line represents data from NIST. [19]

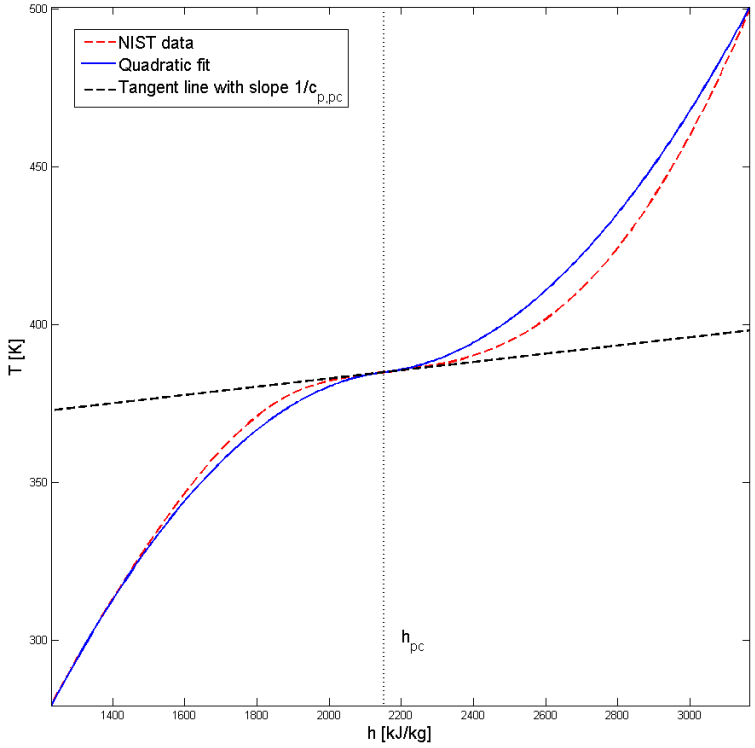

Figure 2.4: Approximation of temperature. The red dotted line represents data from NIST [19]. Figure adapted from Lippens [15].

Lastly also the thermal conductivity was approximated, with a linear function in the low enthalpy region and an exponential function in the high enthalpy region. Again, both the approximation and its slope are continuous around the pseudo-critical point [15].

$$\lambda_f = \begin{cases} -\beta_0 H_0 + \lambda_{f,b,0} & (H_i < h_{pc}) \\ \lambda_z e^{-\beta_1 H_1} + \lambda_{f,b,1} & (H_i \geq h_{pc}) \end{cases} \tag{2.3}$$

This equation uses the following values for the constants, as determined by Lippens:

$$\beta_0 = -3.2711 \cdot 10^{-7} Wm^{-1}K^{-1}J^{-1}kg \qquad \beta_1 = 1.3694 \cdot 10^{-6} kgJ^{-1}$$
$$\lambda_{f,b,0} = 1.0133 Wm^{-1}K^{-1} \qquad \lambda_{f,b,1} = 7.0154 \cdot 10^{-2} Wm^{-1}K^{-1} \qquad \lambda_z = 4.5553 Wm^{-1}K^{-1}$$

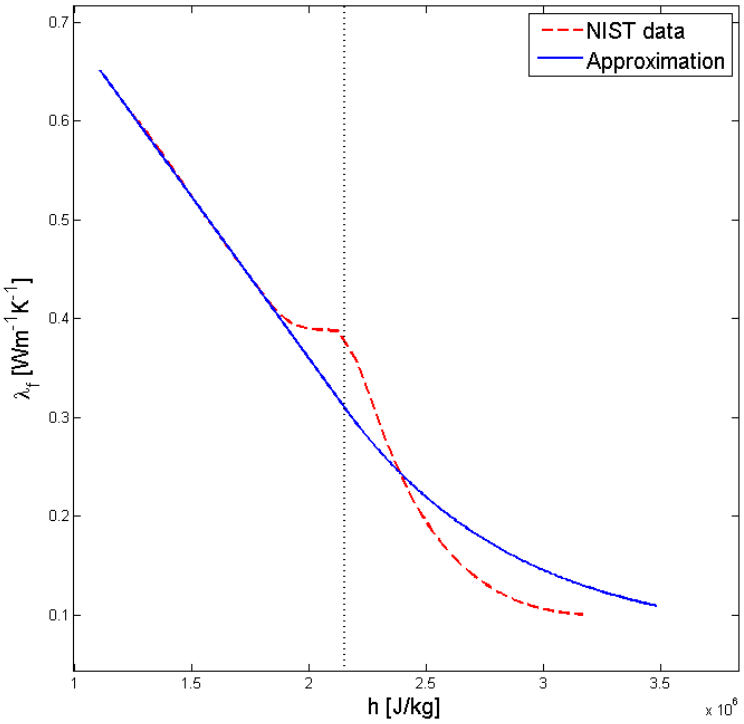

Figure 2.5: Approximation of thermal conductivity. The red dotted line represents data from NIST [19]. Figure adopted from Lippens [15].

2.3. Conservation balances

After defining these water properties, transport balances are set up for mass, energy and momentum for every node in the system. The set of balances was then reduced, by leaving out constant variables and redundant balance equations for several nodes in the loop.

As the balances have been derived by Krijger, Lippens and Zonneveld before, they are included in B. However, as this research also involved the momentum balance, this balance will be used as an example. Please note that there is one difference in the momentum balance with respect to all other energy and mass balances: the momentum balance is the integral of the pressure drops due to gravity, friction and acceleration over the entire loop, whereas all the other balances are set up for the quantities going in and out of one particular node.

The equations below show the momentum balances for the low heating model and high heating model respectively.

$$\underline{\text{I}_{\text{LHM}}}: \quad AL\frac{\mathrm{d}}{\mathrm{d}t}W_0 + AL_R\frac{\mathrm{d}}{\mathrm{d}t}W_R + \frac{\mathrm{d}}{\mathrm{d}t}V_B W_0 + AL_D\frac{\mathrm{d}}{\mathrm{d}t}W_0 = \cdots$$
$$\cdots - \left(\frac{f_0 L}{D_H} + K_0\right)\frac{W_0^2}{2\rho_0} - \left(\frac{f_R L_R}{D_H} + K_R\right)\frac{W_R^2}{2\rho_R}\cdots$$
$$\cdots - \left(\frac{f_D L_D}{D_H} + K_D\right)\frac{W_0^2}{2\rho_{in}} - A^2 g\rho_0 L - A^2 g\rho_R L_R - A^2 g\rho_{in} L_D \tag{2.4}$$

$$\underline{\text{I}_{\text{HHM}}}: \quad A\frac{\mathrm{d}}{\mathrm{d}t}W_0 L_0 + A\frac{\mathrm{d}}{\mathrm{d}t}W_1 L_1 + AL_R\frac{\mathrm{d}}{\mathrm{d}t}W_R + \frac{\mathrm{d}}{\mathrm{d}t}V_B W_0 + AL_D\frac{\mathrm{d}}{\mathrm{d}t}W_0 = \cdots$$
$$\cdots - \left(\frac{f_0 L_0}{D_H} + K_0\right)\frac{W_0^2}{2\rho_0} - \left(\frac{f_1 L_1}{D_H} + K_1\right)\frac{W_1^2}{2\rho_1} - \left(\frac{f_R L_R}{D_H} + K_R\right)\frac{W_R^2}{2\rho_R}\cdots$$
$$\cdots - \left(\frac{f_D L_D}{D_H} + K_D\right)\frac{W_0^2}{2\rho_{in}} - A^2 g\rho_0 L_0 - A^2 g\rho_1 L_1 \cdots$$
$$\cdots - A^2 g\rho_R L_R - A^2 g\rho_{in} L_D \tag{2.5}$$

In these equations, one can clearly see the terms related to friction (involving the Darcy friction factor f and friction coefficients K_i. Gravitational terms are the ones containing the gravitational acceleration constant g. The High Heating Model is dependent on more variables, as the lengths of L_0 and L_1 change with operating conditions, always summing up to the total length of the core node.

For the steady state momentum balance the steady state mass flow rate $\bar{W}$ can be calculated. In steady state the gravity drives circulation and the friction limits the flow, so the pressure drop related to gravity and friction within the loop have to be equal. The equation for $\bar{W}$ for the low heating model and a similar equation used for the calculation of $\bar{W}$ in the HHM are shown below.

$$\bar{W}_{LHM}^2 = gA^2\frac{\rho_{in}L_D - \bar{\rho}_0 L - \bar{\rho}_R L_R}{\frac{1}{2}(\frac{f_0 L}{D_{H,0}} + K_0)\frac{1}{\bar{\rho}_0} + \frac{1}{2}(\frac{f_D L_D}{D_{H,D}} + K_D)\frac{1}{\bar{\rho}_i n} + \frac{1}{2}(\frac{f_R L_R}{D_{H,R}} + K_R)\frac{1}{\bar{\rho}_0}} \tag{2.6}$$

$$\bar{W}_{HHM}^2 = gA^2\frac{\rho_{in}L_D - \bar{\rho}_0\bar{L}_0 - \bar{\rho}_1(\bar{L}_1 + L_R)}{\frac{1}{2}(\frac{f_0 L}{D_{H,1}} + K_0)\frac{1}{\bar{\rho}_0} + \frac{1}{2}(\frac{f_D L_D}{D_{H,D}} + K_D)\frac{1}{\bar{\rho}_i n} + \frac{1}{2}(\frac{f_R L_R}{D_{H,R}} + K_R + \frac{f_1 L_1}{D_{H,1}} + K_1)\frac{1}{\bar{\rho}_1}} \tag{2.7}$$

2.4. Dimensionless balances

Variables in the equations are made dimensionless, to make comparisons with literature easier. The two tables below show how all variables are made dimensionless.

Table 2.1: Dimensionless variables adopted from Krijger (left column) and Lippens (right column).

$\underline{\overline{L_i}} = \frac{\overline{L_i}}{L}$	Length, steady state	$\underline{T_i} = \left(\frac{\lambda_{f,pc}L}{Q}\right)T_i$	Temperature
$\underline{\check{l}_i} = \frac{\check{l}_i}{L}$	Length, perturbation	$\underline{\check{\theta}_i} = \left(\frac{\lambda_{f,pc}L}{Q}\right)\check{\theta}_i$	Temperature, perturbation
$\underline{t} = \frac{t\overline{W}v_{pc}}{AL}$	Time	$\underline{\alpha_i}\left(\frac{Q\lambda_{f,pc}L}{Q}\right)\alpha_i$	Quadratic temperature approximation coefficient
$\underline{\overline{W_i}} = \frac{\overline{W_i}}{\overline{W}} = 1$	Mass flow, steady state	$\underline{c_{p,i}} = \frac{\overline{W}c_{p,i}}{\lambda_{f,pc}L}$	Specific heat capacity
$\underline{\check{w}_i} = \frac{\check{w}_i}{\overline{W}}$	Mass flow, perturbation	$\underline{P_{in}} = \frac{P_{in}}{L}$	Contact perimeter between channel and wall
$\underline{\overline{H_i}} = \frac{\overline{H_i}\,\overline{W}}{Q}$	Specific enthalpy, steady state	$\underline{\lambda_w} = \frac{\lambda_w A}{\lambda_{f,pc}L^2}$	Wall thermal conductivity

Table 2.1: (continued)

$\underline{\check{h}_i} = \frac{\check{h}_i \overline{W}}{Q}$	Specific enthalpy, perturbation	$\underline{A_w} = \frac{A_w}{A}$	Wall cross-sectional area
$\underline{\overline{\rho}_i} = \overline{\rho}_i \upsilon_{pc}$	Density, steady state	$\underline{\lambda_f} = \frac{\lambda_f}{\lambda_{f,pc}}$	Coolant fluid thermal conductivity
$\underline{\check{\rho}_i} = \check{\rho}_i \upsilon_{pc}$	Density, perturbation	$\underline{\beta_0} = \frac{\beta_0 Q}{\lambda_{f,pc} \overline{W}}$	Coolant thermal conductivity linear approximation coefficient
$\underline{D_H} = \frac{D_H}{L}$	Hydraulic diameter	$\underline{\beta_1} = \beta_1 \frac{Q}{\overline{W}}$	Coolant thermal conductivity exponential approximation coefficient
$\underline{\overline{V}_B} = \frac{\overline{V}_B}{AL}$	Buffer volume, steady state	$\underline{\widehat{Nu_0}} = \frac{\widehat{Nu_0}}{\lambda_{f,pc}^{0.66}}$	Adjusted Nusselt number

Table 2.2: Dimensionless variables adopted from Zonneveld.

$\underline{\overline{n}} = \overline{n} AL$	Neutron concentration, steady state	$\underline{\overline{C}_i} = \overline{C}_i AL$	Precursor concentration, steady state
$\underline{\check{n}} = \check{n} AL$	Neutron concentration, perturbation	$\underline{\check{C}_i} = \check{C}_i AL$	Precursor concentration, perturbation
$\underline{\overline{Q}_w} = \frac{\overline{Q}_w}{Q}$	Channel wall heat flux, steady state	$\underline{\lambda_i} = \lambda_i \frac{AL}{\overline{W} \upsilon_{pc}}$	Decay constant
$\underline{\check{q}_w} = \frac{\check{q}_w}{Q}$	Channel wall heat flux, perturbation	$\underline{\Lambda} = \Lambda \frac{\overline{W} \upsilon_{pc}}{AL}$	Neutron generation time
$\underline{\alpha_r} = \alpha_r \rho_{pc}$	Density reactivity feedback coefficient	$\underline{\Sigma_f} = \Sigma_f L$	Macroscopic neutron cross section
$\underline{\upsilon_n} = \upsilon_n \frac{AL^2}{\overline{W} \upsilon_{pc}}$	Neutron velocity	$\underline{E_f} = E_f \frac{\upsilon_{pc}}{AL h_{pc}}$	Energy released per fission event
$\underline{\tau} = \tau \frac{\overline{W} \upsilon_{pc}}{AL}$	Fuel heat transfer time constant	$\underline{V_f} = \frac{V_f}{AL}$	Fuel volume

The dimensionless variables reduce the momentum balances to the following dimensionless balances:

$$
\begin{aligned}
\underline{\mathrm{I_{LHM}}}: \quad & \frac{\mathrm{d}}{\mathrm{d}\underline{t}}\underline{W_0} + \underline{L_R}\frac{\mathrm{d}}{\mathrm{d}\underline{t}}\underline{W_R} + \underline{V_B}\frac{\mathrm{d}}{\mathrm{d}\underline{t}}\underline{W_0} + \underline{L_D}\frac{\mathrm{d}}{\mathrm{d}\underline{t}}\underline{W_0} = \\
& -\underline{W_0}\frac{\underline{W_R} - \underline{W_0}}{\underline{\rho_{in}}} - \left(\frac{f_0}{\underline{D_H}} + K_0\right)\frac{\underline{W_0^2}}{2\underline{\rho_0}} - \left(\frac{f_R\underline{L_R}}{\underline{D_H}} + K_R\right)\frac{\underline{W_R^2}}{2\underline{\rho_R}} \cdots \\
& \cdots - \left(\frac{f_D\underline{L_D}}{\underline{D_H}} + K_D\right)\frac{\underline{W_0^2}}{2\underline{\rho_{in}}} - \frac{\underline{\rho_0 L_0}}{N_{Fr}} - \frac{\underline{\rho_R L_R}}{N_{Fr}} + \frac{\underline{\rho_{in} L_D}}{N_{Fr}}
\end{aligned} \tag{2.8}
$$

$$
\begin{aligned}
\underline{\mathrm{I_{HHM}}}: \quad & -\underline{W_0}\frac{\mathrm{d}}{\mathrm{d}\underline{t}}\underline{L_1} + (1-\underline{L_1})\frac{\mathrm{d}}{\mathrm{d}\underline{t}}\underline{W_0} + \frac{\mathrm{d}}{\mathrm{d}\underline{t}}\underline{W_1 L_1} + \underline{L_R}\frac{\mathrm{d}}{\mathrm{d}\underline{t}}\underline{W_R} + \underline{V_B}\frac{\mathrm{d}}{\mathrm{d}\underline{t}}\underline{W_0} + \underline{L_D}\frac{\mathrm{d}}{\mathrm{d}\underline{t}}\underline{W_0} = \cdots \\
& -\underline{W_0}\frac{\underline{W_R} - \underline{W_0}}{\underline{\rho_{in}}} - \left(\frac{f_0\underline{L_0}}{\underline{D_H}} + K_0\right)\frac{\underline{W_0^2}}{2\underline{\rho_0}} - \left(\frac{f_1\underline{L_1}}{\underline{D_H}} + K_1\right)\frac{\underline{W_1^2}}{2\underline{\rho_1}} \cdots \\
& \cdots - \left(\frac{f_R\underline{L_R}}{\underline{D_H}} + K_R\right)\frac{\underline{W_R^2}}{2\underline{\rho_R}} - \left(\frac{f_D\underline{L_D}}{\underline{D_H}} + K_D\right)\frac{\underline{W_0^2}}{2\underline{\rho_{in}}} \cdots \\
& \cdots - \frac{\underline{\rho_0 L_0}}{N_{Fr}} - \frac{\underline{\rho_1 L_1}}{N_{Fr}} - \frac{\underline{\rho_R L_R}}{N_{Fr}} + \frac{\underline{\rho_{in} L_D}}{N_{Fr}}
\end{aligned} \tag{2.9}
$$

Apart from inserting the dimensionless variables, also the gravitational terms have been adapted by inserting the Froude number, which is defined as the ratio between flow inertia of the coolant and the gravitational force. As the steady state mass flow is already calculated, it can be substituted in the Froude number.

$$
N_{Fr} = \frac{\bar{W}^2 v_{pc}^2}{gLA^2} \tag{2.10}
$$

2.5. Linearized balances

Eventually the model is solved using linear methods. The model equations must thus be linearised, in order to use linear solving techniques. All time-dependent variables are split into a steady state value and a perturbed part, being a small fluctuation from the steady state value:

$$
X = \overline{X} + \check{x} \tag{2.11}
$$

Taylor expansions are used for water properties and all dimensionless variables. The assumption that perturbations are small allows us to neglect second order terms. As products of perturbations with each other or with time derivatives of other perturbations are discarded, only linear terms are left. As long as perturbation stay small compared to their steady state variables, this simplification does not drastically affect the accuracy of the model. After all, the products of perturbations will be even smaller.

The following is an example of this linearisation process:

$$
\begin{aligned}
XY &= \left(\overline{X} + \check{x}\right)\left(\overline{Y} + \check{y}\right) \\
&= \overline{XY} + \overline{X}\check{y} + \overline{Y}\check{x} + \check{x}\check{y} \\
&\approx \overline{XY} + \overline{X}\check{y} + \overline{Y}\check{x}
\end{aligned} \tag{2.12}
$$

Finally, the steady-state solutions $\overline{XY}$ are subtracted from both sides of the equations, leaving a system of n first-order linear differential equations with n unknown variables. By doing so, the solution is investigated around its steady state. After linearisation, the low heating model is left with 13 linearised equations and 13 unknown perturbed variables. The high heating model consists of 16 linearised equations and 16 unknown perturbed variables.

To show how linearisation affects the dimensionless equations, the momentum balances are again given below:

$$
\begin{aligned}
\underline{\mathrm{I_{LHM}}}: \quad & (1+\underline{L_D}+\underline{V_B})\frac{\mathrm{d}}{\mathrm{d}\underline{t}}\underline{\breve{w}_0}+\underline{L_R}\frac{\mathrm{d}}{\mathrm{d}\underline{t}}\underline{\breve{w}_R}=-\left(\left(\frac{f_R\underline{L_R}}{\underline{D_H}}+K_R\right)\underline{\overline{v_R}}+\underline{v_{in}}\right)\underline{\breve{w}_R}\cdots \\
& \cdots+\frac{1}{2}C_1N_{\Delta h}h_{pc}v_{pc}\left(\frac{1}{2}\left(\frac{f_0}{\underline{D_H}}+K_0\right)\frac{1}{\underline{\overline{\rho}_0^2}}-\frac{1}{N_{Fr}}\right)\underline{\breve{h}_{out}}\cdots \\
& \cdots+C_1N_{\Delta h}h_{pc}v_{pc}\left(\frac{1}{2}\left(\frac{f_R\underline{L_R}}{\underline{D_H}}+K_R\right)\frac{1}{\underline{\overline{\rho}_R^2}}-\frac{\underline{L_R}}{N_{Fr}}\right)\underline{\breve{h}_R}\cdots \\
& \cdots\left(\underline{v_{in}}-\left(\frac{f_0}{\underline{D_H}}+K_0\right)\underline{\overline{v}_0}-\left(\frac{f_D\underline{L_D}}{\underline{D_H}}+K_D\right)\underline{v_{in}}\right)\underline{\breve{w}_0} \qquad (2.13) \\
\underline{\mathrm{I_{HHM}}}: \quad & (1+\underline{\overline{L}_1}+\underline{L_D}+\underline{V_B})\frac{\mathrm{d}}{\mathrm{d}\underline{t}}\underline{\breve{w}_0}+\underline{L_1}\frac{\mathrm{d}}{\mathrm{d}\underline{t}}\underline{\breve{w}_1}+\underline{L_R}\frac{\mathrm{d}}{\mathrm{d}\underline{t}}\underline{\breve{w}_R}= \\
& \left(\frac{1}{2}\left(\frac{f_0\underline{v_0}}{\underline{D_H}}-\frac{f_1\underline{\overline{v}_1}}{\underline{D_H}}\right)+\frac{1}{N_{Fr}\underline{v_0}}-\frac{1}{N_{Fr}\underline{\overline{v}_1}}\right)\underline{\breve{l}_1}\cdots \\
& \cdots-\left(\left(\frac{f_0\underline{\overline{L}_0}}{\underline{D_H}}+K_0\right)\underline{\overline{v}_0}+\left(\frac{f_D\underline{\overline{L}_D}}{\underline{D_H}}+K_D\right)\underline{\overline{v_{in}}}-\underline{v_{in}}\right)\underline{\breve{w}_0}\cdots \\
& \cdots-\left(\frac{f_1\underline{\overline{L}_1}}{\underline{D_H}}+K_1\right)\underline{\overline{v}_1\breve{w}_1}+\left(-\frac{1}{2}\left(\frac{f_1\underline{\overline{L}_1}}{\underline{D_H}}+K_1\right)\cdots\right. \\
& \left.\cdots+\frac{\underline{\overline{L}_1}}{N_{Fr}\underline{\overline{v}_R^2}}\right)\frac{C_1N_{\Delta h}h_{pc}}{vpc}\underline{\breve{h}_1}\cdots \\
& \cdots-\left(\frac{f_R\underline{\overline{L}_R}}{\underline{D_H}}+K_R+\frac{v_{in}}{\underline{\overline{v}_R}}\right)\underline{\overline{v}_R\breve{w}_R}+\left(-\frac{1}{2}\left(\frac{f_R\underline{\overline{L}_R}}{\underline{D_H}}+K_R\right)\cdots\right. \\
& \left.\cdots+\frac{\underline{\overline{L}_R}}{N_{Fr}\underline{\overline{v}_R^2}}\right)\frac{C_1N_{\Delta h}h_{pc}}{vpc}\underline{\breve{h}_R} \qquad (2.14)
\end{aligned}
$$

Apart from the linearisation, the steady state mass flow is now expressed in dimensionless number $N_{\Delta h}$, which will be explained in more detail in chapter 3.

3

Method of Stability Investigation

3.1. Solving the matrix equation

The linearised balances left in section 2.5 form a matrix equation according to equation 3.1. In this equation, A is a coefficient matrix that concerns all time-derivatives of perturbed variables, whereas B is a coefficient matrix for the variables. The sets of matrices for both the LHM and the HHM are shown in appendix A.

$$A\frac{\mathrm{d}}{\mathrm{d}t}\vec{x} = B\vec{x} \tag{3.1}$$

If the coefficient matrices A and B are filled in for certain operating values, the loop model is reduced to one matrix equation. The matrix equation has solutions of the form $\vec{x} = \vec{v}e^{\lambda t}$, in which the vector $\vec{v}$ contains the amplitude and phase shift of the initial perturbation. Filling in the solution for $\vec{x}$, results in $A\lambda v e^{\lambda t} = B v e^{\lambda t}$. Dividing the equation by $e^{\lambda t}$, the following generalised eigenvalue problem is left.

$$A\lambda\vec{v} = B\vec{v} \tag{3.2}$$

The eigenvalues and eigenvectors can be found by calculating lambda for $det[B - A\lambda] = 0$. According to Koren [12] the eigenvalues λ and eigenvectors $\vec{v}$ can be decomposed in the following way:

$$\lambda = a + ib \text{ where } a = Re\{\lambda\} \text{ and } b = Im\{\lambda\} \tag{3.3}$$

$$v_k = \alpha_k e^{i\beta_k} \text{ where } \alpha_k = |v_k| \text{ and } \beta_k = \angle v_k \tag{3.4}$$

In equation 3.4, a complex eigenvector $\vec{v}$ is split into its magnitude and corresponding angle in the complex plane. The magnitude of eigenvector will later define the initial amplitude of a perturbation, whereas the angle will determine its phase shift.

3.1.1. Interpretation of the solution

Calculating $det(B - A\lambda) = 0$ can result in a λ with both real and imaginary parts. If for one of the eigenvalues $Re(\lambda) > 0$, this corresponds to an unstable solution, because the decay ratio of the corresponding oscillation will be larger than one. Even if only one eigenvalue has a real part that is larger than zero, eventually the system would diverge in the time-dependent solution. If each λ of $\vec{x}$ is negative, the loop is considered stable under this operating condition, since then $e^{\lambda t}$ will never become larger than 1.

Imaginary eigenvalues always come with their conjugate counterparts, as in the solution of a characteristic polynomial there will be another eigenvalue with the same real part but an opposite imaginary sign. Single imaginary values would otherwise lead to exponential development of a perturbation in the imaginary

plane, which has no physical meaning. Two conjugate eigenvalues form a sinusoid accord to this formulation:

$$\alpha_k e^{at}(e^{i(\beta_k+bt))} + e^{-i(\beta_k+bt))}) = 2\alpha_k e^{at} cos(\beta_k + bt) \tag{3.5}$$

With the imaginary part of λ the frequency of a the perturbed oscillation can be investigated. By knowing $Im(\lambda)$ we know the frequency of the oscillation caused by a perturbation.

3.1.2. Time-dependent solution

Since the model was always meant to evaluate the stability only, the time-dependent solution was not needed before. In order to look at the development of perturbed variables as a function of time, the expression for a perturbed variable in time had to be known. The eigenvalue determines the frequency and decay ratio of a perturbed variable, whereas the eigenvector stands for the initial phase shift and magnitude, thus being both essential for determining the value of a perturbed variable at a certain moment. Given the eigenvalues and eigenvectors, the time-dependent vector of perturbed variables $\vec{x}$ can now be calculated as following:

$$\vec{x} = \sum_{j=1}^{n} c_j \cdot \vec{v}_j \cdot e^{\lambda_j t} \tag{3.6}$$

In this equation, c_j are constants, $\vec{v}_j$ are eigenvectors, and λ_j are eigenvalues. In the eigenvector decomposition of equation 3.4 this would be denoted as following for each perturbed variable x_k [12]:

$$x_k = \sum_{j=1}^{n} c_j \alpha_{k,j} e^{a_j t} e^{i(\beta_{k,j}+b_j t)} \tag{3.7}$$

In this equation, the constants c_j are depending on the initial conditions $x_{k,0}$ at $t = 0$. For $t = 0$, the equation for a perturbed variable reduces to $x_{k,0} = \sum_{j=1}^{n} c_j \alpha_{k,j}$. As there are just as many unknown constants as the number of equations and initial perturbation values, all constants can be determined.

The initial values $\vec{x}_0$ correspond to the disturbance in variables at $t = 0$. By setting the initial value of each perturbed variable to 0, thus making $\vec{x}_0$ a zero-vector, one reduces all time-dependent values of the variables to zero. This will be the trivial solution in which perturbations do not take place. If $\vec{x}_0$ is set to zero except for the first value, as shown in equation 3.8, this means only perturbed value x_1 is disturbed at $t = 0$.

$$\vec{x}_0 = \begin{bmatrix} c_1\alpha_{1,1} + c_2\alpha_{1,2} + \cdots \\ c_1\alpha_{2,1} + c_2\alpha_{2,2} + \cdots \\ c_1\alpha_{3,1} + c_2\alpha_{3,2} + \cdots \\ \vdots \end{bmatrix} = \begin{bmatrix} 1 \\ 0 \\ 0 \\ \vdots \end{bmatrix} \tag{3.8}$$

If the matrix equation 3.8 is solved, values for c_j are found, and the full expression for equation 3.7 is known for each perturbed variable x_k. The initial conditions turned out not to change the stability behaviour of the loop at a certain operating condition, only the amplitudes of perturbed variables. The decay ratios for a perturbed variable stayed unchanged as the initial conditions were varied.

3.2. Defining the operating conditions

To evaluate the stability characteristics of the system at every possible set of operating conditions, a convenient choice was made in how to define these conditions. Throughout literature, many dimensionless numbers are used as measures for the heating power, inlet temperature and mean flow rate, the three main operating conditions. As we are looking at a system driven by natural convection, the flow rate and heating power are directly related.

Although many different dimensionless numbers are adopted throughout literature, most of them differ by a factor only. Krijger chose to use slightly modified versions of the dimensionless numbers used by T'Joen and Rohde [30], which Lippens and Zonneveld adopted for their analysis. The same measures are used in this research as well.

The pseudo phase change number is a measure for the power in the core, made dimensionless as shown in equation 3.9. By the division shown, $N_{\Delta h}$ becomes a measure for the change in enthalpy that occurs in the reactor core. The pseudo phase change number operates in the positive spectrum only, for the core power is always positive, resulting in a positive steady state mass flow.

$$N_{\Delta h} \equiv \frac{Q}{\overline{W} h_{pc}} \tag{3.9}$$

The subcooling number N_{sub} is a measure for the inlet enthalpy, and thus the inlet temperature of the coolant. The subcooling number only operates in the range between 0 and 1 in this model. The inlet enthalpy cannot be negative and therefore the upper limit of N_{sub} is 1. Moreover, the inlet enthalpy is expected to be lower than the pseudo-critical enthalpy, so the lower limit of N_{sub} is 0. This assumption is made as the water would be supercritical throughout the entire loop if N_{sub} is negative. According to our model, the coolant can only become supercritical in the core section, and it will always be subcritical after the buffer, due to the local heat exchange.

$$N_{sub} \equiv 1 - \frac{H_{in}}{h_{pc}} \tag{3.10}$$

The border between the low heating model and the high heating model is defined by $N_{sub} = N_{\Delta h}$. At these operating conditions, $\frac{Q}{\overline{W}} = h_{pc} - h_{in}$, so the coolant is precisely heated to the pseudo-critical temperature (shown in table 1.1) at the end of the core. If $N_{sub} \geq N_{\Delta h}$, the water does not reach supercritical state, so the low heating model applies. The high heating model applies for $N_{sub} < N_{\Delta h}$. Knowing the eigenvalues after solving the eigenvalue problem, a stability map can be plotted with N_{sub} on the vertical axis and $N_{\Delta h}$ on the horizontal axis like in figure 1.10.

4

Computational implementation

The previous chapters provided a theoretical introduction and mathematical foundation for the code used in this research. In this chapter, the Matlab algorithm and the steps to create a stability map are discussed. After this, three additional methods for stability investigation used in the model are introduced.

4.1. Considerations

The main goal for the code has been to be robust, clearly structured and flexible for different parameters and resolutions. The emphasis during coding has always been on readability and not on the computational speed [13]. This choice was made since the calculations are relatively fast and the main goal of this model is to give qualitative information rather than quantitative HPLWR data. At low resolution in N_{sub} and $N_{\Delta h}$, instability maps can be calculated within minutes. As the code has been enhanced with new implementations throughout the last years, the model tends to get more complex and calculation times of MATLAB keep increasing. At high resolutions the calculations may take several hours.

4.2. MATLAB algorithm

Figure 4.1 shows the basic algorithm structure used in MATLAB. After defining several loop parameters and both the range and resolution for the operating conditions (N_{sub} and $N_{\Delta h}$), two FOR loops are assigned to calculate the stability for each unique operating condition.

All variables independent of operating conditions are defined at the beginning of the code, before the two FOR loops of N_{sub} and $N_{\Delta h}$. The steady state solutions needed for filling in the matrices are calculated within the second FOR loop, as they depend on both dimensionless numbers. For the high heating model, the steady state solutions for L_1 and H_1 are calculated by substitution of N_{sub} and $N_{\Delta h}$ in their equations. Using the linear approximations for water properties, the other steady state variables can be defined. The steady-state mass flow rate and the dimensionless Reynolds number are dependent on each other, so they are calculated by an iterative process, using a WHILE loop until the value between the mass flow of two consecutive is less than a set reference value without exceeding the iteration limit set at 1000 iterations. For high resolution calculation, the reference value is set at 10^{-12} while for lower resolutions 10^{-9} is sufficient. After this, wall temperatures, and dimensionless numbers like the Nusselt number and Froude number can be calculated.

The coefficient matrices A and B are filled with values from the balance equations in appendix B. After the coefficient matrices A and B are set up, the stability is investigated by calculating the corresponding eigenvalues. By letting MATLAB do the maths, a matrix is built filled with ones and zeros. Each '1' represents a stable point, whereas a '0' represents an unstable point. A stability map can be created with N_{sub} on the vertical axis and $N_{\Delta h}$ on the horizontal axis. The stable zones are shown in blue and the unstable zones are shown in red.

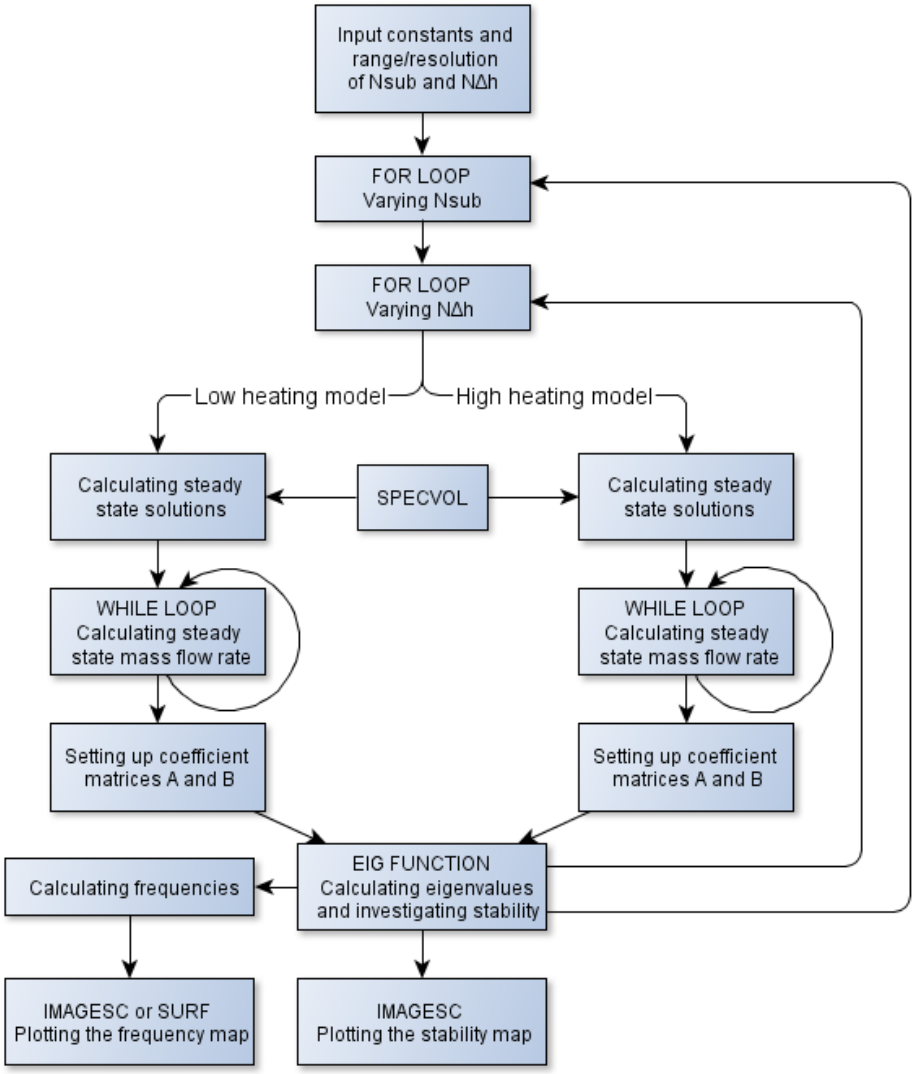

Figure 4.1: Flow chart of the general structure of the algorithm used to generate stability maps. [13]

4.2.1. Filtering of eigenvalues

If all values of coefficient matrices A and B are filled in corresponding to appendix A, the eigenvalue problem can be solved. A generalized eigenvalue problem can be solved by MATLAB's function 'eig'. If matrix A is singular, which is the case, QZ factorization is needed to solve the determinant $det(B - A\lambda) = 0$. MATLAB uses QZ factorization in its 'eig' function [13].

"[V,D] = eig(B,A);" Is executed with A and B as coefficient matrices for the perturbed variable equations. This MATLAB function produces a diagonal matrix D of generalized eigenvalues and a full matrix V whose columns are the corresponding eigenvectors such that $A \cdot V \cdot D = B \cdot V$ applies.

Whereas a regular eigenvalue problem has as many eigenvalues as the dimension of its square coefficient matrices, a generalised eigenvalue problem can have less eigenvalues. The algebraic multiplicity of an eigenvalue is equal to the highest order of a characteristic polynomial as a solution of the determinant. If the sum of all eigenvalue algebraic multiplicities is less than the dimension of its square matrix, MATLAB returns $\lambda = \infty$ for the non-existing eigenvalues. A simple example of MATLAB returning these eigenvalues is shown by Koren [12]. The number of infinite eigenvalues is equal to the size of the matrix minus the degree of a determinant [13].

Until now, the infinite values have not been taken into account in the stability investigation, as Krijger concluded they would correspond to similar other eigenvalues in the solution. If we know that these eigenvalues are equivalent to other eigenvalues, then the infinite values can be disregarded, because for the general solu-

tion and stability problem we only need to know if one of the eigenvalues is positive. Therefore in determining unstable regions, eigenvalues with $\lambda > 10^{12}$ have been set to $\lambda = 0$ and thus have been neglected.

As the infinite eigenvalues have no physical meaning whilst determining the time-dependent solution either, the eigenvalues with $\lambda > 10^{12}$ have been set to $\lambda = 0$ in this research once again. Hereby it was assured that the time-dependent behaviour of perturbed variables was not influenced by the non-existent eigenvalues.

Apart from infinite values, MATLAB may also return extremely small real parts of eigenvalues, due to rounding errors in calculations. If $\lambda < 10^{-12}$, they are set to $\lambda = 0$. After filtering out these eigenvalues, the remaining eigenvalues are analysed for instability analysis.

4.3. Additional analyses

4.3.1. Frequency analysis

After stable and unstable regions have been defined and plotted in a stability map, the frequency of operational points in the unstable area can be investigated. Knowing a frequency, one could make predictions regarding the nature of an instability. As a lot is known about the common frequencies of certain types of instabilities in a BWR, for instance the frequencies of type I and type II DWO, we can predict that similar frequencies will occur in our supercritical water loop model and, eventually, an HPLWR. For the determination of the frequencies only the imaginary parts belonging to the eigenvalues with the largest real parts are taken into account, as they are most dominant. These values can be displayed on the dimensionless stability maps, using a color legend to show their respective frequencies. By showing these frequencies per location, the relative differences between unstable regions and zero-frequency unstable zones can be clearly seen.

4.3.2. Parametric studies

Krijger implemented a feature in the code to investigate the influence of any parameter of choice on the system. To find the neutral stability boundary, every element of a stability map that neighbours an unstable 'pixel' will be located. The neutral stability boundaries for the investigated values of that parameter are then displayed in one figure. This allows easy investigations of a parameter's impact on the stability of the loop.

4.3.3. Ledinegg instabilities

Krijger states that under certain conditions, Ledinegg instabilities occur in the loop [13]. Since there is no external pump characteristic to satisfy the stability condition in equation 1.1, Krijger used another method to find Ledinegg instability. Figure 4.2 shows that there are multiple possible mass flow rates occurring at one heating power. The existence of these multiple solutions makes flow excursion possible. Hence the flow rate may abruptly switch to one of the other possible values. Krijger included the way to calculate these operating conditions in the model, and made it possible to overlay the instability map with the Ledinegg unstable area.

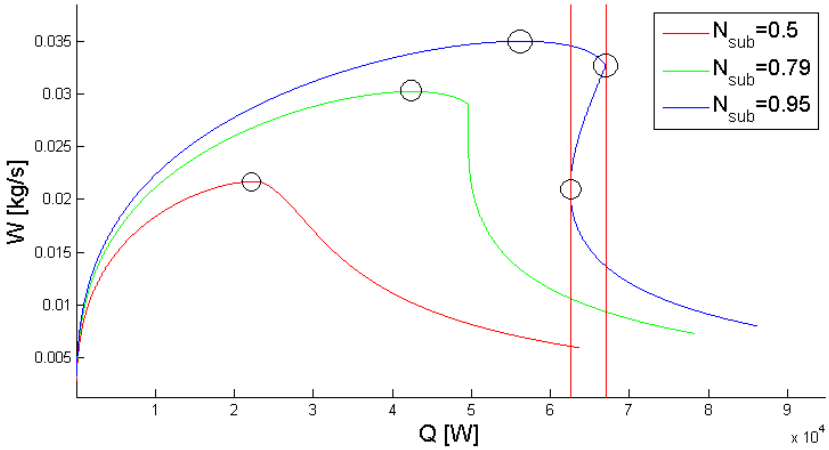

Figure 4.2: Mass flow rate vs. core heating power characteristic for various subcooling numbers, adopted from Krijger. Sign swaps are indicated by black circles. The vertical line shows the Ledinegg unstable region. [13]

5

Results

5.1. Dependency on the hydraulic diameter of the riser

The hydraulic diameter of the single channel in the model has been set constant in every section of the loop. Besides the fact that the diameter of a riser is usually wider than that of a reactor core, for example in a Economic Simplified Boiling Water Reactor [16], also the different inner geometry of the core channel compared to the riser has been neglected. In the core, the coolant flows around fuel rods (described by a single tube in the current model), thereby having a much smaller hydraulic diameter than the open channel of the riser. As the hydraulic diameter of the riser might deviate from the hydraulic diameter in the core by a factor of $n = 76$, like in an ESBWR [16], the stability effects of the riser could be misinterpreted significantly.

As stated in section 2.3, the pressure drop due to friction can be calculated as following:

$$\Delta P_{fric} = \left(\frac{fL}{D_H} + K \right) \frac{W^2}{2\rho} \tag{5.1}$$

(5.2)

In this equation, both the mass flow rate $\bar{W}$ and the friction factor f (depending on the Reynolds number) are dependent on the hydraulic diameter. The equations for the steady state mass flow rate $\bar{W}$ in the LHM and the HHM are shown in section 2.3.

For example, we investigate the case that the hydraulic diameter of the riser D_H, r is increased by a factor n. Since we analyse equation 2.6, we can expect that the steady state mass flow rate $\bar{W}$ will increase with a factor much smaller than n, because the equation is given for $\bar{W}^2$ and $D_{H,r}$ only decreases one of the summed terms in its denominator.

The equations for the friction factor f and the Reynolds number (Re) are shown below.

$$f = 0.316 Re^{-\frac{1}{4}} \qquad \text{for} \qquad (4000 < Re < 10^5) \tag{5.3}$$

$$Re = \frac{\bar{W} D_h}{A\mu} \tag{5.4}$$

As $D_{H,r}$ is increased by factor n, the Reynolds number increases by more than n, as it will also experience a slight increase in $\bar{W}$. As $f \propto \frac{1}{Re^{\frac{1}{4}}}$, the friction factor f will decrease slightly. Since the equations above are all dependent on each other, the exact change in ΔP_{fric} can only be found by an iterative process.

However, a qualitative prediction can be done. It was concluded that if D_H increases by factor n, $\bar{W}^2$ will increase by a factor much smaller than n, and f will decrease by a factor much smaller than n. Since $\Delta P_{fric} \propto$

$\frac{f\bar{W}^2}{D_H}$, and the increase of D_H by n will have the largest influence of these variables, it can be concluded that ΔP_{fric} will decrease.

Looking at the origin of instability, friction-based (type II) DWO might be overestimated, because there is a higher pressure drop due to friction in the riser if its hydraulic diameter is smaller.

This is why a parametric study has been carried out on the hydraulic diameter in the riser, using values for $D_{h,riser}$ shown in 5.1. All other loop variables were chosen according to the reference case in appendix C. In the reference case developed by Krijger [13], the hydraulic diameter of the riser was $5.6 \cdot 10^{-3} m$, equal to the hydraulic diameter of the core. The values for $D_{H,R}$ were chosen larger in the parametric study. If we choose values of $D_{H,R}$ much larger than the hydraulic diameter of the core, the stabilising effect of increasing $D_{H,R}$ gradually diminishes. The result is shown in figure 5.1.

Table 5.1: Values chosen for a parametric study on the hydraulic diameter of the riser

Values for $D_{H,riser}$
$5.6 \cdot 10^{-3}$ m
$1.0 \cdot 10^{-2}$ m
$5.6 \cdot 10^{-2}$ m
$5.6 \cdot 10^{-1}$ m

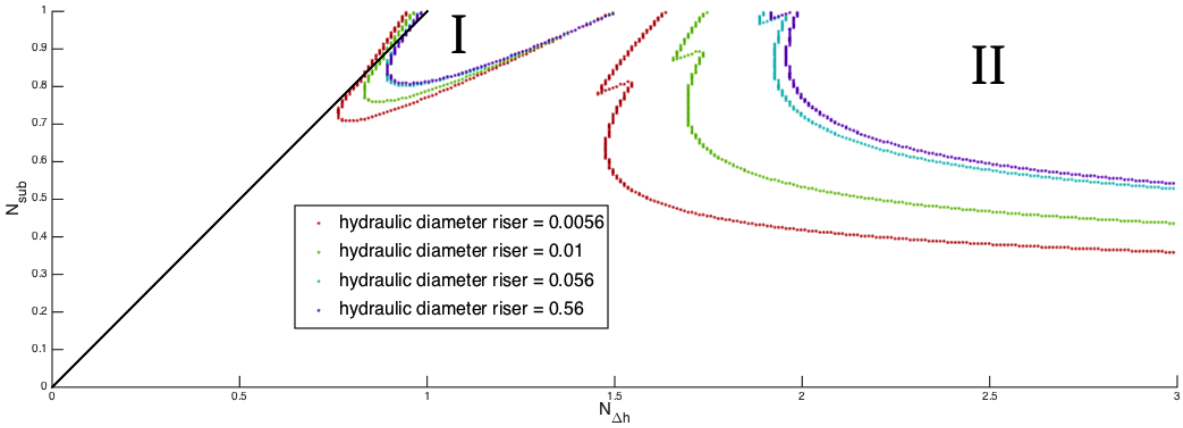

Figure 5.1: Parametric study of the hydraulic diameter of the riser, in which $5.6 \cdot 10^{-3} m$ is the hydraulic diameter (shown in red) of the core and riser in the reference case. Other parameters of the loop were chosen according to the reference case in appendix C.

Stabilisation of the type II DWO zone was expected as the friction in the riser would decrease, however the unstable region that was expected to house type I DWO stabilised too. The cause of this effect might be the increase in mass flow rate due to the reduced friction in the riser. As the mass flow rate is increased while the value of $N_{\Delta h}$ has been kept constant, it might be better to make a comparison between two operating conditions that have the same mass flow rate, instead of the same dimensionless variable.

5.2. Dependency on the riser length

Increasing the hydraulic diameter of the riser did not result in destabilising the unstable zone expected to house type I DWO. The accordance of stability maps with that of a BWR [31] or the Delight facility [29] did not improve. To investigate the effect of other geometric variables on this unstable zone, other parametric studies were done.

The parametric study on the riser length was comparable to Krijger's investigation in 2013, however now the adjustments made to the model by both Lippens and Zonneveld were included. The riser length chosen in the reference case was $4.2m$. In this parametric study, both higher and lower values were chosen, as shown in 5.2. The results are shown in figure 5.2

Table 5.2: Values chosen for a parametric study on the riser length.

Values for L_{riser}
2 m
4.2 m
8 m
12 m
20 m

Increasing the riser length does affect the stability of the system near the $N_{sub} = N_{\Delta h}$ region. As the riser length was increased, both region I and region II destabilise towards lower values for N_{sub} and $N_{\Delta h}$. At a value of $L_r = 10m$ a small unstable region appears in the LHM. The origin of this region is not known. The adjustments made by Lippens and Zonneveld cause the system to destabilise less under variation of the

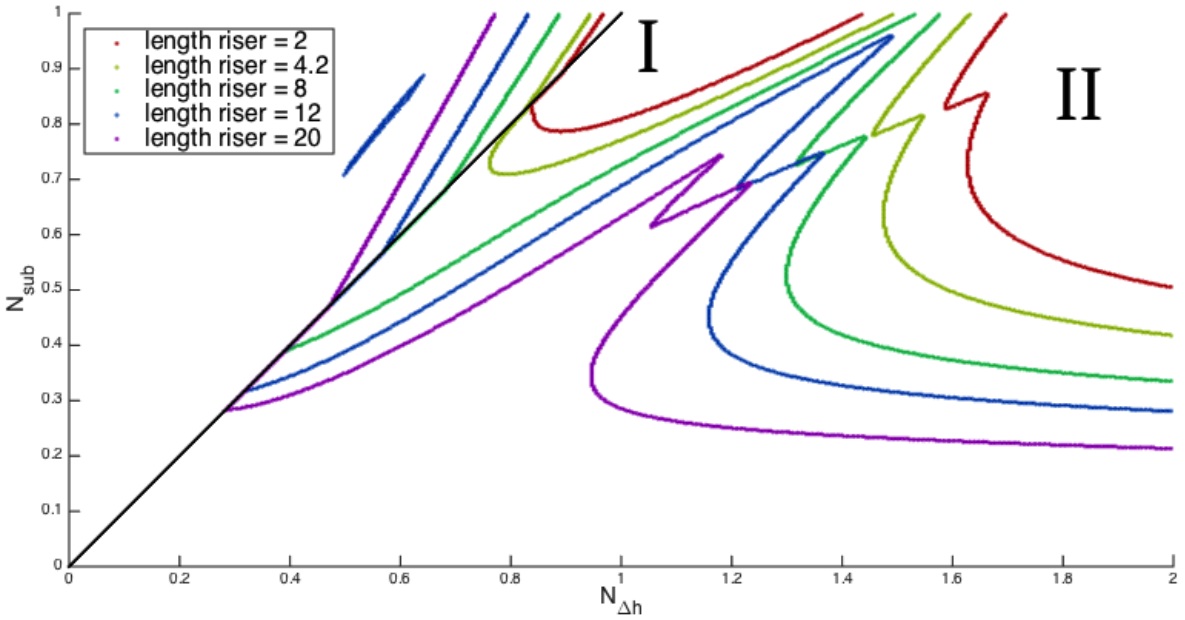

Figure 5.2: Parametric study of the riser length, in which $4.2m$ is the length of the riser in the reference case (shown in light green). Other parameters of the loop were kept chosen according to the reference case in appendix C.

riser length than the more simple model of Krijger. In a comparable parametric study, de system destabilized towards values of $N_{sub} = 0.2$ at riser lentgh of only 8 m.

5.3. Dependency on the buffer volume

In order to investigate the influence of the buffer volume on the stability of the loop, a parametric study was also carried out on buffer volume. Mostly values smaller than $10^{-2}m^3$ chosen in the reference case were chosen, however one larger value was also chosen, as shown in table 5.3.

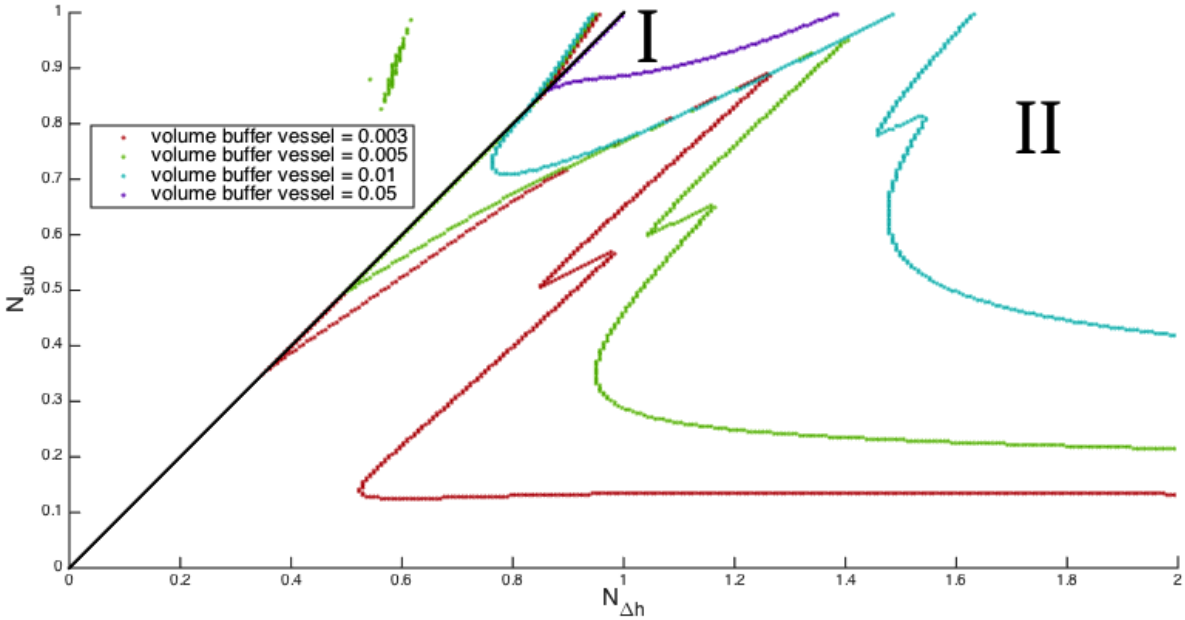

Figure 5.3: Parametric study for the volume of the buffer vessel, in which $10^{-2}m^3$ is the volume of the buffer vessel in the reference case (shown in turquoise). Other parameters of the loop were chosen according to the reference case in appendix C.

A decrease in the buffer volume resulted in significant destabilisation in both region I and II. Varying the buffer volume seems to have a larger effect on unstable region II than region I. At a buffer volume of $10^{-2}m$ an unstable region appears in the subcritical zone. The operating conditions at which this region appears are comparable to those of the unstable region appearing at $L_r = 10m$ in the previous parametric study. The cause of this small unstable area could not be found.

Table 5.3: Values chosen for a parametric study on the buffer volume.

Values for V_{buffer}
$3 \cdot 10^{-3}$ m
$5 \cdot 10^{-3}$ m
10^{-2} m
$5 \cdot 10^{-2}$ m

If the riser length is increased or the buffer volume is decreased, the stability map shows greater similarity to those of a BWR, as found by Van Bragt [31], than the reference case. If gravitation-based (Type I) DWO are the cause of the instability at lower powers in the generated maps, the values chosen for the riser length and volume of the buffer vessel clearly have a larger effect on Type I instabilities than the hydraulic diameter of the riser in our model.

To investigate the origin of both unstable regions in the stability map, it would be useful to compare the impact of gravitational pressure drop and frictional pressure drop on destabilising the model. In this way, proof could be found for the origin of unstable zones in our stability map.

$$R_{fg} = \frac{\Delta P_{fric}}{\Delta P_{grav}} \tag{5.5}$$

By the use of a friction-to-gravitation ratio, denoted by R_{fg}, the influence of both could be analysed quantitatively. For example, if $R_{fg} >> 1$, the influence of friction would be largest under a certain operating condition, and if $R_{fg} \approx 1$ both would contribute similarly.

$$\Delta P_{fric} = \left(\frac{fL}{D_H} + K \right) \frac{W^2}{2\rho} \tag{5.6}$$

$$\Delta P_{grav} = A^2 g \rho L \tag{5.7}$$

$$\tag{5.8}$$

At first, the values of gravitational and frictional pressure drop in the conservation balances were compared. The steady state influences of friction and gravity even out, as they both drive and restrict the steady state mass flow (see section 2.3).

Since the development of instability is caused by time-dependent perturbations, actual comparisons can only be made between the perturbed gravitational and frictional terms out of the linearised momentum balance, presented in 2.5. In the linearised momentum balance, these terms are multiplied by the time dependent value of the corresponding perturbed variable, as will be shown in 5.5.

5.4. Comparison time-dependent solution with stability

In order to know the time-dependent value of a perturbed variable, the eigenvalue problem was solved with respect to time. According to the derivation made in 3.1 perturbed variables were calculated by summing constants, eigenvectors and eigenvalues according to the following equation (earlier presented as equation 3.6):

$$\vec{x} = \sum_{j=1}^{n} c_j \cdot \vec{v}_j \cdot e^{\lambda_j t} \tag{5.9}$$

In this equation, the row of one perturbed variable x_k in x corresponds to the column of this perturbed variable in the coefficient matrices presented in Appendix A. The code was enhanced so that the time-dependent values of selected perturbed variables could be calculated. Additionally, plots were made of the perturbed mass flow rate in the riser, subcritical core and supercritical core for both stable and unstable operating conditions.

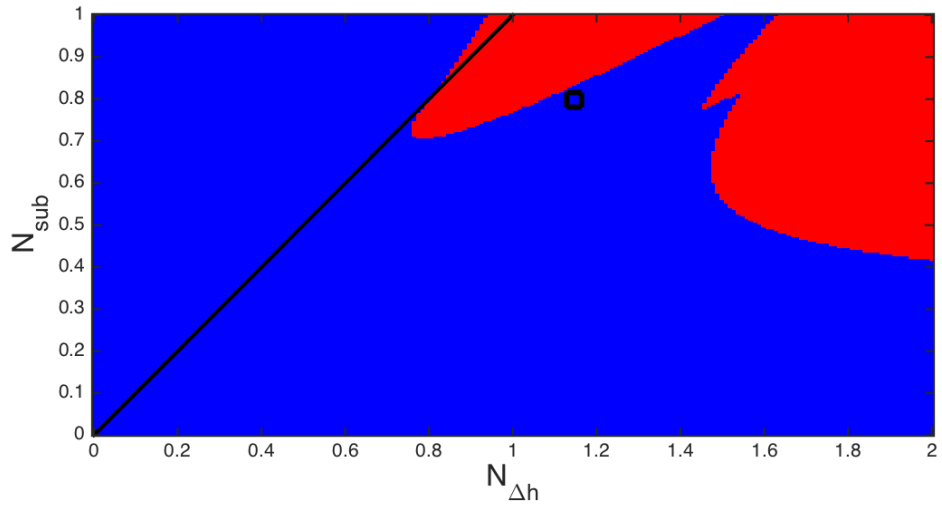

(a)

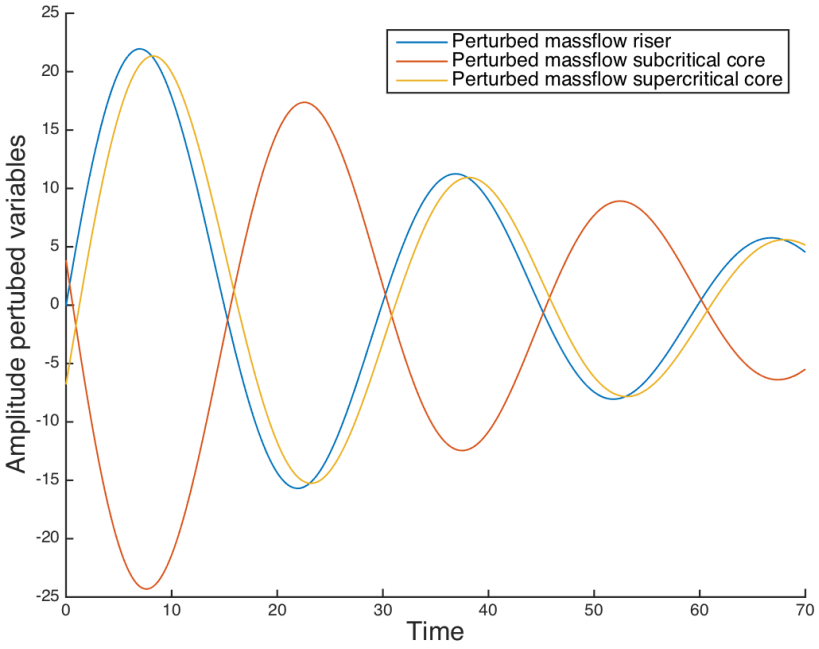

(b)

Figure 5.4: (a) shows the entire instability map. (b) shows the perturbed parameters as a function of time at the stable operational conditions $N_{sub} = 0.7992$ and $N_{\Delta h} = 1.1462$ as indicated in (a)

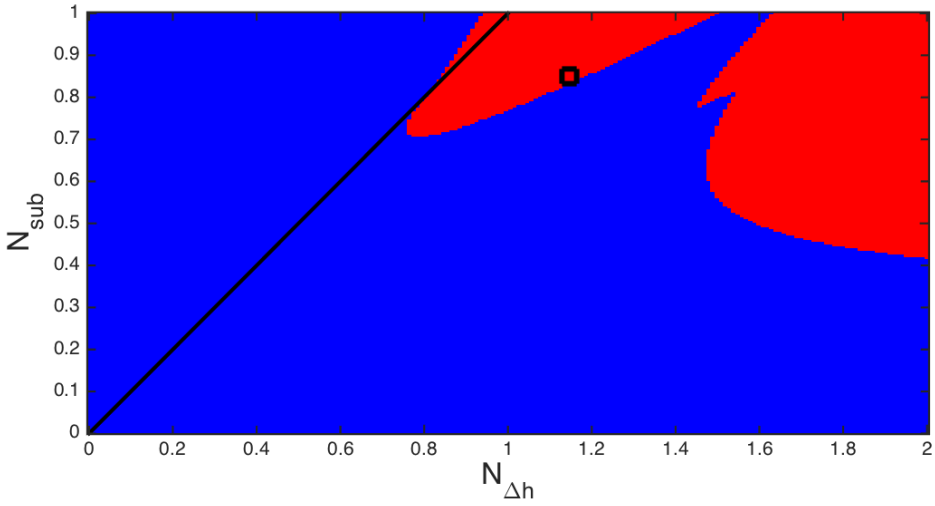

(a)

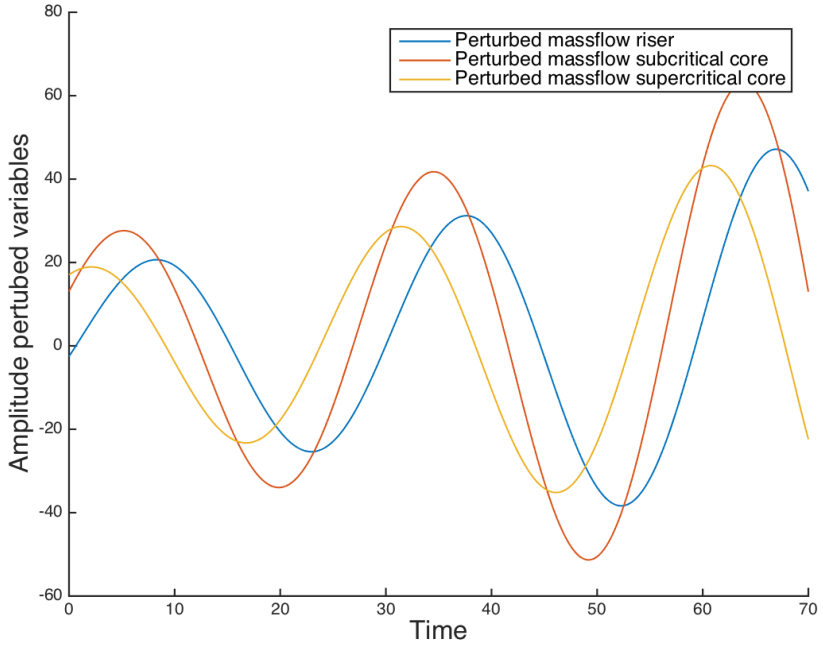

(b)

Figure 5.5: (a) shows the entire instability map. (b) shows the perturbed parameters as a function of time at the unstable operational conditions $N_{sub} = 0.8494$ and $N_{\Delta h} = 1.1462$ as indicated in (a)

As figure 5.4 and figure 5.5 show, the code was augmented such that a selection of wanted operating conditions and a time frame of interest could be chosen. The expected results were as following: under unstable operating conditions, the perturbed variable values would eventually diverge, as at least one eigenvalue has a positive real part. As shown in figure 5.4 and figure 5.5, the perturbed variables do show convergence or divergence dependent on stable or unstable operating conditions respectively. It can be concluded that the perturbed variables behave according to the eigenvalue problem.

5.5. The influence of gravity and friction on destabilisation

Now we can have a look at equations 2.13 and 2.14 again. The terms related to friction contain the Darcy friction factor f and friction coefficients K_i. Gravitational terms are the ones containing the dimensionless Froude Number N_{Fr}. Taking out the gravitation and friction related terms and summing them in the following way, we can look at the temporal changes in friction and gravitation within the system and compare both. The equations described below are used to evaluate the friction and gravity perturbations throughout the LHM and HHM respectively.

$$F_{LHM} = -\left(\left(\frac{f_R \underline{L_R}}{\underline{D_H}} + K_R\right)\underline{\overline{v_R}}\right)\underline{\breve{w}_R} + \frac{1}{2}C_1 N_{\Delta h} h_{pc} v_{pc}\left(\frac{1}{2}\left(\frac{f_0}{\underline{D_H}} + K_0\right)\frac{1}{\underline{\overline{\rho}_0^2}}\right)\underline{\breve{h}_{out}} \cdots$$

$$\cdots + C_1 N_{\Delta h} h_{pc} v_{pc}\left(\frac{1}{2}\left(\frac{f_R \underline{L_R}}{\underline{D_H}} + K_R\right)\frac{1}{\underline{\overline{\rho}_R^2}}\right)\underline{\breve{h}_R} - \left(\left(\left(\frac{f_0}{\underline{D_H}} + K_0\right)\underline{\overline{v}_0} - \left(\frac{f_D \underline{L_D}}{\underline{D_H}} + K_D\right)\underline{v_{in}}\right)\underline{\breve{w}_0}\right) \tag{5.10}$$

$$G_{LHM} = \frac{1}{2}C_1 N_{\Delta h} h_{pc} v_{pc}\left(-\frac{1}{N_{Fr}}\right)\underline{\breve{h}_{out}} + C_1 N_{\Delta h} h_{pc} v_{pc}\left(-\frac{\underline{L_R}}{N_{Fr}}\right)\underline{\breve{h}_R} \tag{5.11}$$

$$F_{HHM} = \left(\frac{1}{2}\left(\frac{f_0 \underline{v_0}}{\underline{D_H}} - \frac{f_1 \underline{\overline{v}_1}}{\underline{D_H}}\right)\right)\underline{\breve{l}_1} - \left(\left(\frac{f_0 \underline{\overline{L}_0}}{\underline{D_H}} + K_0\right)\underline{\overline{v}_0} + \left(\frac{f_D \underline{\overline{L}_D}}{\underline{D_H}} + K_D\right)\underline{\overline{v_{in}}}\right)\underline{\breve{w}_0} \cdots$$

$$\cdots - \left(\frac{f_1 \underline{\overline{L}_1}}{\underline{D_H}} + K_1\right)\underline{\overline{v}_1 \breve{w}_1} + \left(-\frac{1}{2}\left(\frac{f_1 \underline{\overline{L}_1}}{\underline{D_H}} + K_1\right)\right)\frac{C_1 N_{\Delta h} h_{pc}}{vpc}\underline{\breve{h}_1} \cdots$$

$$\cdots - \left(\frac{f_R \underline{\overline{L}_R}}{\underline{D_H}} + K_R\right)\underline{\overline{v}_R \breve{w}_R} + \left(-\frac{1}{2}\left(\frac{f_R \underline{\overline{L}_R}}{\underline{D_H}} + K_R\right)\right)\frac{C_1 N_{\Delta h} h_{pc}}{vpc}\underline{\breve{h}_R} \tag{5.12}$$

$$G_{HHM} = \left(\frac{1}{N_{Fr}\underline{v_0}} - \frac{1}{N_{Fr}\underline{\overline{v}_1}}\right)\underline{\breve{l}_1} + \frac{\underline{\overline{L}_1}}{N_{Fr}\underline{\overline{v}_R^2}}\frac{C_1 N_{\Delta h} h_{pc}}{vpc}\underline{\breve{h}_1} + \frac{\underline{\overline{L}_R}}{N_{Fr}\underline{\overline{v}_R^2}}\frac{C_1 N_{\Delta h} h_{pc}}{vpc}\underline{\breve{h}_R} \tag{5.13}$$

In figure 5.7 several plots were made for the values of the gravitation and friction perturbations throughout time for different operating conditions shown in figure 5.6. The operating conditions chosen are not round as a result of the resolution chosen for N_{sub} and N_{Deltah}. Comparing these two figures, it can easily be seen that both signals converge to zero at stable operating conditions, while they diverge at unstable operating conditions. It was noted that, depending the value of the real parts of the destabilizing eigenvalues, the real timespan in which destabilisation became visible could be several seconds to ten minutes. As the destabilising eigenvalues are not known before doing a calculation at a certain operating point, setting the right time-scale to display a relevant and visible oscillation often showed to be an iterative process.

The friction fluctuations seem to have a larger amplitude in most cases. In both unstable regions at points (b) and (d) shown in figure 5.6, the difference in amplitude is significant, as figure 5.7 shows. This could be an indication that in our model friction plays a larger role in destabilizing the system.

At point (a), the values for friction and gravitation mostly show exponential decay towards steady state, and only in the friction value some oscillating behaviour can be seen. It was found that under the investigated operating conditions the periodic frequencies of fluctuations are very low. The the frequency can be calculated as following:

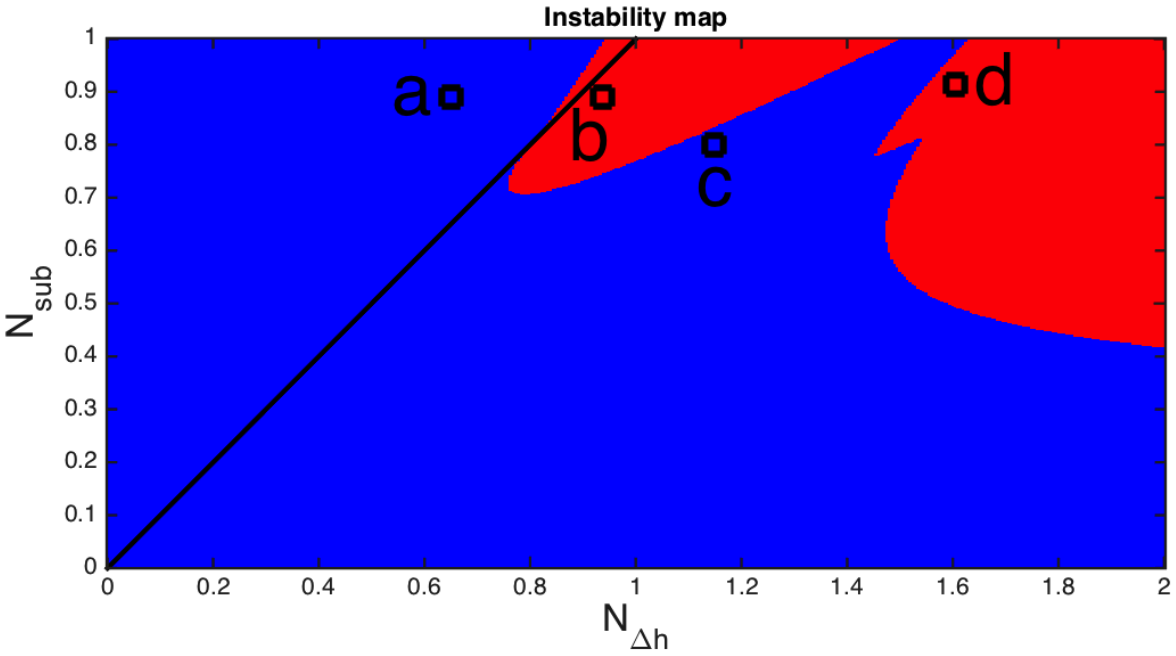

Figure 5.6: The stability map was investigated at four operating points, being depicted with small black circles. The operating conditions were chosen as following: (a) N_{sub} = 0.89981 and N_{Deltah} = 0.64824 (b) N_{sub} = 0.89981 and N_{Deltah} = 0.94609 (c) N_{sub} = 0.7997 and N_{Deltah} = 1.1483 (d) N_{sub} = 0.89981 and N_{Deltah} = 1.5991. All parameters of the loop were chosen according to the reference case in appendix C.

$$f = \frac{1}{T} \tag{5.14}$$

In this equation, T stands for the time of one oscillation period. As $T > 30s$ for points (b), (c) and (d), frequencies are in the order of $f < 0.033Hz$.

Point (d) is the only operational point for which also a higher frequency is visible. This second frequency is in the order of $f = 0.3Hz$. The double oscillatory behaviour can be seen in plot (d) of figure 5.7. Type II DWO are associated with higher frequencies than type I DWO, as explained in 1.4.1. The fact that also higher oscillation frequencies are detected at this point, could give a basis for relating this area to type II DWO instead of type I DWO.

The frequencies found in the fluctuating variables for both friction and gravitation are much lower than the frequencies found in frequency maps plotted earlier by Krijger, Lippens and Zonneveld. This is expected, as in their frequency maps, only the frequency of eigenvalues with the largest real part are investigated.

Oppositely, perturbed variables are composed of all eigenvalues. Most eigenvalues do not have an imaginary part, and their values do only correspond to non-periodic exponential behaviour. In the friction and gravitation terms, also non-periodic terms determine the time dependent behaviour.

The ratio of gravity to friction was also investigated. In most cases $R_{fg} >> 1$, showing that the amplitudes of friction fluctuations are generally higher than gravity fluctuations throughout the system, as had been concluded from figure 5.7 as well. However, due to the oscillatory behaviour and exponential behaviour of both quantities, the time-dependent ratio is quantitatively meaningless.

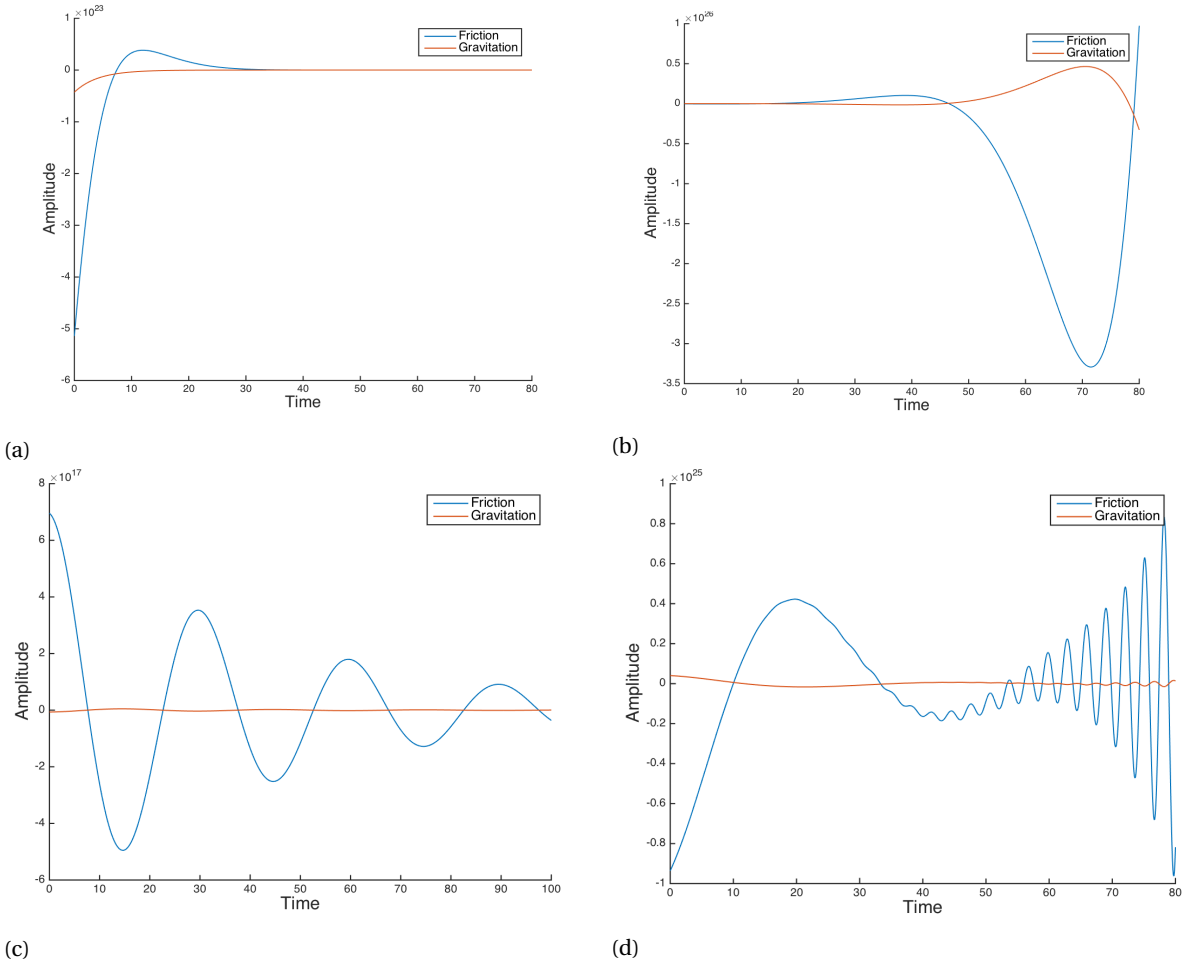

Figure 5.7: The friction and gravitation terms were plotted throughout time for the four respective operating points of figure 5.6.

6

Conclusions and discussion

6.1. Conclusions

In this research the flow instabilities of a simplified model for a High Performance Light Water Reactor have been analysed. A computational model was used to find the stability of operating conditions by investigating the response of the system to introduced perturbations.

It was investigated why numerical results of the HPLWR model deviate from experimental data of comparable systems. Studies on Boiling Water Reactors by van Bragt, show two unstable regions at low and high operational powers respectively [31]. The stability map of a HPLWR is expected to house similar instabilities. Experimental results of the Delight facility, a scaled version of a HPLWR that uses Freon (R-23) as a cooling fluid, confirm the existence of an unstable region at low operational powers [29]. It would be expected that the stability calculated by the current model shows similar trends, however the low power unstable region is much smaller. In this research it was investigated what is the cause of this qualitative difference with respect to these two experimental studies.

Previously, the hydraulic diameter of the system had been kept constant throughout the model. To investigate the implications of this simplification with respect to a real HPLWR, the dependency of the model on the hydraulic diameter of the riser was analysed. Increasing the hydraulic diameter of the riser stabilises the system in both a low and high power unstable area. It was concluded that keeping the hydraulic diameter constant throughout the model was not the cause of a small unstable region at low powers.

In order to investigate which system parameter might cause a larger unstable region at low heating powers of the core, the dependency of the model on several other geometrical parameters was analysed. The stability dependency on the length of the riser was investigated. It was found that increasing the riser length causes significant destabilisation of the regions both the low and high power unstable area. This can be expected from literature, since increasing the riser length caused destabilization at low powers for a BWR [31]. In the Delight facility the riser length is much larger than the length of its heating section. It can be concluded that a smaller riser length might be the cause of a smaller low power unstable region.

After this, the system's dependency on a buffer volume was investigated. Decreasing the volume of the buffer vessel resulted in destabilisation of both unstable areas. More similarity with experimental results found by the experimental Delight facility[29] was found if a smaller buffer volume was chosen, in comparison with values that were chosen as a reference throughout the model.

In order to investigate what physical mechanisms are causing the different unstable operating conditions that occur in our model, the time-dependent fluctuations in steady state variables were studied. Therefore, the generalised eigenvalue problem was solved with respect to time. The time-dependent fluctuations of perturbed variables were plotted and convincingly showed converging and diverging behaviour according to stable and unstable operating conditions respectively.

It was expected that knowing the development of variables related to gravity and friction throughout the system, could improve the understanding of the origin of instabilities that occur in our system. The ratio

between gravity and friction could prove which of the two is more dominant in destabilising the system at certain operating conditions. Perturbed terms for gravity and friction were determined and investigated over time. In general the amplitudes of fluctuations in friction were larger than the amplitudes related to gravitation. It can be concluded that for the operating conditions investigated, fluctuations in friction terms had a larger effect on destabilising the system. However, due to the oscillatory behaviour and exponential behaviour, a time-dependent ratio between gravitation and friction turned out to be quantitatively meaningless. Phase change between the two terms and zero-crossings made the ratio useless.

Further research can be done in analysing the friction and gravitation terms for different system geometries. In this way, it can be found if the influence of gravitation in destabilizing the system is larger if the riser length is increased, or the buffer volume is decreased.

6.2. Discussion

For further research, a significant recommendation is to investigate the effect of parametric studies on the operating conditions itself. For example, if a parametric study is performed for the hydraulic diameter of the riser, stability maps are defined by the operating conditions $N_{\Delta h}$ and N_{sub}. However, the steady state mass flow rate will change as we vary the hydraulic diameter of the riser in a parametric study (see equation 2.6 and 2.7). By an iterative process the core wall temperature and mass flow rate $\bar{W}$ are calculated until they match the dimensionless number $N_{\Delta h}$ within a set accuracy. In this way, when we compare the same location (with the same values for $N_{\Delta h}$ and N_{sub}) on stability maps for two different values of $D_{h,riser}$, we do compare two point with the same value for $N_{\Delta h}$ but they do not have the same mass flow rates or heating power in the core. In this way two points are compared that do not have the same operating conditions, but only share the same dimensionless operating number $N_{\Delta h}$. It would be more intuitive to compare stability maps with dimensionless number N_{sub} on the vertical axis and the steady state mass flow rate $\bar{W}$ or core heating power Q on the horizontal axis of a stability map. In this way one could compare similar operating conditions more easily when a parametric study is carried out. However, it will not be equally easy to see when a coolant reaches supercritical temperature in the core.

Further research can also be done into the unstable regions thought to be caused by type I on and type II DWO. As friction-based perturbations in the model seem to dominate gravity-based perturbations, it is questionable if type 1 DWO is actually taking place in unstable region at lower powers. Alternatively, the more significant presence of friction-based perturbations, even when the riser length or hydraulic diameter are increased, could also be caused by the shifting of operating conditions explained in the paragraph before. Considering the findings of Zonneveld in 2015 [35], it would be interesting to investigate why variation of the fuel heat transfer model time constant and density reactivity feedback coefficient (in the core) seem to effect unstable region expected to house the type I DWO more, contradictory to the expected effect on the type II DWO unstable region.

Another recommendation would be to evaluate the method currently used for finding Ledinegg instability. As our HPLWR-based loop is driven by natural convection, no external pumping characteristics are present. Consequently, for determining Ledinegg instability the internal characteristics of the gravitational driving force have to be used instead of the pumping characteristic. Alternative methods to analyse Ledinegg instability in natural circulation driven loops are presented throughout literature, and the approach of Yu and Che for natural circulation systems seems promising [34].

As the eigenvalue problem is a linearised version of the set of perturbed balances, solving it in time comes with certain complications. Since we are solving a system that originally was non-linear in time, our way of solving only applies for very small perturbations in stable operating conditions. Only if a perturbation is still within the so-called attraction domain of the steady state value for a specific operating condition, it is valid to solve it in time according to equation 3.7. If in future quantitative calculations in time will be required instead of qualitative indications, it would be best to further investigate the implications of linear solving methods on the time-dependent solution of our system. In this way, it will be ensured that the current solving approach is numerically valid.

In our time-dependent solution, infinite eigenvalues generated by Matlab were neglected. A test case was set up in appendix D to improve the understanding of those eigenvalues. The test case confirmed that the $\lambda = \infty$ returned by MATLAB can be neglected, without affecting the stability of an operating condition. In

the test case it was shown that if a generalised eigenvalue problem has fewer eigenvalues then the dimension of its square coefficient matrices, the eigenvalue problem can be reduced to a matrix equation of lower dimensions. It could not be determined easily how the coefficient matrices in our model could be reduced to a lower order problem, whilst keeping a simple equation for every perturbed variable. If the dimension of the coefficient matrices could be reduced in such way that the infinite eigenvalues do no longer appear, the time-dependent solution of the new eigenvalue problem could be compared with the current approach, proving if it mathematically correct. Further investigation could be done into this simplification of the original problem.

As the model has been extended and enhanced throughout the last several years, the size of matrices and number of calculations to create a stability map have increased. Therefore, it takes longer to produce a stability map of similar resolution. Given the fact MATLAB is using less RAM per vectorized calculation, it is worth considering to vectorise the entire model, avoiding FOR loops and increasing its calculation speed. Also, preallocating arrays and matrices by first setting them to zero-filled ones greatly increases calculation speed. Storing MATLAB data into columns instead of vectors and avoiding unnecessary variables by overwriting old ones increases calculation time as well [17].

To match the reality of a HPLWR more accurately, the core of the model could be split up into 3 nodes, reflecting the three-pass heating core model proposed by Schulenberg [25]. In this way, also axial position of the fuel in the core could play a bigger role in the heat transfer and reactivity feedback of the coolant. However, even with two or three core nodes, the model will remain far from the real case. At least, this would increase the similarities between the model ans the HPLWR, though it does not improve the simplicity of the model.

In the approximation of water properties attention has been paid to make both the thermal conductivity and its slope continuous at the pseudo-critical point. The same has been done in the approximation of temperature, being only dependent on the section's enthalpy [15]. However, the linear approximation of density in the equation of state of Krijger [13], is only continuous in its value, and not in its slope. A new (exponential or quadratic) approximation which has a continuous slope could increase the accuracy of the stability behaviour around the pseudo-critical border ($N_{\Delta h} = N_{sub}$). Also a better approximation could be made if more than two segments were used in the equation of state. This would be possible if the core were split up in the same amount of segments. It would result in a less rigorous transition would be modelled between the LHM and the HHM.

Although the basis of the current model is to solve the balance equations by linear methods, the model would be valid for larger perturbation if the quadratic terms and time-derivatives of perturbations were not neglected. However, as the goal of this model is to give qualitative indications for instability, linearising the equations greatly simplifies the model and increases its speed.

The model could be enhanced by modelling the dynamic viscosity as a function of temperature. Hereby, the Darcy friction factor will be calculated more accurately. Krijger predicted a maximum deviation of 20% caused by keeping the dynamic viscosity constant throughout the loop [13]. If the specific materials for the core wall and loop wall in general would be known the roughness height could be specified differently per section, which would also increase the accuracy of friction factors.

The thin layer of gas present in fuel rods, often referred to as gap, is neglected in this research. For adequate modelling of the heat transfer the effects of a gap could be taken into account [35].

In this thesis the dependency of specific heat on the Prandtl number is only taken into account in the steady state calculations, but it is not considered to be of large effect for the perturbed calculations. For the sake of accuracy, it could be added to these calculations, although it might be time-consuming to involve this depency in every calculation. A parametric study might be carried out to determince the importance of the implementation [15].

Further research could be done on the effects of fuel enrichment on the stability of the model. Looking back at the results of a parametric study carried out by Zonneveld [35], the effects of changing the enrichment were expected to be much larger than they turned out to be in the model.

To conclude, the further development of a HPLWR driven by natural convection is not discouraged by the results of this thesis. According to the model, the great variety of stable operating conditions under various loop geometries presents a promising reactor design.

Acknowledgments

I would like to thank my supervisor Martin Rohde for all his knowledge and time. I have enjoyed our numerous conversations about type 1 and type 2 instabilities, as well as international evening and coffee brakes at NERA. I have learned a bunch of getting lost in subjects that were far beyond my level of knowledge at that time. I admire his perseverance and determination that pushed this project further than I could have ever come on my own.

I would like to thank all people at NERA for the interesting conversations that were both work-related and personal.

I would like to thank Dr. H. Kneppers (Functional Analysis at the faculty of Applied Mathematics) for his help and enthusiasm when I got stuck on the mathematics of generalized eigenvalue problems. I would like to thank Dr. M. van Gijzen (Numerical Analysis, at the faculty of Applied Mathematics) for his help explaining the origin of infinite eigenvalues returned by MATLAB and the implications of the presence of singular matrices in non-linear systems. I would like to thank Dr. Ir. W. van Horssen (Mathematical Physics at the faculty of Applied Mathematics) for his patience in explaining the constraints for solving a generalised eigenvalue problem in time.

I would also like to thank my family, housemates and other friends for their interest and support during my research.

A

Coefficient Matrices

This appendix presents the coefficient matrices A and B that have been used in the stability analyses in this work. Because of the large size of the matrices, they have been split up into parts.

In order to make the indexation of the matrices clear: the rows of matrices in the LHM correspond to balances M_0, E_0, E_r, I, E_w, n, C_i (1 until 6) and E_f respectively, while the columns correspond to the perturbed variables $\check{h}_{out}$, $\check{h}_r$, $\check{w}_0$, $\check{w}_r$, $\check{\theta}_w$, $\check{n}$, $\check{C}_1$, $\check{C}_2$, $\check{C}_3$,$\check{C}_4$, $\check{C}_5$, $\check{C}_6$ and $\check{q}_w$ respectively.

A.1. Low heating model

COEFFICIENT MATRIX A:
Columns 1 to 5

$$\begin{pmatrix}
\frac{1}{2}C_1N_{\Delta h}h_{pc}v_{pc} & C_1N_{\Delta h}h_{pc}v_{pc}\underline{L_R} & 0 & 0 & 0 \\
\frac{1}{2}(C_1N_{\Delta h}h_{pc}v_{pc}\underline{\overline{H}_0}+\underline{\rho_0} & C_1N_{\Delta h}h_{pc}v_{pc}\underline{\overline{H}_{out}L_R} & 0 & 0 & 0 \\
0 & \underline{L_R\overline{\rho}_R}+\underline{L_R}C_1N_{\Delta h}h_{pc}v_{pc}(\underline{\overline{H}_R}-\underline{\overline{H}_{out}}) & 0 & 0 & 0 \\
0 & 0 & 1+\underline{L_D}+\underline{\overline{V}_B} & \underline{L_R} & 0 \\
0 & 0 & \underline{0} & \underline{0} & \underline{\rho_w c_{p,w}A_w} \\
0 & \dots & & & \underline{0} \\
\vdots & \ddots & & & \vdots \\
0 & \dots & & & 0
\end{pmatrix}$$

Colums 6 to 13

$$\begin{pmatrix} 0 & & \dots & & & 0 \\ 0 & & & & & \\ 0 & & \ddots & & & \vdots \\ 0 & & & & & \\ 0 & & \dots & & & 0 \\ 1 & 0 & 0 & 0 & 0 & 0 & 0 & 0 \\ 0 & 1 & 0 & 0 & 0 & 0 & 0 & 0 \\ 0 & 0 & 1 & 0 & 0 & 0 & 0 & 0 \\ 0 & 0 & 0 & 1 & 0 & 0 & 0 & 0 \\ 0 & 0 & 0 & 0 & 1 & 0 & 0 & 0 \\ 0 & 0 & 0 & 0 & 0 & 1 & 0 & 0 \\ 0 & 0 & 0 & 0 & 0 & 0 & 1 & 0 \\ 0 & 0 & 0 & 0 & 0 & 0 & 0 & \underline{\tau} \end{pmatrix}$$

COEFFICIENT MATRIX B:
Column 1

$$\begin{pmatrix} 0 \\ -\left(\underline{\widehat{Nu_0}}\frac{P_{in}}{\overline{\overline{D_H}}}\left(\left(\underline{\alpha_0}\left(\underline{H_0}-\underline{h_{pc}}\right)+\frac{1}{2\underline{c_{p,pc}}}\right)\underline{\overline{\lambda}_{f0}^{0.34}}-0.17\underline{\overline{\lambda}_{f0}^{-0.66}}\left(\overline{\underline{T}}_w-\overline{\underline{T}}_0\right)\underline{\beta_0}\right)+1\right) \\ 1 \\ \frac{1}{2}C_1N_{\Delta h}h_{pc}v_{pc}\left(\frac{1}{2}\left(\frac{f_0}{\underline{D_H}}+K_0\right)\frac{1}{\overline{\underline{\rho}}_0^2}-\frac{1}{N_{Fr}}\right) \\ \frac{1}{2}\underline{\widehat{Nu_0}}\frac{P_{in}}{\overline{\overline{D_H}}}\left(\underline{\overline{\lambda}_{f0}^{0.34}}\left(2\underline{\alpha_0}\left(\underline{H_0}-\underline{h_{pc}}\right)+\frac{1}{\underline{c_{p,pc}}}\right)-0.34\underline{\overline{\lambda}_{f0}^{-0.66}}\left(\overline{\underline{T}}_w-\overline{\underline{T}}_0\right)\underline{\beta_0}\right) \\ \frac{C_1N_{\Delta h}h_{pc}v_{pc}\underline{\alpha_r}\overline{\underline{n}}}{2\underline{\Lambda}} \\ 0 \\ 0 \\ 0 \\ 0 \\ 0 \\ 0 \\ 0 \end{pmatrix}$$

Columns 2, 3

$$\begin{pmatrix} 0 & 1 \\ 0 & \overline{\underline{H}}_{in} \\ -1 & 0 \\ \frac{1}{2}C_1N_{\Delta h}h_{pc}v_{pc}\left(\frac{1}{2}\left(\frac{f_R\underline{L_R}}{\underline{D_H}}+K_R\right)\frac{1}{\overline{\underline{\rho}}_R^2}-\frac{\underline{L_R}}{\overline{N_{Fr}}}\right) & \left(\underline{v_{in}}\left(\frac{f_0}{\underline{D_H}}+K_0\right)\overline{\underline{v}}_0-\left(\frac{f_D\underline{L_D}}{\underline{D_H}}+K_D\right)\underline{v_{in}}\right) \\ 0 & 0 \\ 0 & 0 \\ 0 & 0 \\ 0 & 0 \\ 0 & 0 \\ 0 & 0 \\ 0 & 0 \\ 0 & 0 \\ 0 & 0 \end{pmatrix}$$

Columns 4, 5, 6

$$\begin{pmatrix} -1 & 0 & 0 \\ -\underline{\overline{H}_{out}} & \underline{\widehat{Nu_0}\overline{\lambda}_{f0}^{-0.34}\frac{P_{in}}{\overline{D_H}}} & 0 \\ \underline{\overline{H}_{out}-\overline{H}_R} & 0 & 0 \\ -\left(\left(\frac{f_R L_R}{\underline{D_H}}+K_R\right)\underline{\overline{v_R}}+\underline{v_{in}}\right) & 0 & 0 \\ 0 & -\underline{\widehat{Nu_0}\overline{\lambda}_{f0}^{-0.34}\frac{P_{in}}{\overline{D_H}}} & 0 \\ 0 & 0 & -\frac{\beta}{\underline{\Lambda}} \\ 0 & 0 & \frac{\beta_1}{\underline{\Lambda}} \\ 0 & 0 & \frac{\beta_2}{\underline{\Lambda}} \\ 0 & 0 & \frac{\beta_3}{\underline{\Lambda}} \\ 0 & 0 & \frac{\beta_4}{\underline{\Lambda}} \\ 0 & 0 & \frac{\beta_5}{\underline{\Lambda}} \\ 0 & 0 & \frac{\beta_6}{\underline{\Lambda}} \\ 0 & 0 & \underline{\Sigma_f E_f V_f v_n} \end{pmatrix}$$

Columns 7 to 13

$$\begin{pmatrix} 0 & & & \dots & & & 0 \\ 0 & & & & & & \\ 0 & & & \ddots & & & \vdots \\ 0 & & & & & & 0 \\ 0 & & & \dots & & 0 & 1 \\ \underline{\lambda_1} & \underline{\lambda_2} & \underline{\lambda_3} & \underline{\lambda_4} & \underline{\lambda_5} & \underline{\lambda_6} & 0 \\ -\underline{\lambda_1} & 0 & 0 & 0 & 0 & 0 & 0 \\ 0 & -\underline{\lambda_2} & 0 & 0 & 0 & 0 & 0 \\ 0 & 0 & -\underline{\lambda_3} & 0 & 0 & 0 & 0 \\ 0 & 0 & 0 & -\underline{\lambda_4} & 0 & 0 & 0 \\ 0 & 0 & 0 & 0 & -\underline{\lambda_5} & 0 & 0 \\ 0 & 0 & 0 & 0 & 0 & -\underline{\lambda_6} & 0 \\ 0 & 0 & 0 & 0 & 0 & 0 & -1 \end{pmatrix}$$

A.2. High heating model

In order to make the indexation of the matrices clear: the rows of matrices in the LHM correspond to balances M_0, M_1, M_R, E_1, E_r, I, E_{w0}, E_{w1}, n, C_i (1 until 6) and E_f respectively, while the columns correspond to the perturbed variables $\check{l}_1$, $\check{h}_1$, $\check{h}_r$, $\check{w}_0$, $\check{w}_1$, $\check{w}_r$, $\check{\theta}_w 0$, $\check{\theta}_w 1$, $\check{n}$, $\check{C}_1$, $\check{C}_2$, $\check{C}_3$,$\check{C}_4$, $\check{C}_5$, $\check{C}_6$ and $\check{q}_w$ respectively.

COEFFICIENT MATRIX A:

Columns 1 to 3

$$\begin{pmatrix}
\underline{\rho_0}\left(\frac{H_0}{\underline{\overline{h_{pc}}}}-1\right) & 0 & 0 \\
\left(\frac{1}{\underline{\overline{v_1}}}-\frac{H_0}{\underline{\overline{h_{pc}}}\underline{\rho_0}}\right) & -\frac{\overline{\underline{L_1}}C_1N_{\Delta h}h_{pc}}{vpc\underline{\overline{v_1}^2}} & 0 \\
0 & 0 & -\frac{\overline{\underline{L_R}}C_1N_{\Delta h}h_{pc}}{vpc\underline{\overline{v_R}^2}} \\
\left(\frac{\overline{H_1}}{\underline{\overline{v_1}}}-\underline{H_0\rho_0}\right) & \frac{\overline{\underline{L_1}}}{\underline{\overline{v_1}}}\left(1-\frac{\overline{H_1}C_1N_{\Delta h}h_{pc}}{vpc\underline{\overline{v_1}}}\right) & 0 \\
0 & 0 & \left(\underline{L_R\overline{\rho}_R}-\underline{L_R}C_1N_{\Delta h}h_{pc}v_{pc}(\underline{\overline{H_R}}-\underline{\overline{H_{out}}})\right) \\
0 & 0 & 0 \\
-\underline{\rho_w c_{p,w}A_w\overline{T}_{w,0}} & 0 & 0 \\
\underline{\rho_w c_{p,w}A_w\overline{T}_{w,1}} & 0 & 0 \\
0 & 0 & 0 \\
\vdots & \vdots & \vdots \\
0 & 0 & 0
\end{pmatrix}$$

Columns 4 to 8

$$\begin{pmatrix}
0 & \cdots & 0 \\
0 & & \\
0 & \ddots & \vdots \\
0 & & \\
0 & \cdots & 0 \\
1-\underline{\overline{L_1}}+\underline{L_D}+\underline{\overline{V}_B} \quad \underline{\overline{L_1}} \quad \underline{L_R} & 0 & 0 \\
0 \quad 0 \quad 0 & \underline{\rho_w c_{p,w}A_w\overline{L_0}} & 0 \\
0 \quad 0 \quad 0 & 0 & \underline{\rho_w c_{p,w}A_w\overline{L_1}} \\
0 \quad 0 \quad 0 & 0 & 0 \\
\vdots & \vdots & \vdots \\
0 \quad 0 \quad 0 & 0 & 0
\end{pmatrix}$$

Colums 9 to 16

$$\begin{pmatrix}
0 & \cdots & 0 \\
0 & & \\
0 & & \\
0 & \ddots & \vdots \\
0 & & \\
0 & & \\
0 & & \\
0 & \cdots & 0 \\
1\ 0\ 0 & 0\ 0\ 0\ 0 & 0 \\
0\ 1\ 0 & 0\ 0\ 0\ 0 & 0 \\
0\ 0\ 1 & 0\ 0\ 0\ 0 & 0 \\
0\ 0\ 0 & 1\ 0\ 0\ 0 & 0 \\
0\ 0\ 0 & 0\ 1\ 0\ 0 & 0 \\
0\ 0\ 0 & 0\ 0\ 1\ 0 & 0 \\
0\ 0\ 0 & 0\ 0\ 0\ 1 & 0 \\
0\ 0\ 0 & 0\ 0\ 0\ 0 & \underline{\tau}
\end{pmatrix}$$

Column 1

$$\begin{pmatrix} \frac{1}{h_{pc}} \\ -\frac{1}{h_{pc}} \\ 0 \\ \frac{P_{in}}{D_H}\left(\widehat{Nu_1}\,\overline{\lambda}_{f1}^{0.34}\left(\overline{T}_{w,1}-\overline{T_1}\right)-\widehat{Nu_0}\,\overline{\lambda}_{f0}^{0.34}\left(\overline{T}_{w,0}-\overline{T_0}\right)\right) \\ 0 \\ \frac{1}{2}\left(\frac{f_0 v_0}{D_H}-\frac{f_1 \overline{v}_1}{D_H}\right)+\frac{1}{N_{Fr} v_0}-\frac{1}{N_{Fr}\overline{v}_1} \\ \frac{\widehat{Nu_0}\,\overline{\lambda}_{f0}^{0.34}\frac{P_{in}}{D_H}\left(\overline{T}_{w,0}-T_0\right)-1}{1-\widehat{Nu_1}\,\overline{\lambda}_{f1}^{0.34}\frac{P_{in}}{D_H}\left(\overline{T}_{w,1}-\overline{T_1}\right)} \\ 0 \\ \vdots \\ 0 \end{pmatrix}$$

Column 2

$$\begin{pmatrix} 0 \\ 0 \\ 0 \\ -\left(\widehat{Nu_1}\frac{P_{in}\overline{L}_1}{D_H}\left(\left(2\alpha_1\left(\overline{H}_1-h_{pc}\right)+\frac{1}{c_{p,pc}}\right)\overline{\lambda}_{f1}^{-0.34}+0.34\left(\overline{T}_{w,1}-\overline{T_1}\right)\overline{\lambda}_{f1}^{-0.66}\beta_1\lambda_z e^{-\beta_1\overline{H}_1}\right)+1\right) \\ 1 \\ \left(-\frac{1}{2}\left(\frac{f_1\overline{L}_1}{D_H}+K_1\right)+\frac{\overline{L}_1}{N_{Fr}\overline{v}_R^2}\right)\frac{C_1 N_{\Delta h} h_{pc}}{vpc} \\ 0 \\ \widehat{Nu_1}\frac{P_{in}\overline{L}_1}{D_H}\left(\left(2\alpha_1\left(\overline{H}_1-h_{pc}\right)+\frac{1}{c_{p,pc}}\right)\overline{\lambda}_{f1}^{-0.34}+0.34\left(\overline{T}_{w,1}-\overline{T_1}\right)\overline{\lambda}_{f1}^{-0.66}\beta_1\lambda_z e^{-\beta_1\overline{H}_1}\right) \\ -\frac{C_2 N_{\Delta h} h_{pc}\alpha_r \overline{L}_1 \overline{n}}{v_{pc}\Lambda\overline{v}_1^2} \\ 0 \\ \vdots \\ 0 \end{pmatrix}$$

Column 3

$$\begin{pmatrix} 0 \\ 0 \\ 0 \\ 0 \\ -1 \\ \left(-\frac{1}{2}\left(\frac{f_R\overline{L}_R}{D_H}+K_R\right)+\frac{\overline{L}_R}{N_{Fr}\overline{v}_R^2}\right)\frac{C_1 N_{\Delta h} h_{pc}}{vpc} \\ 0 \\ \vdots \\ 0 \end{pmatrix}$$

Columns 4, 5

$$\begin{pmatrix} 1-\frac{H_{in}}{h_{pc}} & 0 \\ \frac{H_{in}}{h_{pc}} & -1 \\ 0 & 1 \\ \frac{H_{in}}{\overline{H}_1} & -\frac{\overline{H}_1}{\overline{H}_1} \\ -\left(\left(\frac{f_0\overline{L}_0}{D_H}+K_0\right)\overline{v}_0\left(\frac{f_D\overline{L}_D}{D_H}+K_D\right)\overline{v_{in}}-v_{in}\right) & -\left(\frac{f_1\overline{L}_1}{D_H}+K_1\right)\overline{v}_1 \\ 0 & 0 \\ \vdots & \vdots \\ 0 & 0 \end{pmatrix}$$

Columns 6, 7, 8

$$\begin{pmatrix}
0 & 0 & 0 \\
0 & 0 & 0 \\
-1 & 0 & 0 \\
0 & \underline{\widehat{Nu_0}\overline{\lambda}_{f0}^{0.34}\frac{P_{in}\overline{L}_0}{\overline{D_H}}} & \underline{\widehat{Nu_1}\overline{\lambda}_{f1}^{0.34}\frac{P_{in}\overline{L}_1}{\overline{D_H}}} \\
-\underline{\overline{H}_R} & 0 & 0 \\
-\left(\underline{\frac{f_R\overline{L}_R}{\overline{D_H}}} + K_R + \underline{\frac{v_{in}}{\overline{v}_R}}\right)\underline{\overline{v}_R} & 0 & 0 \\
0 & -\left(\underline{\widehat{Nu_0}\overline{\lambda}_{f0}^{0.34}\frac{P_{in}\overline{L}_0}{\overline{D_H}}} + 2\underline{\lambda_w A_w}\right) & 2\underline{\lambda_w A_w} \\
0 & 2\underline{\lambda_w A_w} & -\left(\underline{\widehat{Nu_1}\overline{\lambda}_{f1}^{0.34}\frac{P_{in}\overline{L}_1}{\overline{D_H}}} + 2\underline{\lambda_w A_w}\right) \\
0 & 0 & 0 \\
\vdots & \vdots & \vdots \\
0 & 0 & 0
\end{pmatrix}$$

Columns 9 to 16

$$\begin{pmatrix}
0 & \cdots & 0 \\
0 & & \\
0 & \ddots & \vdots \\
0 & & \\
0 & & \\
0 & & 0 \\
0 & \cdots & 0 \quad 1-\underline{L_1} \\
0 & \cdots & 0 \quad \underline{L_1} \\
-\frac{\beta}{\Lambda} & \underline{\lambda_1} \quad \underline{\lambda_2} \quad \underline{\lambda_3} \quad \underline{\lambda_4} \quad \underline{\lambda_5} \quad \underline{\lambda_6} & 0 \\
\frac{\beta_1}{\Lambda} & -\underline{\lambda_1} \quad 0 \quad 0 \quad 0 \quad 0 \quad 0 & 0 \\
\frac{\beta_2}{\Lambda} & 0 \quad -\underline{\lambda_2} \quad 0 \quad 0 \quad 0 \quad 0 & 0 \\
\frac{\beta_3}{\Lambda} & 0 \quad 0 \quad -\underline{\lambda_3} \quad 0 \quad 0 \quad 0 & 0 \\
\frac{\beta_4}{\Lambda} & 0 \quad 0 \quad 0 \quad -\underline{\lambda_4} \quad 0 \quad 0 & 0 \\
\frac{\beta_5}{\Lambda} & 0 \quad 0 \quad 0 \quad 0 \quad -\underline{\lambda_5} \quad 0 & 0 \\
\frac{\beta_6}{\Lambda} & 0 \quad 0 \quad 0 \quad 0 \quad 0 \quad -\underline{\lambda_6} & 0 \\
\underline{\Sigma_f E_f V_f v_n} & 0 \quad 0 \quad 0 \quad 0 \quad 0 \quad 0 & -1
\end{pmatrix}$$

B

Balance equations (Krijger, 2013 and Lippens, 2014)

This thesis is based on research conducted by Krijger in 2013, Lippens in 2014 and Zonneveld in 2015. Krijger set up the initial system of balances that was extended by the two others. The balance equations are given in this appendix.

The underlined text shows which equation pertains to which node. M refers to a mass balance, E to an energy balance, and I to the momentum balance. There is only a single momentum balance for the entire loop, but the mass and energy balances are specified for each node individually. This is indicated by the inclusion of a letter or digit specifying which node the equation governs. A key for which character refers to which node is included in the nomenclature, under *Subscripts*.

As before, the dimensionless variant of variable X is denoted $\underline{X}$, the steady-state value $\overline{X}$, and the perturbation $\check{x}$.

B.1. Transport balances – low heating model

$$\underline{\text{M0:}} \quad AL\frac{\mathrm{d}}{\mathrm{d}t}\rho_0 = W_0 - W_{out} \tag{B.1}$$

$$\underline{\text{MR:}} \quad AL_R\frac{\mathrm{d}}{\mathrm{d}t}\rho_R = W_{out} - W_R \tag{B.2}$$

$$\underline{\text{MB:}} \quad \rho_{in}\frac{\mathrm{d}}{\mathrm{d}t}V_B = W_R - W_0 \tag{B.3}$$

$$\underline{\text{E0:}} \quad AL\frac{\mathrm{d}}{\mathrm{d}t}\rho_0 H_0 = W_0 H_{in} - W_{out}H_{out} + \frac{Nu_0\lambda_{f,0}}{D_H}P_{in}L(T_w - T_0) \tag{B.4}$$

$$\underline{\text{ER:}} \quad AL_R\frac{\mathrm{d}}{\mathrm{d}t}\rho_R H_R = W_{out}H_{out} - W_R H_R \tag{B.5}$$

$$\begin{aligned}\underline{\text{I:}} \quad & AL\frac{\mathrm{d}}{\mathrm{d}t}W_0 + AL_R\frac{\mathrm{d}}{\mathrm{d}t}W_R + \frac{\mathrm{d}}{\mathrm{d}t}V_B W_0 + AL_D\frac{\mathrm{d}}{\mathrm{d}t}W_0 = \cdots \\ & \cdots - \left(\frac{f_0 L}{D_H} + K_0\right)\frac{W_0^2}{2\rho_0} - \left(\frac{f_R L_R}{D_H} + K_R\right)\frac{W_R^2}{2\rho_R}\cdots \\ & \cdots - \left(\frac{f_D L_D}{D_H} + K_D\right)\frac{W_0^2}{2\rho_{in}} - A^2 g\rho_0 L - A^2 g\rho_R L_R - A^2 g\rho_{in}L_D\end{aligned} \tag{B.6}$$

$$\underline{\text{EF:}} \quad \tau\frac{\partial}{\partial t}\frac{Q''_w(t)}{\overline{Q''_w}} + \frac{Q''_w(t) - \overline{Q''_w}}{\overline{Q''_w}} = \frac{Q(t) - \overline{Q}}{\overline{Q}} \tag{B.7}$$

$$\underline{\text{Ew:}} \quad \rho_w c_{p,w} A_w L\frac{\mathrm{d}}{\mathrm{d}t}T_w = Q_w - \frac{Nu_0\lambda_f}{D_H}P_{in}L(T_w - T_0) \tag{B.8}$$

$$\underline{\text{n:}} \quad \frac{\mathrm{d}}{\mathrm{d}t}n(t) = \frac{\mathscr{R}(t) - \beta}{\Lambda}n(t) + \sum_{i=1}^{6}\lambda_i C_i(t) \tag{B.9}$$

$$\underline{\text{C}_\text{i}\text{:}} \quad \frac{\mathrm{d}}{\mathrm{d}t}C_i(t) = \frac{\beta_i}{\Lambda}n(t) - \lambda_i C_i(t), \quad \text{for } i = 1\ldots6 \tag{B.10}$$

(B.11)

B.2. Transport balances – high heating model

$$\underline{\text{M0:}} \quad A\rho_0 \frac{\mathrm{d}}{\mathrm{d}t} L_0 = W_0 - W_{pc} \tag{B.12}$$

$$\underline{\text{M1:}} \quad A \frac{\mathrm{d}}{\mathrm{d}t} \rho_1 L_1 = W_{pc} - W_1 \tag{B.13}$$

$$\underline{\text{MR:}} \quad AL_R \frac{\mathrm{d}}{\mathrm{d}t} \rho_R = W_1 - W_R \tag{B.14}$$

$$\underline{\text{MB:}} \quad \rho_{in} \frac{\mathrm{d}}{\mathrm{d}t} V_B = W_R - W_0 \tag{B.15}$$

$$\underline{\text{E0:}} \quad A\rho_0 H_0 \frac{\mathrm{d}}{\mathrm{d}t} L_0 = W_0 H_{in} - W_{pc} H_{pc} + \frac{Nu_0 \lambda_f}{D_H} P_{in} L_0 (T_w, 0 - T_0) \tag{B.16}$$

$$\underline{\text{E1:}} \quad A \frac{\mathrm{d}}{\mathrm{d}t} \rho_1 L_1 H_1 = W_{pc} H_{pc} - W_1 H_1 + \frac{Nu_1 \lambda_f}{D_H} P_{in} L_1 (T_w, 1 - T_1) \tag{B.17}$$

$$\underline{\text{ER:}} \quad AL_R \frac{\mathrm{d}}{\mathrm{d}t} \rho_R H_R = W_1 H_1 - W_R H_R \tag{B.18}$$

$$\begin{aligned} \underline{\text{I:}} \quad & A \frac{\mathrm{d}}{\mathrm{d}t} W_0 L_0 + A \frac{\mathrm{d}}{\mathrm{d}t} W_1 L_1 + AL_R \frac{\mathrm{d}}{\mathrm{d}t} W_R + \frac{\mathrm{d}}{\mathrm{d}t} V_B W_0 + AL_D \frac{\mathrm{d}}{\mathrm{d}t} W_0 = \cdots \\ & \cdots - \left(\frac{f_0 L_0}{D_H} + K_0 \right) \frac{W_0^2}{2\rho_0} - \left(\frac{f_1 L_1}{D_H} + K_1 \right) \frac{W_1^2}{2\rho_1} - \left(\frac{f_R L_R}{D_H} + K_R \right) \frac{W_R^2}{2\rho_R} \cdots \\ & \cdots - \left(\frac{f_D L_D}{D_H} + K_D \right) \frac{W_0^2}{2\rho_{in}} - A^2 g \rho_0 L_0 - A^2 g \rho_1 L_1 \cdots \\ & \cdots - A^2 g \rho_R L_R - A^2 g \rho_{in} L_D \end{aligned} \tag{B.19}$$

$$\begin{aligned} \underline{\text{Ew0:}} \quad & \rho_w c_{p,w} A_w \frac{\mathrm{d}}{\mathrm{d}t} L_0 T_{w,0} = Q_w \frac{L_0}{L} - \frac{Nu_0 \lambda_f}{D_H} P_{in} L_0 (T_{w,0} - T_0) \cdots \\ & \cdots \frac{2\lambda_w}{L} A_w (T_{w,1} - T_{w,0}) \end{aligned} \tag{B.20}$$

$$\begin{aligned} \underline{\text{Ew1:}} \quad & \rho_w c_{p,w} A_w \frac{\mathrm{d}}{\mathrm{d}t} L_1 T_{w,1} = Q_w \frac{L_1}{L} - \frac{Nu_1 \lambda_f}{D_H} P_{in} L_1 (T_{w,1} - T_1) \cdots \\ & \cdots \frac{2\lambda_w}{L} A_w (T_{w,1} - T_{w,0}) \end{aligned} \tag{B.21}$$

$$\underline{\text{n:}} \quad \frac{\mathrm{d}}{\mathrm{d}t} n(t) = \frac{\frac{L_1}{L} \mathscr{R}(t) - \beta}{\Lambda} n(t) + \sum_{i=1}^{6} \lambda_i C_i(t) \tag{B.22}$$

$$\tag{B.23}$$

B.3. Dimensionless balances – low heating model

$$\underline{\text{M0:}} \quad \frac{\mathrm{d}}{\mathrm{d}\underline{t}}\underline{\rho_0} = \underline{W_0} - \underline{L_R}\frac{\mathrm{d}}{\mathrm{d}\underline{t}}\underline{\rho_R} - \underline{W_R} \tag{B.24}$$

$$\begin{aligned}\underline{\text{E0:}} \quad & \frac{\mathrm{d}}{\mathrm{d}\underline{t}}\underline{\rho_0 H_0} = \underline{W_0 H_{in}} - \underline{H_{out}}\left(\underline{L_R}\frac{\mathrm{d}}{\mathrm{d}\underline{t}}\underline{\rho_R} + \underline{W_R}\right)\cdots \\ & + \underline{\widehat{Nu_0}\lambda_{f0}^{0.34}}\frac{\underline{P_{in}}}{\underline{D_H}}\left(\underline{T_w} - \underline{T_{pc}} - \underline{\alpha_0}\left(\underline{H_0} - h_{pc}\right)^2\cdots\right. \\ & \left.\cdots - \frac{1}{\underline{c_{p,pc}}}\left(\underline{H_0} - h_{pc}\right)\right)\end{aligned} \tag{B.25}$$

$$\underline{\text{ER:}} \quad \underline{L_R}\frac{\mathrm{d}}{\mathrm{d}\underline{t}}\underline{\rho_R H_R} = \underline{H_{out}}\left(\underline{L_R}\frac{\mathrm{d}}{\mathrm{d}\underline{t}}\underline{\rho_R} + \underline{W_R}\right) - \underline{W_R H_R} \tag{B.26}$$

$$\begin{aligned}\underline{\text{I:}} \quad & \frac{\mathrm{d}}{\mathrm{d}\underline{t}}\underline{W_0} + \underline{L_R}\frac{\mathrm{d}}{\mathrm{d}\underline{t}}\underline{W_R} + \underline{V_B}\frac{\mathrm{d}}{\mathrm{d}\underline{t}}\underline{W_0} + \underline{L_D}\frac{\mathrm{d}}{\mathrm{d}\underline{t}}\underline{W_0} = \\ & - \underline{W_0}\frac{\underline{W_R} - \underline{W_0}}{\underline{\rho_{in}}} - \left(\frac{f_0}{\underline{D_H}} + K_0\right)\frac{\underline{W_0^2}}{2\underline{\rho_0}} - \left(\frac{\underline{f_R}\underline{L_R}}{\underline{D_H}} + K_R\right)\frac{\underline{W_R^2}}{2\underline{\rho_R}}\cdots \\ & \cdots - \left(\frac{\underline{f_D}\underline{L_D}}{\underline{D_H}} + K_D\right)\frac{\underline{W_0^2}}{2\underline{\rho_{in}}} - \frac{\underline{\rho_0}\underline{L_0}}{\underline{N_{Fr}}} - \frac{\underline{\rho_R}\underline{L_R}}{\underline{N_{Fr}}} + \frac{\underline{\rho_{in}}\underline{L_D}}{\underline{N_{Fr}}}\end{aligned} \tag{B.27}$$

$$\begin{aligned}\underline{\text{Ew:}} \quad & \underline{\rho_w c_{p,w} A_w}\frac{\mathrm{d}}{\mathrm{d}\underline{t}}\underline{T_w} = \underline{Q_w} - \underline{\widehat{Nu_0}\lambda_{f0}^{0.34}}\frac{\underline{P_{in}}}{\underline{D_H}}\left(\underline{T_w} - \underline{T_{pc}}\cdots\right. \\ & \left.\cdots - \underline{\alpha_0}\left(\underline{H_0} - h_{pc}\right)^2 - \frac{1}{\underline{c_{p,pc}}}\left(\underline{H_0} - h_{pc}\right)\right)\end{aligned} \tag{B.28}$$

$$\underline{\text{EF:}} \quad \underline{\tau}\frac{\partial}{\partial\underline{t}}\underline{Q_w''} = \underline{\Sigma_f E_f V_f \nu_n n} - \underline{Q_w''} \tag{B.29}$$

$$\underline{\text{n:}} \quad \frac{\mathrm{d}}{\mathrm{d}\underline{t}}\underline{n} = \frac{\mathscr{R} - \beta}{\underline{\Lambda}}\underline{n} + \sum_{i=1}^{6}\underline{\lambda_i C_i} \tag{B.30}$$

$$\underline{\text{C}_\text{i}:} \quad \frac{\mathrm{d}}{\mathrm{d}\underline{t}}\underline{C_i} = \frac{\beta_i}{\underline{\Lambda}}\underline{n} - \underline{\lambda_i C_i} \tag{B.31}$$

B.4. Dimensionless balances – high heating model

$$\underline{\text{M0:}} \quad \underline{\rho_0}\left(\frac{\underline{\underline{H_0}}}{\underline{h_{pc}}}-1\right)\frac{\mathrm{d}}{\mathrm{d}\underline{t}}\underline{L_1}=\left(1-\frac{\underline{\underline{H_{in}}}}{\underline{h_{pc}}}\right)\underline{W_0}-\frac{1}{\underline{h_{pc}}}(1-\underline{L_1}) \tag{B.32}$$

$$\underline{\text{M1:}} \quad \left(\underline{\rho_1}-\frac{\underline{\underline{H_0}}}{\underline{h_{pc}}}\underline{\rho_0}\right)\frac{\mathrm{d}}{\mathrm{d}\underline{t}}\underline{L_1}+\underline{L_1}\frac{\mathrm{d}}{\mathrm{d}\underline{t}}\underline{\rho_1}=\frac{\underline{\underline{H_{in}}}}{\underline{h_{pc}}}\underline{W_0}+\frac{1}{\underline{h_{pc}}}(1-\underline{L_1})-\underline{W_1} \tag{B.33}$$

$$\underline{\text{MR:}} \quad \underline{L_R}\frac{\mathrm{d}}{\mathrm{d}\underline{t}}\underline{\rho_R}=\underline{W_1}-\underline{W_R} \tag{B.34}$$

$$\begin{aligned}\underline{\text{E1:}} \quad & \underline{L_1}\frac{\mathrm{d}}{\mathrm{d}\underline{t}}\underline{\rho_1 H_1}+(\underline{\rho_1 H_1}-\underline{\rho_0 H_0})\frac{\mathrm{d}}{\mathrm{d}\underline{t}}\underline{L_1}=\underline{W_0 H_{in}}-\underline{W_1 H_1}\cdots\\ & \cdots+\underline{\widehat{Nu_0}\lambda_{f0}^{0.34}}\frac{\underline{\underline{P_{in}}}(1-\underline{L_1})}{\underline{D_H}}\left(\underline{T_{w,0}}-\underline{T_{pc}}-\underline{\alpha_0}\left(\underline{H_0}-h_{pc}\right)^2\cdots\right.\\ & \left.\cdots-\frac{1}{\underline{c_{p,pc}}}\left(\underline{H_0}-h_{pc}\right)\right)\cdots\\ & \cdots+\underline{\widehat{Nu_1}\lambda_{f1}^{0.34}}\frac{\underline{\underline{P_{in}}}\underline{L_1}}{\underline{D_H}}\left(\underline{T_{w,1}}-\underline{T_{pc}}-\underline{\alpha_1}\left(\underline{H_1}-h_{pc}\right)^2\cdots\right.\\ & \left.\cdots-\frac{1}{\underline{c_{p,pc}}}\left(\underline{H_1}-h_{pc}\right)\right)\end{aligned} \tag{B.35}$$

$$\underline{\text{ER:}} \quad \underline{L_R}\frac{\mathrm{d}}{\mathrm{d}\underline{t}}\underline{\rho_R H_R}=\underline{W_1 H_1}-\underline{W_R H_R} \tag{B.36}$$

$$\begin{aligned}\underline{\text{I:}} \quad & -\underline{W_0}\frac{\mathrm{d}}{\mathrm{d}\underline{t}}\underline{L_1}+(1-\underline{L_1})\frac{\mathrm{d}}{\mathrm{d}\underline{t}}\underline{W_0}+\frac{\mathrm{d}}{\mathrm{d}\underline{t}}\underline{W_1 L_1}+\underline{L_R}\frac{\mathrm{d}}{\mathrm{d}\underline{t}}\underline{W_R}+\underline{V_B}\frac{\mathrm{d}}{\mathrm{d}\underline{t}}\underline{W_0}+\underline{L_D}\frac{\mathrm{d}}{\mathrm{d}\underline{t}}\underline{W_0}=\cdots\\ & -\underline{W_0}\frac{\underline{\underline{W_R}}-\underline{W_0}}{\underline{\rho_{in}}}-\left(\frac{f_0\underline{L_0}}{\underline{D_H}}+K_0\right)\frac{\underline{\underline{W_0^2}}}{2\underline{\rho_0}}-\left(\frac{f_1\underline{L_1}}{\underline{D_H}}+K_1\right)\frac{\underline{\underline{W_1^2}}}{2\underline{\rho_1}}\cdots\\ & \cdots-\left(\frac{f_R\underline{L_R}}{\underline{D_H}}+K_R\right)\frac{\underline{\underline{W_R^2}}}{2\underline{\rho_R}}-\left(\frac{f_D\underline{L_D}}{\underline{D_H}}+K_D\right)\frac{\underline{\underline{W_0^2}}}{2\underline{\rho_{in}}}\cdots\\ & \cdots-\frac{\underline{\underline{\rho_0 L_0}}}{N_{Fr}}-\frac{\underline{\underline{\rho_1 L_1}}}{N_{Fr}}-\frac{\underline{\underline{\rho_R L_R}}}{N_{Fr}}+\frac{\underline{\underline{\rho_{in} L_D}}}{N_{Fr}}\end{aligned} \tag{B.37}$$

$$\begin{aligned}\underline{\text{Ew0:}} \quad & \underline{\rho_w c_{p,w} A_w}\left(1-\underline{L_1}\right)\frac{\mathrm{d}}{\mathrm{d}\underline{t}}\underline{T_{w,0}}-\underline{\rho_w c_{p,w} A_w T_{w,0}}\frac{\mathrm{d}}{\mathrm{d}\underline{t}}\underline{L_1}=\underline{Q_w}-\underline{L_1}\cdots\\ & \cdots-\underline{\widehat{Nu_0}\lambda_{f0}^{0.34}}\frac{\underline{\underline{P_{in}}}\,(1-\underline{L_1})}{\underline{D_H}}\left(\underline{T_{w,0}}-\underline{T_{pc}}-\underline{\alpha_0}\left(\underline{H_0}-h_{pc}\right)^2\cdots\right.\\ & \left.\cdots-\frac{1}{\underline{c_{p,pc}}}\left(\underline{H_0}-h_{pc}\right)\right)+2\underline{\lambda_w A_w}\left(\underline{T_{w,1}}-\underline{T_{w,0}}\right)\end{aligned} \tag{B.38}$$

$$\begin{aligned}\underline{\text{Ew1:}} \quad & \underline{\rho_w c_{p,w} A_w L_1}\frac{\mathrm{d}}{\mathrm{d}\underline{t}}\underline{T_{w,1}}+\underline{\rho_w c_{p,w} A_w T_{w,1}}\frac{\mathrm{d}}{\mathrm{d}\underline{t}}\underline{L_1}=\underline{Q_w}+\underline{L_1}\cdots\\ & \cdots-\underline{\widehat{Nu_1}\lambda_{f1}^{0.34}}\frac{\underline{\underline{P_{in}}}\underline{L_1}}{\underline{D_H}}\left(\underline{T_{w,1}}-\underline{T_{pc}}-\underline{\alpha_1}\left(\underline{H_1}-h_{pc}\right)^2\cdots\right.\\ & \left.\cdots-\frac{1}{\underline{c_{p,pc}}}\left(\underline{H_1}-h_{pc}\right)\right)-2\underline{\lambda_w A_w}\left(\underline{T_{w,1}}-\underline{T_{w,0}}\right)\end{aligned} \tag{B.39}$$

$$\underline{\text{n:}} \quad \frac{\mathrm{d}}{\mathrm{d}\underline{t}}\underline{n}=\frac{\underline{\underline{L_1\mathscr{R}}}-\beta}{\underline{\Lambda}}\underline{n}+\sum_{i=1}^{6}\underline{\lambda_i C_i} \tag{B.40}$$

B.5. Linearised balances – low heating model

$$\underline{\text{M0:}} \quad C_1 N_{\Delta h} h_{pc} v_{pc} \left(\frac{1}{2} \frac{\mathrm{d}}{\mathrm{d}\underline{t}} \check{h}_{out} + \underline{L_R} \frac{\mathrm{d}}{\mathrm{d}\underline{t}} \check{h}_R \right) = \underline{\check{w}_0} - \underline{\check{w}_R} \tag{B.41}$$

$$\begin{aligned} \underline{\text{E0:}} \quad & \left(\frac{1}{2} \underline{\overline{\rho}_0} + \frac{1}{2} C_1 N_{\Delta h} h_{pc} v_{pc} \underline{\overline{H}_0} \right) \frac{\mathrm{d}}{\mathrm{d}\underline{t}} \underline{\check{h}_{out}} + C_1 N_{\Delta h} h_{pc} v_{pc} \underline{\overline{H}_{out} L_R} \frac{\mathrm{d}}{\mathrm{d}\underline{t}} \underline{\check{h}_R} = \\ & - \underline{\check{w}_R \overline{H}_{out}} + \underline{\check{w}_0 \overline{H}_{in}} + \underline{\widehat{Nu_0} \overline{\lambda}_{f0}^{-0.34}} \frac{\overline{P_{in}}}{\underline{D_H}} \underline{\check{\theta}_w} \cdots \\ & \cdots - \left(\underline{\widehat{Nu_0}} \frac{\overline{P_{in}}}{\underline{D_H}} \left(\left(\underline{\alpha_0} \left(\underline{H_0} - \underline{h_{pc}} \right) + \frac{1}{2 \underline{c_{p,pc}}} \right) \underline{\overline{\lambda}_{f0}^{-0.34}} \cdots \right. \right. \\ & \left. \left. \cdots - 0.17 \underline{\overline{\lambda}_{f0}^{-0.66}} \left(\underline{\overline{T}_w} - \underline{\overline{T}_0} \right) \underline{\beta_0} \right) + 1 \right) \underline{\check{h}_{out}} \end{aligned} \tag{B.42}$$

$$\begin{aligned} \underline{\text{ER:}} \quad & \left(\underline{L_R \overline{\rho}_R} - \underline{L_R} C_1 N_{\Delta h} h_{pc} v_{pc} (\underline{\overline{H}_R} - \underline{\overline{H}_{out}}) \right) \frac{\mathrm{d}}{\mathrm{d}\underline{t}} \underline{\check{h}_R} = \\ & \underline{\check{h}_{out}} + \underline{\overline{H}_{out}} \underline{\check{w}_R} - \underline{\check{h}_R} - \underline{\check{w}_R \overline{H}_R} \end{aligned} \tag{B.43}$$

$$\begin{aligned} \underline{\text{I:}} \quad & (1 + \underline{L_D} + \underline{V_B}) \frac{\mathrm{d}}{\mathrm{d}\underline{t}} \underline{\check{w}_0} + \underline{L_R} \frac{\mathrm{d}}{\mathrm{d}\underline{t}} \underline{\check{w}_R} = - \left(\left(\frac{f_R \underline{L_R}}{\underline{D_H}} + K_R \right) \underline{\overline{v_R}} + \underline{v_{in}} \right) \underline{\check{w}_R} \cdots \\ & \cdots + \frac{1}{2} C_1 N_{\Delta h} h_{pc} v_{pc} \left(\frac{1}{2} \left(\frac{f_0}{\underline{D_H}} + K_0 \right) \frac{1}{\underline{\overline{\rho}_0^2}} - \frac{1}{N_{Fr}} \right) \underline{\check{h}_{out}} \cdots \\ & \cdots + C_1 N_{\Delta h} h_{pc} v_{pc} \left(\frac{1}{2} \left(\frac{f_R \underline{L_R}}{\underline{D_H}} + K_R \right) \frac{1}{\underline{\overline{\rho}_R^2}} - \frac{\underline{L_R}}{N_{Fr}} \right) \underline{\check{h}_R} \cdots \\ & \cdots \left(\underline{v_{in}} - \left(\frac{f_0}{\underline{D_H}} + K_0 \right) \underline{\overline{v}_0} - \left(\frac{f_D \underline{L_D}}{\underline{D_H}} + K_D \right) \underline{v_{in}} \right) \underline{\check{w}_0} \end{aligned} \tag{B.44}$$

$$\begin{aligned} \underline{\text{Ew:}} \quad & \underline{\rho_w c_{p,w} A_w} \frac{\mathrm{d}}{\mathrm{d}\underline{t}} \underline{\check{\theta}_w} = \underline{\check{q}_w} - \underline{\widehat{Nu_0} \overline{\lambda}_{f0}^{-0.34}} \frac{\overline{P_{in}}}{\underline{D_H}} \underline{\check{\theta}_w} \cdots \\ & \cdots + \frac{1}{2} \underline{\widehat{Nu_0}} \frac{\overline{P_{in}}}{\underline{D_H}} \left(\underline{\overline{\lambda}_{f0}^{-0.34}} \left(2 \underline{\alpha_0} \left(\underline{H_0} - \underline{h_{pc}} \right) + \frac{1}{\underline{c_{p,pc}}} \right) \cdots \right. \\ & \left. \cdots - 0.34 \underline{\overline{\lambda}_{f0}^{-0.66}} \left(\underline{\overline{T}_w} - \underline{\overline{T}_0} \right) \underline{\beta_0} \right) \underline{\check{h}_{out}} \end{aligned} \tag{B.45}$$

$$\underline{\text{EF:}} \quad \underline{\tau} \frac{\partial}{\partial \underline{t}} \underline{\check{q}_w} = \underline{\Sigma_f E_f V_f \nu_n \check{n}} - \underline{\check{q}_w} \tag{B.46}$$

$$\underline{\text{n:}} \quad \frac{\mathrm{d}}{\mathrm{d}\underline{t}} \underline{\check{n}} = \frac{\underline{\alpha_r \overline{n}} C_1 N_{\Delta h} h_{pc} v_{pc} \underline{\check{h}_0} - \beta \underline{\check{n}}}{\underline{\Lambda}} + \sum_{i=1}^{6} \underline{\lambda_i \check{C}_i} \tag{B.47}$$

$$\underline{\text{C}_\text{i}:} \quad \frac{\mathrm{d}}{\mathrm{d}\underline{t}} \underline{\check{C}_i} = \frac{\underline{\beta_i}}{\underline{\Lambda}} \underline{\check{n}} - \underline{\lambda_i \check{C}_i} \tag{B.48}$$

(B.49)

B.6. Linearised balances – high heating model

$$\underline{\text{M0:}} \quad \underline{\rho_0}\left(\frac{\underline{\overline{H_0}}}{\underline{h_{pc}}}-1\right)\frac{\mathrm{d}}{\mathrm{d}\underline{t}}\underline{\check{l}_1}=\left(1-\frac{\underline{\overline{H_{in}}}}{\underline{h_{pc}}}\right)\underline{\check{w}_0}+\frac{1}{\underline{h_{pc}}}\underline{\check{l}_1} \tag{B.50}$$

$$\underline{\text{M1:}} \quad \left(\frac{1}{\underline{\overline{v}_1}}-\frac{\underline{H_0}}{\underline{h_{pc}}}\underline{\rho_0}\right)\frac{\mathrm{d}}{\mathrm{d}\underline{t}}\underline{\check{l}_1}-\frac{\underline{\overline{L}_1}C_1N_{\Delta h}h_{pc}}{\nu pc\underline{\overline{v}_1^2}}\frac{\mathrm{d}}{\mathrm{d}\underline{t}}\underline{\check{h}_1}=$$
$$\frac{\underline{\overline{H_{in}}}}{\underline{h_{pc}}}\underline{\check{w}_0}-\frac{1}{\underline{h_{pc}}}\underline{\check{l}_1}-\underline{\check{w}_1} \tag{B.51}$$

$$\underline{\text{MR:}} \quad -\frac{\underline{\overline{L}_R}C_1N_{\Delta h}h_{pc}}{\nu pc\underline{\overline{v}_R^2}}\frac{\mathrm{d}}{\mathrm{d}\underline{t}}\underline{\check{h}_R}=\underline{\check{w}_1}-\underline{\check{w}_R} \tag{B.52}$$

$$\underline{\text{E1:}} \quad \frac{\underline{\overline{L}_1}}{\underline{\overline{v}_1}}\left(1-\frac{\underline{\overline{H}_1}C_1N_{\Delta h}h_{pc}}{\nu pc\underline{\overline{v}_1}}\right)\frac{\mathrm{d}}{\mathrm{d}\underline{t}}\underline{\check{h}_1}+\left(\frac{\underline{\overline{H}_1}}{\underline{\overline{v}_1}}-\underline{H_0\rho_0}\right)\frac{\mathrm{d}}{\mathrm{d}\underline{t}}\underline{\check{l}_1}=$$
$$\underline{H_{in}\check{w}_0}-\underline{\overline{H}_1\check{w}_1}+\underline{\widehat{Nu_0}\overline{\lambda}_{f0}^{0.34}}\frac{\underline{P_{in}\overline{L}_0}}{\underline{D_H}}\underline{\check{\theta}_{w,0}}\cdots$$
$$\cdots-\left(\underline{\widehat{Nu_1}}\frac{\underline{P_{in}\overline{L}_1}}{\underline{D_H}}\left(\left(2\underline{\alpha_1}\left(\underline{\overline{H}_1}-\underline{h_{pc}}\right)+\frac{1}{\underline{c_{p,pc}}}\right)\underline{\overline{\lambda}_{f1}^{-0.34}}\cdots\right.\right.$$
$$\left.\cdots+0.34\left(\underline{\overline{T}_{w,1}}-\underline{\overline{T}_1}\right)\underline{\overline{\lambda}_{f1}^{-0.66}\beta_1\lambda_z e^{-\beta_1\overline{H}_1}}\right)+1\Big)\underline{\check{h}_1}\cdots$$
$$\cdots+\underline{\widehat{Nu_1}\overline{\lambda}_{f1}^{0.34}}\frac{\underline{P_{in}\overline{L}_1}}{\underline{D_H}}\underline{\check{\theta}_{w,1}}+\frac{\underline{P_{in}}}{\underline{D_H}}\left(\underline{\widehat{Nu_1}\overline{\lambda}_{f1}^{0.34}}\left(\underline{\overline{T}_{w,1}}-\underline{\overline{T}_1}\right)\cdots\right.$$
$$\left.\cdots-\underline{\widehat{Nu_0}\overline{\lambda}_{f0}^{0.34}}\left(\underline{\overline{T}_{w,0}}-\underline{\overline{T}_0}\right)\right)\underline{\check{l}_1} \tag{B.53}$$

$$\underline{\text{ER:}} \quad \frac{\underline{\overline{L}_R}}{\underline{\overline{v}_R}}\left(1-\frac{\underline{\overline{H}_R}C_1N_{\Delta h}h_{pc}}{\nu pc\underline{\overline{v}_R}}\right)\frac{\mathrm{d}}{\mathrm{d}\underline{t}}\underline{\check{h}_R}=\underline{\check{h}_1}+\underline{\overline{H}_1\check{w}_1}-\underline{\check{h}_R}-\underline{\overline{H}_R\check{w}_R} \tag{B.54}$$

$$\underline{\text{I:}} \quad (1+\underline{\overline{L}_1}+\underline{L_D}+\underline{V_B})\frac{\mathrm{d}}{\mathrm{d}\underline{t}}\underline{\check{w}_0}+\underline{L_1}\frac{\mathrm{d}}{\mathrm{d}\underline{t}}\underline{\check{w}_1}+\underline{L_R}\frac{\mathrm{d}}{\mathrm{d}\underline{t}}\underline{\check{w}_R}=$$
$$\left(\frac{1}{2}\left(\frac{\underline{f_0\upsilon_0}}{\underline{D_H}}-\frac{\underline{f_1\overline{v}_1}}{\underline{D_H}}\right)+\frac{1}{N_{Fr}\underline{\upsilon_0}}-\frac{1}{N_{Fr}\underline{\overline{v}_1}}\right)\underline{\check{l}_1}\cdots$$
$$\cdots-\left(\left(\frac{\underline{f_0\overline{L}_0}}{\underline{D_H}}+K_0\right)\underline{\overline{v}_0}+\left(\frac{\underline{f_D\overline{L}_D}}{\underline{D_H}}+K_D\right)\underline{\overline{v_{in}}-v_{in}}\right)\underline{\check{w}_0}\cdots$$
$$\cdots-\left(\frac{\underline{f_1\overline{L}_1}}{\underline{D_H}}+K_1\right)\underline{\overline{v}_1\check{w}_1}+\left(-\frac{1}{2}\left(\frac{\underline{f_1\overline{L}_1}}{\underline{D_H}}+K_1\right)\cdots\right.$$
$$\left.\cdots+\frac{\underline{\overline{L}_1}}{N_{Fr}\underline{\overline{v}_R^2}}\right)\frac{C_1N_{\Delta h}h_{pc}}{\nu pc}\underline{\check{h}_1}\cdots$$
$$\cdots-\left(\frac{\underline{f_R\overline{L}_R}}{\underline{D_H}}+K_R+\frac{\underline{\upsilon_{in}}}{\underline{\overline{v}_R}}\right)\underline{\overline{v}_R\check{w}_R}+\left(-\frac{1}{2}\left(\frac{\underline{f_R\overline{L}_R}}{\underline{D_H}}+K_R\right)\cdots\right.$$
$$\left.\cdots+\frac{\underline{\overline{L}_R}}{N_{Fr}\underline{\overline{v}_R^2}}\right)\frac{C_1N_{\Delta h}h_{pc}}{\nu pc}\underline{\check{h}_R} \tag{B.55}$$

$$\underline{\text{Ew0:}} \quad \underline{\rho_w c_{p,w}A_w\overline{L}_0}\frac{\mathrm{d}}{\mathrm{d}\underline{t}}\underline{\check{\theta}_{w,0}}-\underline{\rho_w c_{p,w}A_w\overline{T}_{w,0}}\frac{\mathrm{d}}{\mathrm{d}\underline{t}}\underline{\check{l}_1}=$$
$$\left(1-\underline{L_1}\right)\underline{\check{q}_w}+\left(\underline{\widehat{Nu_0}\overline{\lambda}_{f0}^{0.34}}\frac{\underline{P_{in}}}{\underline{D_H}}\left(\underline{\overline{T}_{w,0}}-\underline{T_0}\right)-1\right)\underline{\check{l}_1}\cdots$$
$$\cdots-\left(\underline{\widehat{Nu_0}\overline{\lambda}_{f0}^{0.34}}\frac{\underline{P_{in}\overline{L}_0}}{\underline{D_H}}+2\underline{\lambda_w A_w}\right)\underline{\check{\theta}_{w,0}}+2\underline{\lambda_w A_w\check{\theta}_{w,1}} \tag{B.56}$$

(B.57)

$$
\begin{aligned}
\underline{\text{Ew1:}} \quad & \underline{\rho_w c_{p,w} A_w \overline{L_1}} \frac{\mathrm{d}}{\mathrm{d}\underline{t}} \underline{\check{\theta}_{w,1}} + \underline{\rho_w c_{p,w} A_w \overline{T}_{w,1}} \frac{\mathrm{d}}{\mathrm{d}\underline{t}} \underline{\check{l}_1} = \\
& \underline{L_1 \check{q}_w} + \left(1 - \underline{\widehat{Nu_1}\, \overline{\lambda}_{f1}^{-0.34}} \frac{\underline{P_{in}}}{\underline{D_H}} \left(\underline{\overline{T}_{w,1}} - \underline{\overline{T_1}} \right) \right) \underline{\check{l}_1} \cdots \\
& \cdots + \underline{\widehat{Nu_1}} \frac{\underline{P_{in}} \overline{L}_1}{\underline{D_H}} \left(\left(2\underline{\alpha_1} \left(\underline{\overline{H}_1} - \underline{h_{pc}} \right) + \frac{1}{\underline{c_{p,pc}}} \right) \underline{\overline{\lambda}_{f1}^{-0.34}} \cdots \right. \\
& \cdots + 0.34 \left(\underline{\overline{T}_{w,1}} - \underline{\overline{T_1}} \right) \underline{\overline{\lambda}_{f1}^{-0.66}} \beta_1 \lambda_z e^{-\beta_1 \overline{H}_1} \Big) \underline{\check{h}_1} \cdots \\
& \cdots + 2\underline{\lambda_w A_w \check{\theta}_{w,0}} - \left(\underline{\widehat{Nu_1}\, \overline{\lambda}_{f1}^{-0.34}} \frac{\underline{P_{in}} \overline{L}_1}{\underline{D_H}} + 2\underline{\lambda_w A_w} \right) \underline{\check{\theta}_{w,1}}
\end{aligned} \tag{B.58}
$$

$$
\underline{\text{n:}} \quad \frac{\mathrm{d}}{\mathrm{d}\underline{t}} \underline{\check{n}} = - \frac{C_2 N_{\Delta h} h_{pc} \underline{\alpha_r} \overline{L}_1 \overline{n}}{v_{pc} \underline{\Lambda} \overline{v}_1^2} \underline{\check{h}_1} - \frac{\beta}{\underline{\Lambda}} \underline{\check{n}} + \sum_{i=1}^{6} \underline{\lambda_i \check{C}_i} \tag{B.59}
$$

C

Reference case parameters and constants

Krijger [13] set up a reference case for the model used in this thesis as the baseline for comparison. Lippens [15] and Zonneveld [35] extended the reference case for the thermal inertia of the core wall and the parameters governing the neutronics of the system respectively.

Table C.1: Design parameters for the reference case

PARAMETER	VALUE
Volume buffer vessel	10^{-2}m^3
Riser length	4.2m
Core length	4.2m
Channel hydraulic diameter	$5.6 \cdot 10^{-3}$m
Channel flow area	$3.55 \cdot 10^{-5}$m^2
Wall cross-sectional area	$3.55 \cdot 10^{-5}$m^2
Fuel volume per rod	$1.48 \cdot 10^{-4}$m^3
Inlet pressure loss coefficient	1
Downcomer pressure loss coefficient	1
Riser pressure loss coefficient	20

Table C.2: Material, thermodynamic and neutronic properties for the reference case

PROPERTY	VALUE
Water specific enthalpy, pseudo-critical point	$2.1529 \cdot 10^6$J kg^{-1}
Water specific volume, pseudo-critical point	$3.1564 \cdot 10^{-3}$m^3 kg^{-1}
Water specific heat capacity, pseudo-critical point	$7.6444 \cdot 10^4$ J kg^{-1} K^{-1}
Dynamic viscosity of water	$4.2797 \cdot 10^{-5}$ N s m^{-2}
Fuel density	$10.96 \cdot 10^3$kg m^{-3}
Wall density	$7.850 \cdot 10^3$kg m^{-3}
Wall specific heat capacity	490 J kg^{-1} K^{-1}
Wall thermal conductivity	43 W m^{-1} K^{-1}
Fuel heat transfer time constant	6 s
Energy per fission event	$2.81 \cdot 10^{-11}$J
Fuel enrichment	4% by mass
Neutron velocity	$5.72958 \cdot 10^3$ m s^{-1}

Table C.3: Delayed neutron fractions and decay constants [35]

Table C.3: (continued)

FRACTIONS (%)		DECAY CONSTANTS (s^{-1})	
β_1	0.026	λ_1	0.0127
β_2	0.1459	λ_2	0.0317
β_3	0.1288	λ_3	0.115
β_4	0.2788	λ_4	0.311
β_5	0.0877	λ_5	1.40
β_6	0.0178	λ_6	3.87

D

Test case generalised eigenvalue problem with singular matrix

As coefficient matrix A in equation 3.1 is singular, the number of eigenvalues is not necessarily the same as the size of both matrices. A test case similar to the one presented by Koren [12] in 2010 has been carried out, however this time 3-dimensional matrices were used for A and B within the known equation $A\frac{\mathrm{d}}{\mathrm{d}t}\vec{x} = B\vec{x}$.

$$\begin{bmatrix} 1 & 0 & 0 \\ 1 & 0 & 0 \\ 0 & 1 & 2 \end{bmatrix} \frac{d}{dt} \begin{bmatrix} x_1 \\ x_2 \\ x_3 \end{bmatrix} = \begin{bmatrix} 3 & 0 & 0 \\ 1 & -1 & 1 \\ 1 & 0 & 1 \end{bmatrix} \begin{bmatrix} x_1 \\ x_2 \\ x_3 \end{bmatrix} \tag{D.1}$$

If the system is reduced to $A\lambda\vec{v} = B\vec{v}$, solving the determinant of $(\lambda A - B) = 0$ results in a characteristic polynomial of $3\lambda^2 - 10\lambda + 3 = (\lambda - \frac{1}{3})(\lambda - 3) = 0$, giving two eigenvalues $\lambda_1 = \frac{1}{3}$ and $\lambda_2 = 3$.

The original system can also be written in three differential equations:

$$\dot{x}_1 = 3x_1 \tag{D.2}$$
$$\dot{x}_1 = x_1 - x_2 + x_3 \tag{D.3}$$
$$\dot{x}_2 + 2\dot{x}_3 = x_1 + x_3 \tag{D.4}$$

However, as matrix A is singular, one component of x can easily be expressed in the other two. For example:

$$3x_1 = x_1 - x_2 + x_3 \tag{D.5}$$
$$x_3 = 2x_1 + x_2 \tag{D.6}$$

Substituting this definition for x_3 in the earlier given equations brings the differential equation back to a lower dimension generalised eigenvalue problem:

$$\dot{x}_1 = 3x_1 \tag{D.7}$$
$$\dot{x}_2 + 2\frac{d}{dt}(2x_1 + x_2) = x_1 + (2x_1 + x_2) \tag{D.8}$$

The last line reduces to $4\dot{x}_1 + 3\dot{x}_2 = 3x_1 + x_2$. In matrix notation the system will now look like:

$$\begin{bmatrix} 1 & 0 \\ 4 & 3 \end{bmatrix} \frac{d}{dt} \begin{bmatrix} x_1 \\ x_2 \end{bmatrix} = \begin{bmatrix} 3 & 0 \\ 3 & 1 \end{bmatrix} \begin{bmatrix} x_1 \\ x_2 \end{bmatrix} \tag{D.9}$$

Hereby the system is reduced to a 2 dimensional eigenvalue problem with 2 eigenvalues. This transformation naturally corresponds to bringing the first matrix to its echelon form.

x_1 and x_2 are both a linear combination of the eigenvalues and eigenvectors according to equation 3.6. x_3 is a linear combination of x_1 and x_2 according to equation D.6. Thus x_3 is a linear combination of the same set of eigenvectors and eigenvalues.

To confirm that MATLAB tackles this situation in the same way, the following script was tested:

```
A1=[1 0 0; 1 0 0; 0 1 2];
B1=[3 0 0; 1 -1 1; 1 0 1];
lambda1=eig(B1,A1)
A2=[1 0; 4 3];
B2=[3 0; 3 1];
lambda2=eig(B2,A2)
```

Proving the assumption, MATLAB returned λ_1 and λ_2 as the following.

$$\lambda_1 = \begin{bmatrix} 0.3333 \\ Inf \\ 3.0000 \end{bmatrix} \tag{D.10}$$

$$\lambda_2 = \begin{bmatrix} 0.3333 \\ 3.0000 \end{bmatrix} \tag{D.11}$$

As x_3 is a linear combination of x_1 and x_2, it is composed out the eigenvalues found by the smaller matrix equation only. This test case again confirms that the $\lambda = \infty$ returned by MATLAB can be neglected in stability research. The time-dependent solutions can be formed by all finite eigenvalues returned by MATLAB.

Bibliography

[1] W. Ambrosini. Flow stability of heated channels with supercritical pressure fluids. 2011.

[2] P. A. M. Boomkamp. *Stability of Parallel Two-Phase Flow*. 1998. ISBN 9036510767.

[3] J.A. Bouré. Review of two-phase flow instability.Pdf, 1972.

[4] V. Chatoorgoon, A. Voodi, and D. Fraser. The stability boundary for supercritical flow in natural convection loops: Part I: H2O studies. *Nuclear Engineering and Design*, 235(24):2570–2580, 2005. ISSN 00295493. doi: 10.1016/j.nucengdes.2005.06.003.

[5] E. M. Chiapero. *Two phase flow instabilities and flow mal-distribution in parallel channels*. PhD thesis, NTNU, 2013.

[6] GIF. A technology roadmap for generation IV nuclear energy systems. *Nuclear Energy Research Advisory Committee and the ...*, pages 1–97, 2002. doi: 10.2172/859029. URL `http://www.gen-4.org/PDFs/GenIVRoadmap.pdf$\delimiter"026E3B2$nhttp://scholar.google.com/scholar?hl=en{&}btnG=Search{&}q=intitle:A+Technology+Roadmap+for+Generation+IV+Nuclear+Energy+Systems{#}0`.

[7] O. Gomez. Stability Analysis of the High Performance Light Water Reactor. 2009.

[8] G Guido, J Converti, and A Clausse. Density-wave oscillations in parallel channels - an analytical approach. 125:121–136, 1991.

[9] P. K. Jain and Rizwan-Uddin. Numerical analysis of supercritical flow instabilities in a natural circulation loop. *Nuclear Engineering and Design*, 238(8):1947–1957, 2008. ISSN 00295493. doi: 10.1016/j.nucengdes.2007.10.034.

[10] F.A.L. Kam. Development of a one-dimensional model for stability analysis of a natural circulation supercritical water reactor. 2011.

[11] H Khartabil, D Brady, and T Schulenberg. Supercritical water-cooled reactor (SCWR) development through GIF collaboration. pages 1–9, 2009. URL `http://inis.iaea.org/search/search.aspx?orig{_}q=RN:41033478`.

[12] G.B. Koren. Linear stability analysis of a supercritical water loop driven by natural convection. 2010.

[13] D Krijger. A linear stability analysis of a water loop driven by natural convection at supercritical conditions. (July), 2013.

[14] M. Ledinegg. Instability of flow during natural and forced circulation. *Die Wärme, 61, 891-898*, 1938.

[15] G. I. A. Lippens. Linear analysis of thermal inertia effect on the thermal-hydraulic stability of a natural circulation driven supercritical water loop. Technical Report 9, 2014.

[16] C. P. Marcel. *Experimental and numerical stability investigations on natural circulation boiling water reactors*. PhD thesis, Delft University of Technology, 2007.

[17] S. Mcgarrity. Maximizing Code Performance by Optimizing Memory Access. *Memory*, (June):2–5, 2007.

[18] A. K. Nayak and P. K. Vijayan. Flow instabilities in boiling two-phase natural circulation systems: A review. *Science and Technology of Nuclear Installations*, 2008, 2008. ISSN 16876075. doi: 10.1155/2008/573192.

[19] National Institute of Standards and Technology. Thermophysical properties of fluid systems. *NIST Standard Reference Database*.

[20] Y. Oka. An Advanced Course in Nuclear Engineering : Nuclear Reactor Design. *Springer*, 2010. doi: 10.1007/978-4-431-54898-0.

[21] M. Rohde, C. P. Marcel, C. T'Joen, A. G. Class, and T. H J J Van Der Hagen. Downscaling a supercritical water loop for experimental studies on system stability. *International Journal of Heat and Mass Transfer*, 54(1-3):65–74, 2011. ISSN 00179310. doi: 10.1016/j.ijheatmasstransfer.2010.09.063. URL http://dx.doi.org/10.1016/j.ijheatmasstransfer.2010.09.063.

[22] L. C. Ruspini. *Carlos Ruspini Experimental and numerical investigation on two-phase flow*. 2013. ISBN 9788247134047.

[23] R. Jain S. Lomperski, D. Cho and M. Corradini. Stability of a natural circulation loop with a fluid heated through the thermodynamic pseudo-critical point. *Proceedings of the 2004 International Congress on Advances in Nuclear Power Plants, ICAPP'04 pp. 1736–1741*, 2004.

[24] T. K. F. Schenderling. Numerical analysis of the influence of wall thermal inertia on the stability of natural circulation driven supercritical water reactors. 2013.

[25] T. Schulenberg, J. Starflinger, and J. Heinecke. Three pass core design proposal for a high performance light water reactor. *Progress in Nuclear Energy*, 50(2-6):526–531, 2008. ISSN 01491970. doi: 10.1016/j.pnucene.2007.11.038.

[26] M. Sharabi and W. Ambrosini. Discussion of heat transfer phenomena in fluids at supercritical pressure with the aid of CFD models. *Annals of Nuclear Energy*, 36(1):60–71, 2009. ISSN 03064549. doi: 10.1016/j.anucene.2008.10.006. URL http://dx.doi.org/10.1016/j.anucene.2008.10.006.

[27] J. Spoelstra. Numerical stability analysis of natural circulation driven supercritical water reactors. *ISSCWR-6 Proceedings*, (December), 2013. URL http://www.isscwr6.com.

[28] B. T. Swapnalee, P. K. Vijayan, M. Sharma, and D. S. Pilkhwal. Steady state flow and static instability of supercritical natural circulation loops. *Nuclear Engineering and Design*, 245:99–112, 2012. ISSN 00295493. doi: 10.1016/j.nucengdes.2012.01.002. URL http://dx.doi.org/10.1016/j.nucengdes.2012.01.002.

[29] C. G. A. T'Joen. Experimental study on the stability of a natural circulation driven Super-Critical Water Cooled Reactor. (2011).

[30] C. G. A. T'Joen, M. Rohde, and M. De Paepe. Linear Stabitlity Analysis of a Supercritical Loop. *9th International Conference on Heat Transfer, Fluid Mechanics and Thermodynamics (HEFAT 2012)*, (July): 242–250, 2012.

[31] D. D. B. van Bragt. Analytical modeling of Boiling Water Reactor Dynamics, 1998.

[32] T. H. J. J. Van Der Hagen. Fuel heat transfer modelling in reduced-order boiling water reactor dynamics models.pdf, 1998.

[33] P. K. Vijayan, A. K. Nayak, D. Saha, and M. R. Gartia. Effect of loop diameter on the steady state and stability behaviour of single-phase and two-phase natural circulation loops. *Science and Technology of Nuclear Installations*, 2008, 2008. ISSN 16876075. doi: 10.1155/2008/672704.

[34] J. Yu, S. Che, R. Li, and B. Qi. Analysis of Ledinegg flow instability in natural circulation at supercritical pressure. *Progress in Nuclear Energy*, 53(6):775–779, 2011. ISSN 01491970. doi: 10.1016/j.pnucene.2011.04.001. URL http://dx.doi.org/10.1016/j.pnucene.2011.04.001.

[35] A. Zonneveld. Linear analysis of the influence of neutronic-thermal-hydraulic coupling on the stability of a natural convection driven supercritical water loop. 2015.

[36] N. Zuber. Hydronamic aspects of boiling heat transfer. *Final report NASA-11422*, 1966.